MIKE Powered by DHI

# Littoral Processes FM

## All Modules

## Scientific Documentation

**DHI headquarters**
Agern Allé 5
DK-2970 Hørsholm
Denmark

+45 4516 9200 Telephone
+45 4516 9333 Support
+45 4516 9292 Telefax

mike@dhigroup.com
www.mikepoweredbydhi.com

# PLEASE NOTE

# CONTENTS

Littoral Processes FM
All Modules
Scientific Documentation

# 1 Introduction

This document presents the scientific background for the calculations carried out within the Littoral Processes FM module. The module is a part of the MIKE Powered by DHI software.

The Littoral Processes FM module is an integrated modelling system that simulates non-cohesive transport in points and along quasi-uniform coastlines. Using functionality to calculate and save representative littoral drift transport rates into format specified binary tables it is possible to simulate the evolution of coastlines affected by structures, sediment sources and/or climate changes.

Littoral Processes FM contains four calculation modules:

- Transport in point
- Littoral drift
- Littoral drift table generation
- Coastline evolution

These modules may be used individually or in combination. The common model engine is developed such that common functionalities in the modules are embedded as indicated in Figure 1.1.

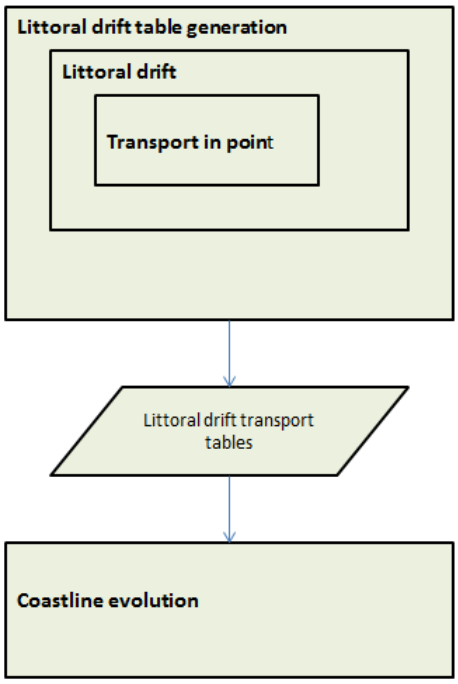


Figure 1.1 Outline of model integration

# 2 Basic Sediment Transport

## 2.1 Introduction

The core of the sand transport calculations in the Littoral Processes FM module is a Quasi Three-Dimensional Sediment Transport model (STPQ3D).

The STPQ3D model calculates instantaneous and time-averaged hydrodynamics and sediment transport in two horizontal directions in a point. The model calculates the bed load and the suspended load separately, and it sums the values to the total load.

The essence of the Quasi-3D hydrodynamics model is the solution of the force balance across the water column

$$\tau = \rho \nu_t \left| \frac{\partial \overline{U}}{\partial z} \right| \tag{2.1}$$

from which the time averaged flow velocity $\overline{U}$ is found by integration.

The temporal and vertical variations of shear stress, turbulence, flow velocity and sediment concentrations are resolved. The time evolution of the boundary layer due to combined wave/current motion is solved by means of the integrated momentum approach of Fredsøe (1984). The force balance includes contributions from the near bed wave orbital motion, forces associated with wave breaking (gradients of radiation stresses) and the sloping water surface.

In the following the different aspects of the STPQ3D model are described.

### 2.1.1 Vertical distribution

The vertical grid resolution of the water column is defined by a maximum number of grid points, $j_{max}$. To resolve the finer details of the flow near the bed, the water column is divided into two main areas:

1. The lower 10% of the water column is described by 50% of the grid points using a log-normal distribution
2. The upper 90% of the water column is described by the remaining grid points using linear distribution

The vertical distribution can be described as follows:

$$z(j) = a \cdot e^{bj} \quad for \quad j < 0.5 \cdot j_{\max}$$

$$z(j) = z(j-1) + \frac{0.9D}{0.5 \cdot j_{\max}} \quad for \quad j \le 0.5 \cdot j_{\max} \tag{2.2}$$

$$a = 2.0 d_{50} + h_r \tag{2.3}$$

$$b = \frac{\log\left(0.1 \cdot D / a\right)}{0.5 \cdot j_{\max}} \tag{2.4}$$

Where

| | |
|---|---|
| $d_{50}$ | is the mean grain diameter |
| $D$ | is the water depth, and |
| $H_r$ | is the ripple height (if any) |

An example is shown in Figure 2.1.

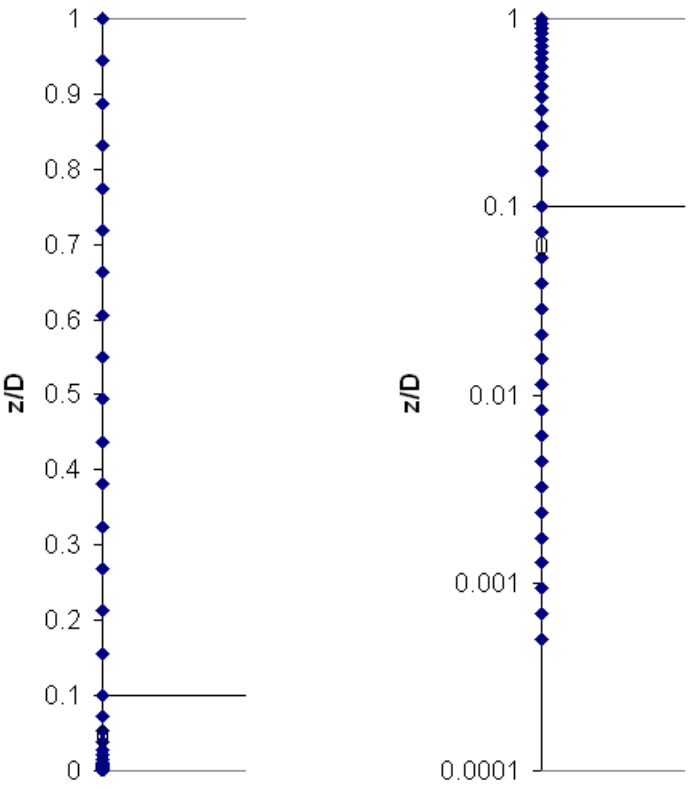


Figure 2.1 Example of vertical grid resolution (Depth = 1.0 m, $d_{50}$ = 0.25 mm).
Left: shown on linear z-axis
Right: shown on logarithmic z-axis

## 2.2 Hydrodynamics

### 2.2.1 Mean Flow

Prior to the sediment transport calculations the hydrodynamic flow conditions must be calculated. The mean horizontal velocity component is input parameter to the model. The pre-defined mean discharge is obtained by superposing the wave motion by a steady current driven by a gradient in the water surface elevation and solving the turbulent boundary layer for the combined wave/current motion. The interaction of the undertow, the longshore current and the waves are automatically taken into account. The wave induced mass transport and the discharge in the surface rollers are included in the calculation of the mean flow. The gradients in the water surface elevations in the x and y

directions are not known beforehand and are found through iteration to obtain the prescribed fluxes.

The time-averaged flow velocity distribution is calculated from the vertical distribution of the driving forces and the mean eddy viscosity. By using the no slip condition at the bed, the mean velocity profile is solved by integrating Eq.(2.1).

Figure 2.2 shows an example of the time varying velocity profiles across the vertical in the current direction, and Figure 2.3 shows the corresponding velocity profiles perpendicular to the current direction.

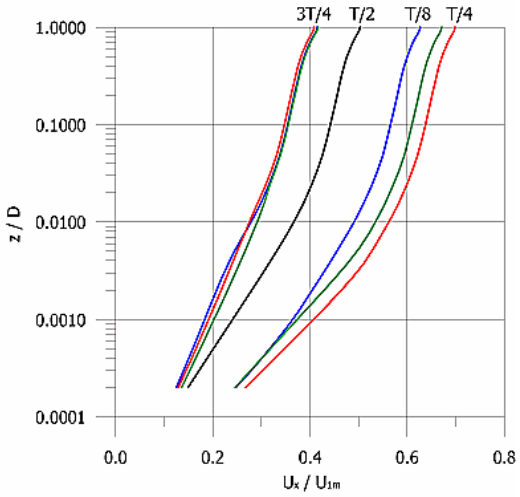


Figure 2.2 Example of velocity profiles in the current direction during one wave period. Test conditions are: Cnoidal 5th order wave theory, $H_{rms}$=1.0 m, $T_z$=6 s, Angle=10 deg., D=2 m, V=0.5 m/s. No wave breaking

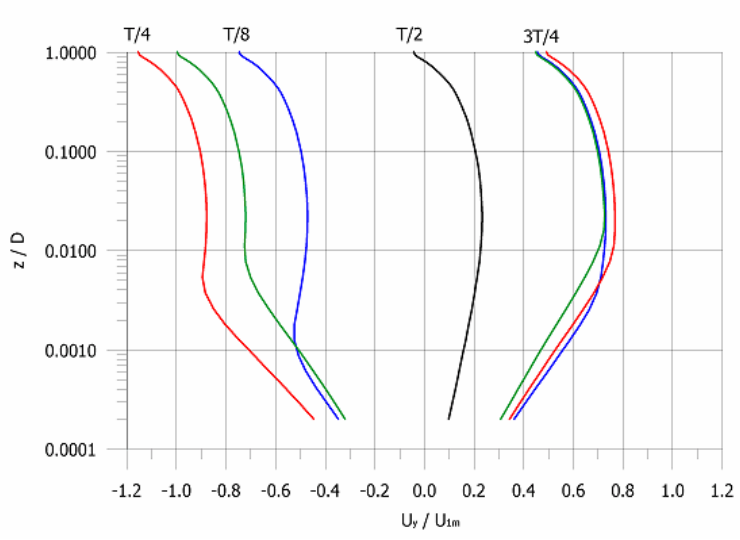


Figure 2.3 Example of velocity profiles perpendicular to the current direction during one wave period. Test conditions as in Figure 2.2

### 2.2.2 Wave Motion

In the model, the wave motion is defined through a number of general wave parameters such as wave height $H$ (or $H_{rms}$ ), wave period $T$ (or $T_z$ ) and angle of incidence $\alpha$ (or MWD). The values in parentheses refer to an irregular wave description.

In shallow water the wave motion becomes non-linear, e.g. the velocities under the wave crest are higher than under the wave trough. This phenomenon is very important in the calculation of cross-shore sediment transport. The time varying water surface and orbital velocities can be calculated from various wave theories.

The wave motion outside the boundary layer is assumed to be inviscid (potential flow). In order to fulfil the requirements of potential theory, the mean bed shear stress due to the wave motion must be zero for pure oscillatory flow. In case of progressive waves, a small but significant mean bed shear stress occurs due to the non-uniformity of the wave boundary layer.

In the model, a small additional constant velocity is added to the wave orbital motion. This velocity is not known beforehand, but must be found by iteration, such that the mean bed shear stress, calculated from the turbulent boundary layer model, corresponds to the pre-defined value. The concept of the additional potential velocity is described in Brøker (1985).

In case of breaking waves, energy is extracted from the organized wave motion and is converted into turbulence. The turbulent energy generated at the water surface is transported downwards into the water column. The amount of turbulence produced at the water surface is calculated from general wave parameters such as wave height and period and the water depth. The production of energy can be calculated according to a regular or an irregular wave description.

#### Near bed orbital velocities

The wave motion outside the bottom boundary layer can be calculated from a number of wave theories. Both classical wave theories as well as semi-empirical theories are available.

The use of non-linear wave theory is important to resolve higher order velocity moments (skewness, asymmetry), which are important for sediment transport. Unfortunately, no wave theory exists today that covers all hydrodynamic conditions satisfactorily. Therefore, a number of the existing ones are included in the model. Each of them is valid in a limited range of hydrodynamic conditions.

The available wave theories and their area of application are listed below.

##### Classic theories:

- Stokes theory 1$^{st}$, 3$^{rd}$ and 5$^{th}$ Order (Fenton 1985).
  Deep water/ Non-breaking waves
- Cnoidal theory (1$^{st}$, 3$^{rd}$ and 5$^{th}$ Order (Fenton 1990).
  Shallow water/ Non-breaking waves
- Vocoidal theory (Swart 1982).
  All water depths/Non breaking waves

### Semi-empirical theories:

- Isobe and Horikawa (1982).
  All water depths/Breaking and Non-breaking waves

- Doering and Bowen (1995).
  All water depths/Breaking and Non-breaking waves

Detailed descriptions of the wave theories can be found in the referred literature. Figure 2.4 shows an example of the near bed velocity, $u_0$, during a wave period.

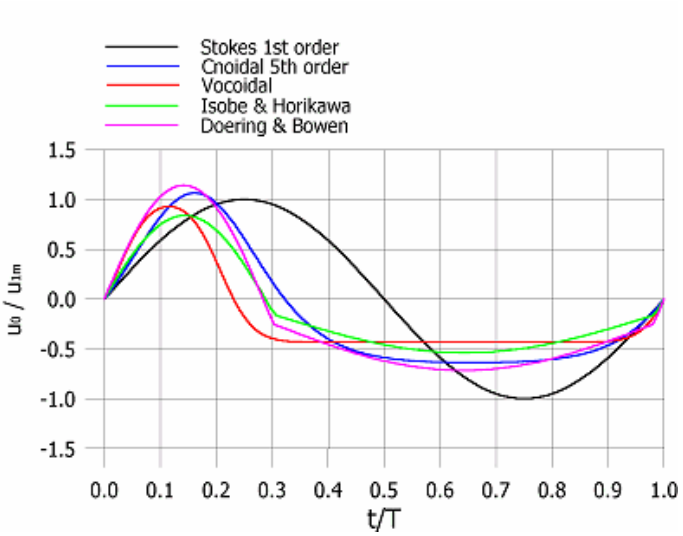


Figure 2.4 Example of near bed velocity $u_0$ for 5 different wave theories

The terms 'shallow' and 'deep' water refer to the Ursell number, $U_s$, which is defined as:

$$U_s = \frac{HL^2}{D^3} \tag{2.5}$$

Where $H$ is the wave height, $L$ is the wave length and $D$ is the water depth.

Deep water corresponds to $U_s < 25$, shallow water corresponds to $U_s > 25$.

Stokes' and Cnoidal wave theories descriptions of orbital velocities can be used for $U_s < 25$ and $U_s > 25$, respectively. In the model an option is available that automatically applies either Stokes' or Cnoidal wave theory, according to the above mentioned validity range. In some cases it is desirable to use linear wave theory regardless of the Ursell number. The model also provides an option for this.

Vocoidal wave theory has the advantage that it is applicable in all water depths, which means that the same theory is used in both deep and shallow water.

The model of Isobe and Horikawa (1982) includes the effect of the bed slope on the time varying orbital velocity. The model is semi-empirical and has not been tested for applications including breaking and broken waves.

The model of Doering and Bowen (1995) relates the skewness of the wave orbital motion to general wave parameters (H,T,D), but does not describe time varying near bed orbital velocities. The description of velocity skewness is valid for both breaking and non-breaking waves. In order to calculate the velocity variation, the semi-empirical description of Isobe and Horikawa (1982) is used in the model, where the ratio between the

maximum velocities at wave crest and wave trough are found by iteration such that the skewness of the velocity distribution corresponds to the model of Doering and Bowen (1995).

### Mass transport

For progressive waves a net mass transport (drift) occurs between the wave trough and the wave crest (Eulerian definition). Under uniform conditions in the longshore direction the net cross-shore discharge must be zero. The mass flux is calculated from the applied wave theory. For the semi-empirical wave theories the mass flux is estimated by using linear wave theory, as no descriptions of mass flux exist for these wave theories.

### Surface roller area

In case of breaking waves a surface roller is present at the water surface. The mass flux in the surface roller and the shear stress exerted on the water surface by the roller are important in the calculation of the undertow. In the present model the surface roller area is calculated according to the model of Dally and Brown (1995), in which the surface roller area *A* is related to the energy dissipation through:

$$\rho A = \frac{Diss}{\beta_d} \tag{2.6}$$

Where *Diss* is the dissipation of wave energy through breaking and $\beta_d$ is an empirical constant between 0.1 and 0.2, which is an input parameter to the model. The default value is 0.15 according to Deigaard et al. (1986). The surface roller area is thus defined in the model by the parameter $\beta_d$ and the energy dissipation, which is calculated either from a regular or an irregular wave description.

## 2.2.3 Bottom Boundary Layer

The development in time of the boundary layer in combined wave-current motion is described by the following first-order differential equation, Fredsøe (1984).

$$\frac{\partial z}{\partial t} = \frac{z\left(1+z-e^z\right)}{e^z\left(z-1\right)+1}\frac{1}{U_0}\frac{dU_0}{dt} + \frac{30\kappa}{k}\frac{\sqrt{\kappa^2 U_0^2 + z^2 U_{f0}^2 + 2\kappa z U_{f0} U_0 \cos\gamma}}{e^z\left(z-1\right)+1} \tag{2.7}$$

Where

| | |
|---|---|
| $\kappa$ | is von Kármán constant |
| *t* | is time |
| *z* | is a parameter related to the boundary layer thickness $\delta$, see Eq. (2.9) |
| $U_0$ | is the near-bed wave orbital velocity |
| $U_{f0}$ | is the friction velocity due to the current inside the wave boundary layer |
| $\gamma$ | is the angle between the current and the waves |
| *k* | is the bed roughness, taken to be equal to 2.5 $d_{50}$ for a plane bed, and 2.5 $d_{50}$ + $k_R$ for a ripple-covered bed |

$d_{50}$ is the median grain size

$k_R$ is the ripple-related roughness, see Eq. (2.37)

The near-bed wave-induced velocity $U_0$ varies in time according to Eq. (3.5):

$$U_0(t) = U(0,t) \tag{2.8}$$

Equation (2.7) is solved by the application of a fourth-order Runge-Kutta method over the wave period. The time step is defined by dividing the wave period *T* into two times *n/2* (defining *n/2+1* evenly spaced calculation points in one half period). It is assumed that a new boundary layer begins to develop each time the flow reverses.

Once *z(t)* is known, the boundary layer thickness $\delta$ is calculated for every time step:

$$\delta = \frac{k}{30}\left(e^{z} - 1\right) \tag{2.9}$$

Figure 2.5 shows an example of the boundary layer thickness during a wave period applying Cnoidal wave theory.

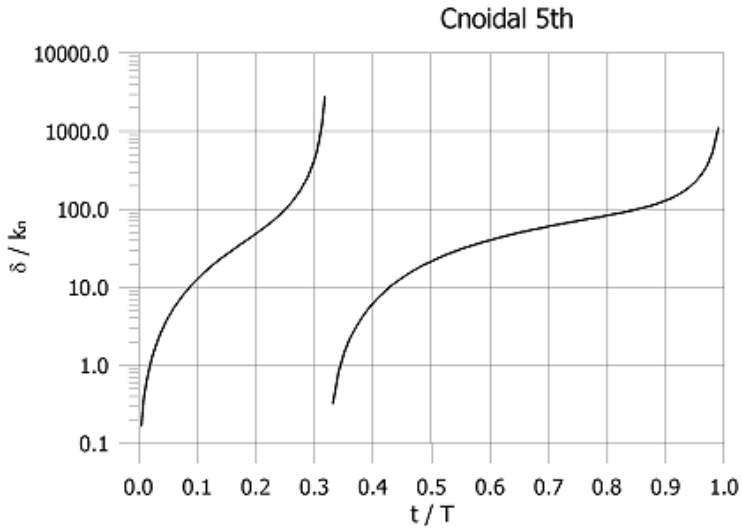


Figure 2.5 Example of boundary layer thickness δ, using Cnoidal wave theory

The friction velocity $U_f(t)$ is derived from the boundary condition for the velocity at the top of the boundary layer.

$$\left[\frac{U_f}{\kappa}\ln\left(\frac{\delta + k/30}{k/30}\right)\right]^2 = \left[\frac{U_{f0}}{\kappa}\ln\left(\frac{\delta + k/30}{k/30}\right) + U_0\cos\gamma\right]^2 + \left[U_0\sin\gamma\right]^2 \tag{2.10}$$

$$\cos\phi = \frac{U_0\kappa\cos\gamma + U_{f0}z}{U_f z} \tag{2.11}$$

$$\sin\phi = \frac{U_0\kappa\sin\gamma}{U_f z} \tag{2.12}$$

Figure 2.6 and Figure 2.7 show examples of the friction velocity $U_f$ in the cross-shore and longshore direction, respectively, for the 5 different wave theories.

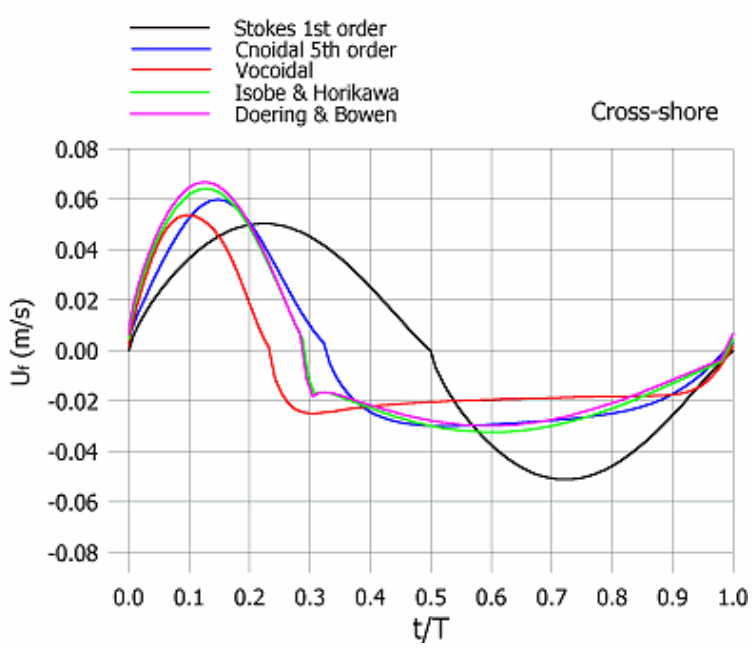


Figure 2.6 Example of friction velocity $U_f$ in the cross-shore direction

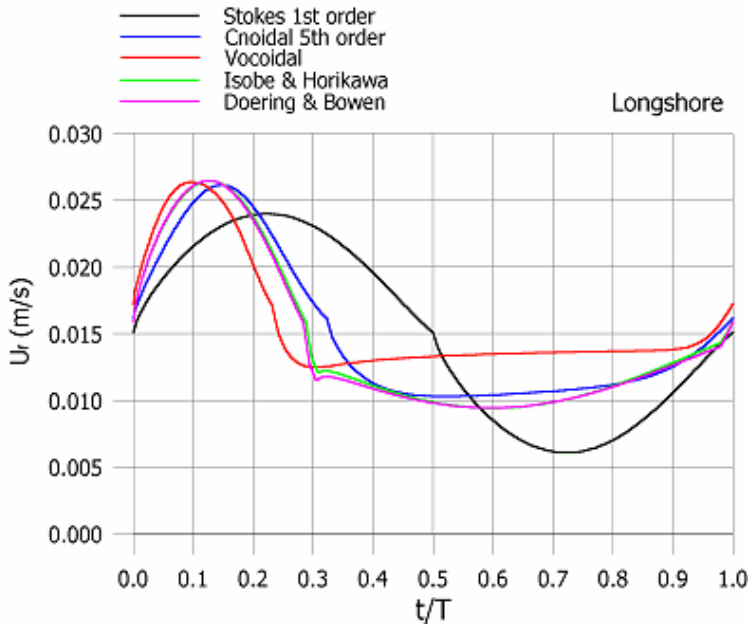


Figure 2.7 Example of friction velocity $U_f$ in the longshore direction

Additional parameters determined by the model are:

$$U_{fc} = \sqrt{\frac{1}{T}\int_0^T U_f^2 \cos\phi \, dt} \tag{2.13}$$

$$\delta_m = \frac{1}{2}\left(\delta\left(t=\frac{T}{4}\right)+\delta\left(t=\frac{3T}{4}\right)\right) \tag{2.14}$$

$$k_w = k\left(\frac{30\delta_m}{k}\right)^{1-\frac{U_{f0}}{U_{fc}}} \tag{2.15}$$

Where

| | |
|---|---|
| $\delta$ | is the instantaneous thickness of the boundary layer |
| $\delta_m$ | is the mean boundary layer thickness |
| $U_f$ | is the friction velocity |
| $U_{fc}$ | is the friction velocity of the mean current $V$ |
| $D$ | is the local water depth |
| $k_w$ | is the apparent bed roughness |
| $\phi$ | is the angle between the instantaneous flow in the boundary layer and the mean current. |

The value of the friction velocity of the current inside the boundary layer $U_{f0}$ is not known beforehand and is found by iteration.

The calculations are repeated until the difference between the value of $U_{fc}$ is given and the value determined through Eq. (2.13) becomes smaller than the chosen tolerance $\varepsilon$.

### 2.2.4 Turbulence

The turbulence originates from 3 different sources:

1. The wave boundary layer
2. The energy dissipation due to wave breaking
3. The mean flow

The three contributions to the eddy viscosity are calculated more or less independently from each other. The contribution from the wave boundary layer is calculated from the boundary layer model of Fredsøe (1984). The contribution from the mean flow is modelled by applying a mixing length concept, see Elfrink et al. (1996) and the eddy viscosity due to wave breaking is calculated from the transport equation for turbulent kinetic energy, see Deigaard et al. (1986).

The total instantaneous eddy viscosity is calculated by summing the three contributions at the energy level:

$$\nu_t^2 = \nu_{bl}^2 + \nu_c^2 + \nu_{br}^2 \tag{2.16}$$

Where $\nu_t$ is the total instantaneous eddy viscosity, $\nu_{bl}$ the eddy viscosity in the bottom boundary layer, $\nu_c$ the eddy viscosity due to the mean current and $\nu_{br}$ the eddy viscosity due to wave breaking.

Figure 2.8 shows an example of the mean total eddy viscosity distribution across the depth for a non-breaking and breaking wave, respectively.

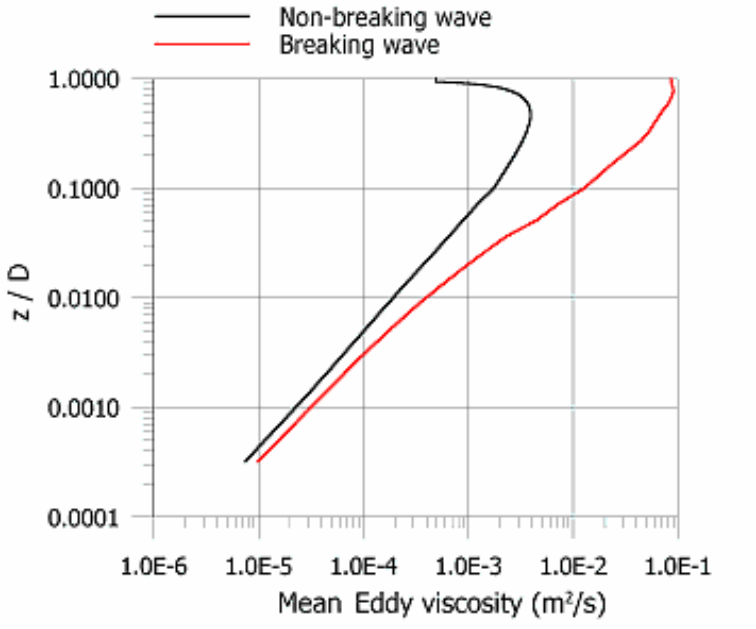


Figure 2.8 Example of mean total eddy viscosity for a non-breaking and breaking wave

## Eddy viscosity in bottom boundary layer

Inside the bottom boundary layer the eddy viscosity is calculated as:

$$\nu_{bl} = \kappa U_f z\left(1-\frac{z}{\delta}\right) \tag{2.17}$$

Where $\delta$ is the instantaneous boundary layer thickness, $U_f$ the instantaneous shear velocity due to the combined wave-current motion and $z$ is the height above the bed.

The shear velocity $U_f$ and the boundary layer thickness $\delta$ are calculated from the model of Fredsøe (1984).

In the case of a ripple-covered bed, an extra contribution to the eddy viscosity $\nu_{bl}$ is added according to Eq. (2.40).

## Eddy viscosity due to mean current

Outside the boundary layer the eddy viscosity due to the mean current is calculated from the mixing length concept:

$$\nu_c = l^2 \frac{d\overline{U}}{dz} \tag{2.18}$$

Where $l$ is the mixing length defined as $l = k\ z\ (1 - z/D)$ and $U$ is the mean current velocity

## Eddy viscosity due to wave breaking

The time-averaged production of turbulent kinetic energy at the water surface is calculated from a regular or an irregular wave description. For regular waves the production of turbulent energy is defined at the input level as a dimensionless factor $f_{br}$ ,

which is defined as the ratio of the actual energy dissipation and the energy dissipation in a steady hydraulic jump, $Diss_j$, which yields:

$$\overline{Diss_j} = \frac{\rho g D}{T}\left(\frac{H^3}{4D^2 - H^2}\right) \tag{2.19}$$

The energy dissipation in the model can thus be varied gradually from $f_{br} = 0$ for non-breaking waves to $f_{br} = 1$ for fully developed breaking waves.

For irregular waves the production of turbulent energy is calculated according to the model of Battjes and Janssen (1978), which yields:

$$Diss = 0.25\alpha Q_b H_{\max}^2 \cdot \frac{\rho g}{T} \cdot \frac{H_{\max}}{D} \tag{2.20}$$

Where $H_{max}$ is the maximal wave height, $Q_b$ the fraction of breaking waves and $\alpha$ the dimension less parameter, taken as 1.

The maximal wave height is:

$$H_{\max} = \frac{\gamma_1}{k}\tanh\left(\frac{\gamma_2 kD}{\gamma_1}\right) \tag{2.21}$$

Where $k$ is the wave number and $D$ the water depth.

In case $kD > 2\pi$, the eddy viscosity due to wave breaking is omitted from the calculations.

The fraction of breaking waves $Q_b$ is:

$$\frac{1 - Q_b}{\ln Q_b} = -\left(\frac{H_{rms}}{H_{\max}}\right)^2 \tag{2.22}$$

The two parameters $\gamma_1$ and $\gamma_2$, which describe the maximum wave steepness $H/L$ and height/depth ratio $H/D$, respectively, are input parameters to the model. As default, the theoretical value of $\gamma_1 = 0.88$ is used. The second parameter, $\gamma_2$ is calculated from the expression as presented in Battjes and Stive (1985):

$$\gamma_2 = 0.5 + 0.4\tanh\left(33 s_0\right) \tag{2.23}$$

Where $s_0$ is the deep-water wave steepness, $H/L_0$, where $L_0$ is the deep-water wave length.

The eddy viscosity due to wave breaking is calculated from the diffusion equation for turbulent kinetic energy according to the model of Deigaard et al. (1986):

$$\frac{\partial k}{\partial t} = \frac{\partial}{\partial z}\left(\frac{\nu_t}{\sigma_n}\frac{\partial k}{\partial z}\right) + \frac{1}{\rho}PROD - c_1\frac{k^{2/3}}{l} \tag{2.24}$$

$$\nu_t = l\sqrt{k} \tag{2.25}$$

Where *PROD* is the production of turbulent kinetic energy due to wave breaking, i.e. total production of turbulent energy equals the dissipation of energy. The 'production' is assumed to take place during the time $T_{diss}$ after passage of the crest and limited to above the trough level.

In case of irregular waves, the time scale $T_{diss}$ over which the turbulent energy is produced, diffused and dissipated is taken as: $T_{diss} = T_p/Q_b$.

### 2.2.5 Shear Stress

The driving forces for the mean flow basically consist of three contributions:

1. The time averaged shear stress associated with the wave motion
2. The shear stress associated with wave breaking
3. The shear stress due to gradients in the water surface

The vertical distribution of the time mean shear stress is illustrated in Figure 2.9.

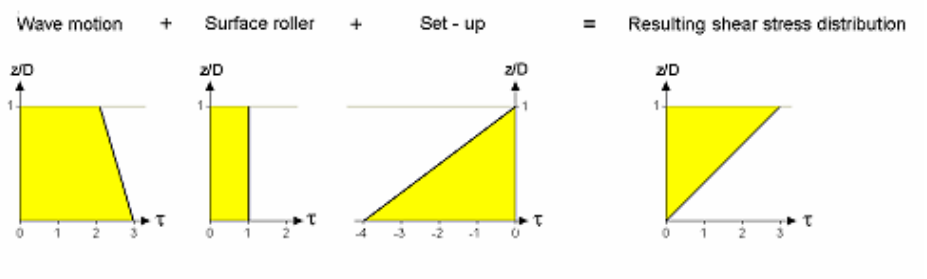


Figure 2.9 Illustration of vertical distribution of mean shear stress

For details reference is given to Fredsøe and Deigaard (1992).

#### Wave motion

**Asymmetric wave orbital motion**
The non-linear wave motion will give rise to a mean bed shear stress in the wave direction. In order to fulfil the requirements of potential theory, a small additional velocity is added to the oscillatory wave motion such that the mean bed shear stress becomes zero.

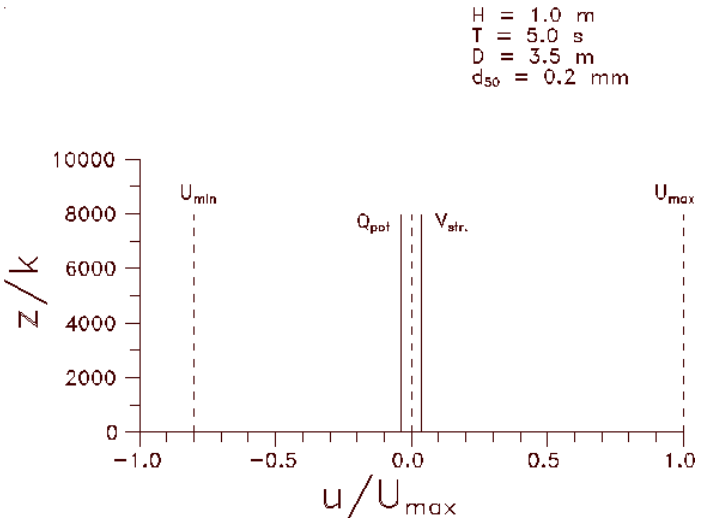


Figure 2.10 Sketch of components in asymmetric wave motion

### Streaming in the boundary layer

In case of progressive waves, a small net shear stress is generated due to the non-uniformity of the wave boundary layer. Brøker (1985) showed that this streaming induced shear stress at the bed can be expressed as:

$$\tau_{str} = \frac{\rho}{c}\overline{U_0 U_f \left|U_f\right|} \tag{2.26}$$

## Radiation stresses

Deigaard et al. (1986) determined the time mean shear stress necessary to balance the gradients in the radiation stresses. It was found that the vertical transfer of horizontal momentum gives a significant contribution to the momentum balance. Deigaard et al. (1994) derived expressions for time mean shear stress at the wave trough level in case of oblique waves by considering the momentum balance for the surface rollers. The shear stress is constant over the water column. In the wave direction it yields:

$$\frac{\overline{\tau_s}}{\rho} \approx -\frac{\overline{Diss}}{c} \tag{2.27}$$

Where *c* is the wave celerity and *Diss* is the time averaged energy dissipation due to wave breaking.

## Water level gradients

On uniform beaches the mean flow in the cross shore direction must balance the mass transport associated with the wave motion and the discharge in the surface roller. In the longshore direction the mean flow corresponds to the time averaged longshore current velocity. In the model the predefined mean flow discharge is obtained by superposing a shear stress arising from a sloping water surface to the shear stress associated with the wave motion (radiation stress, surface roller, streaming). It is noted that this water level gradient not automatically corresponds to the gradient in radiation stress.

This shear stress due to the sloping water surface is zero at the water surface and varies linearly through the water column (hydrostatic pressure). In this model, the pre-defined current may have any magnitude and direction.

### 2.2.6 Ripples

Wave-generated ripples exist for values of the Shield's parameter $\theta_{max}$ less than approximately 1, Nielsen (1979):

$$\theta_{\max} = \frac{U_{f,\max}^2}{(s-1)gd_{50}} \tag{2.28}$$

Where $s$ is the relative density of the bed material, $g$ is the acceleration of gravity and $d_{50}$ is the mean grain size.

For similar values of $\theta_{max}$ the ripples are the largest for pure wave motion and are smoothed out when current superposes the wave motion.

The ripples act on the flow as large roughness elements. The influence of ripples on the sediment transport is considered by calculating:

- The dimensions of the ripples as a function of the characteristics of the waves and the current
- The increased roughness experienced by the flow due to the presence of ripples
- The contribution to the eddy viscosity due to ripples
- The mean concentration at the level of the ripple crest

#### Ripple dimensions

In pure wave motion the ripple dimensions are determined according to Nielsen (1979):

$$h_r = 21 \cdot \psi^{-1.85} \cdot a \tag{2.29}$$

$$\lambda = h_r / \left(0.342 - 0.34 \cdot \theta^{0.25}\right) \tag{2.30}$$

Where

| | |
|---|---|
| $\psi$ | is $U_{1m}^2 / (s-1)gd_{50}$ |
| $h_r$ | is ripple height |
| $\lambda$ | is ripple length |
| $\theta'$ | is Shield's parameter for plane bed case (k = 2.5 $d_{50}$) |
| $a$ | is amplitude of wave orbital motion near the bed |
| $U_{1m}$ | maximum orbital velocity |

In the estimates of ripple dimensions $\theta'_{pn}$ is calculated using Swart's formula for the friction factor (1982):

$$f_w = \exp\left(5.213\left(\frac{2.5d_{50}}{a}\right)^{0.194} - 5.977\right) \tag{2.31}$$

$$\theta'_{pn} = \frac{U_f^2}{(s-1)gd} = \frac{1}{2} f_w \psi \tag{2.32}$$

In cases where current superposes the wave motion, the ripple height is decreased. In the model the effect of current is included by introduction of a 'reduced ripple height'.

The reduced ripple height in combined wave-current motion is estimated as:

$$h_r(wave, current) = h_r(wave) \cdot R_f\left(\frac{U_{fc}}{U_{fw}}\right) \tag{2.33}$$

The reduction factor, $R_f$, is given as follows:

$$R_f = \begin{cases} 1 & for \quad \frac{U_{fc}}{U_{fw}} \le C_1 \\ 0.5 + 0.5 \cdot \cos\left(\left(\frac{U_{fc}}{U_{fw}} - C_1\right) \cdot \frac{\pi}{C_2 - C_1}\right) & for \quad C_1 < \frac{U_{fc}}{U_{fw}} \le C_2 \\ 0 & for \quad \frac{U_{fc}}{U_{fw}} \ge C_2 \end{cases} \tag{2.34}$$

Where $C_1$ and $C_2$ are user-defined constants, having default values of $C_1$ = 0.1 and $C_2$ = 2.

When $C_2$ is set to zero, the influence of ripples on the transport is neglected.

In Eqs. (2.33) and (2.34), $U_{fc}$ is estimated as:

$$U_{fc} = \frac{V}{6 + 2.5 \cdot \ln\left(\frac{D}{k_r + 2.5d_{50}}\right)} \tag{2.35}$$

Where $k_r$ is ripple roughness corresponding to ripples in pure wave motion. $U_{fw}$ is found from:

$$U_{fw} = \sqrt{\frac{1}{2} \cdot f_w \cdot U_{1m}^2} \tag{2.36}$$

The calculation of ripple dimensions becomes less valid with increasing grain diameter. If, $h_r$ *(wave, current)* > *0.1 D* the bed is considered plane and $h_r$ is set to 0.

### Roughness due to ripples

The roughness due to ripples according to Raudkivi (1988) is given by:

$$k_r = \frac{C_3 \cdot h_r^2}{\lambda} \tag{2.37}$$

Where $C_3$ is a constant and the default value is 16.

### Eddy viscosity from ripples

In the case of a ripple-covered bed, an extra contribution $\nu_r$ to the eddy viscosity is added according to the empirical formulation of Nielsen (1979).

$$\nu_r(0) = h_r \cdot \alpha\omega \exp\left(1.5 - 4500 d_{50} - 1.21 n\left(\frac{\alpha\omega}{w}\right)\right) \tag{2.38}$$

It is assumed that the eddy viscosity related to the presence of wave ripples decreases with the distance above the bed according to:

$$\nu_r(y) = \nu_r(0) \cdot \cos\frac{\pi y}{4 h_r C_4} \tag{2.39}$$

Where $C_4$ is an empirical constant and the default value is 3.

The eddy viscosity near the bed is corrected for the presence of ripples according to

$$\nu_{bl}(z,t) = \nu_{bl}(z,t) + \nu_r(z) \tag{2.40}$$

For $y > 2+C_4 h_r$ the ripples have no effect on the eddy viscosity.

## 2.3 Sediment Transport

The sediment transport is calculated as:

$$q_t = q_b + q_s \tag{2.41}$$

Where $q_t$ is the total sediment transport, $q_b$ the bed load transport and $q_s$ is the sediment transport in suspension.

In the STPQ3D model the bed load transport model of Engelund and Fredsøe (1976) is used, where the bed load transport is calculated from the instantaneous Shields parameter.

In case of shingle sized material only bed load is considered to exist and the calculation of the bed load is different from the default description for sand.

The vertical variation of the suspended sediment concentration is calculated from the vertical diffusion equation for suspended sediment, according to Fredsøe et al. (1985).

The omission of the convective terms in the diffusion equation is compensated by adding the Lagrangian flow velocity times the mean concentration to the time averaged product of instantaneous velocity and concentrations.

The suspended sediment transport is calculated as the product of the instantaneous flow velocities and the instantaneous sediment concentration:

$$q_s = \frac{1}{T}\int_0^T \int_{2d}^{D} (uc)\, dz dt \tag{2.42}$$

The time integration of the diffusion equation for suspended sediment is repeated until a periodic solution is obtained.

### 2.3.1 Bed Load Transport in case of Sand sized bed material

The dimensional bed load transport $\Phi_b$ is found by a deterministic approach:

$$\Phi_b = 5p\left(\sqrt{\theta'} - 0.7\sqrt{\theta_c}\right) \tag{2.43}$$

Where *p* is found from Eq. (2.62).

From $\Phi_b$ the following time-averaged quantities are calculated:

$$\Phi_{b1} = \frac{1}{T}\int_0^T \Phi_b(t)\cos\left(\phi(t)\right) dt \tag{2.44}$$

$$\Phi_{b2} = \frac{1}{T}\int_0^T \Phi_b(t)\sin\left(\phi(t)\right) dt \tag{2.45}$$

$$q_{b1} = \Phi_{b1} \cdot \sqrt{(s-1) g d_{50}^3} \tag{2.46}$$

$$q_{b2} = \Phi_{b2} \cdot \sqrt{(s-1) g d_{50}^3} \tag{2.47}$$

Where

| | |
|---|---|
| $\phi(t)$ | is the direction of the instantaneous flow |
| $\Phi_{b1}$ | is the dimension less bed load in the mean current direction |
| $\Phi_{b2}$ | is the dimension less bed load normal to the mean current direction |
| $q_{b1}$ | is the bed load in the mean current direction |
| $q_{b2}$ | is the bed load normal to the mean current direction |

The presence of ripples does not influence the bed transport. This is the reason why $\Phi_b$, *p* and $\lambda$ are evaluated based on $\theta'$.

#### Effect of sloping bed

The bed load transport is influenced by the effect of both a longitudinal slope, $\beta_L$ and a transverse slope, $\beta_T$ on the bed-load transport and on the critical value of the Shields parameter $\theta_c$. The effect on the suspended load is attained indirectly through the inclusion

of $\theta_c$, which accounts for the effect of a sloping bed, in the expression for the bed concentration of suspended sediment, $c_b$.

All the equations presented in the following are valid for small bed slopes, either transverse or longitudinal.

For the general case where the flow is at an angle $\psi$ to the slope $\beta$, the critical Shields parameter is given by:

$$\theta_c = \theta_{c,0} \cdot \left( \frac{-\cos\psi \sin\beta + \sqrt{\mu_s^2 \cos^2\beta - \sin^2\psi \sin^2\beta}}{\mu_s} \right) \tag{2.48}$$

Where $\mu_s$ is a static friction coefficient ($\mu_s = \tan\phi_s$, $\phi_s$ = angle of repose) and $\theta_{c,0}$ is the critical Shields parameter for a plane bed.

The influence of a transversal slope on the bed-load transport is exhibited through a deflection of the transport direction, i.e. that a down-slope component of the transport will appear. This component can be expressed as:

$$q_{by} = \frac{\tan\beta_T}{1.6\sqrt{\theta'}} q_{bx} \tag{2.49}$$

Where $\theta'$ is the dimension less bed shear stress related to skin friction, and $q_{bx}$ is the rate of bed-load transport in the x direction, which is along the strike of the slope.

The influence of a longitudinal slope on the bed-load transport is simply accounted for by modifying the threshold value $\theta_c$ according to Eq. (2.48) and then using this modified value in the bed transport formulation. See Fredsøe and Deigaard (1992) for more details.

### 2.3.2 Bed Load Transport in case of Shingle sized bed material

#### Introduction

The mechanics of transport of coarse material such as shingle are very similar to those of sand. However, a number of important differences occur. The transport of coarse material often occurs as bed load whereas the transport of fine material is often dominated by suspended transport. The importance of suspended load can be expressed in terms of the Rouse number, which is defined in Eq. (2.50).

$$R = \frac{w_s}{\kappa U_f} \tag{2.50}$$

Where $w_s$ is the fall velocity of the suspended sediment, $\kappa$ is the Karman constant and $U_f$ is the shear velocity. Usually the criterion for a particle to be transported in suspension is that $R$ must be smaller than 2.0 to 2.5. For coarse material this can often not be fulfilled. Another difference between transport of coarse and fine material is that for coarse material inertia forces may be of importance, whereas they usually can be neglected for fine sediment.

Finally, shingle beaches often have very steep slopes. Therefore, bed slope effects on the initiation of particle motion and on the transport itself must be included.

## The bed load transport model

We consider a combined wave-current motion on a plane sloping bed. An orthogonal coordinate system (x,y) is introduced. The bed slopes in x and y directions are denoted as $\beta_x$ and $\beta_y$ respectively, defined here as positive upslope.

The angle between the wave propagation and the x-axis is denoted as $\gamma_{x,w}$, the angle between the current direction and the x-axis as $\gamma_{x,c}$, see Figure 2.11.

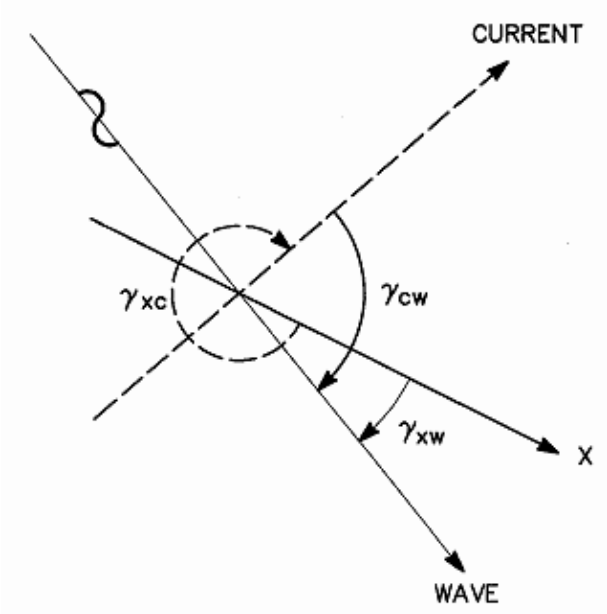


Figure 2.11 Definition sketch

The instantaneous flow angle of the combined wave current motion is denoted as $\varphi_x$. The force balance for a single moving spherical sediment particle can be expressed as:

$$V(s+C_m)\frac{dU_{b,x}}{dt} = 0.5 \cdot C_D A U_{r,x}\left|\overline{U_r}\right| + V_m \frac{dU_{o,x}}{dt} - g(s-1)V(\mu_d \cos(\alpha)\cos(\beta_x) + \sin(\beta_x)) \quad (2.51)$$

in the x-direction and as:

$$V(s+C_m)\frac{dU_{b,y}}{dt} = 0.5 \cdot C_D A U_{r,y}\left|\overline{U_r}\right| + V_m \frac{dU_{o,y}}{dt} - g(s-1)V(\mu_d \sin(\alpha)\cos(\beta_y) + \sin(\beta_y)) \quad (2.52)$$

in the y-direction.

Here V is the volume of the sediment particle = ($\pi D^3/6$), A is the surface area of the sediment particle = ($\pi D^2/4$), and D is the sediment grain diameter. $s$ is the specific density of the sediment, $C_m$ the hydrodynamic mass coefficient, $C_d$ the drag coefficient, $\mu_d$ the dynamic friction coefficient, $\alpha$ a dimensionless coefficient, $U_b$ the particle velocity, $U_o$ the oscillating flow velocity close to the bed and $U_r$ is the relative flow velocity in x-direction: $U_o$-$U_b$.

The subscripts x and y indicate projections in x- and y direction respectively.

Using the Engelund-Fredsøe transport formula (1976) as a basis and including an inertia term and the effect of a bed slope, the bed load can be described as:

$$\rho s \frac{dq_b}{dt} = \tau_b - \tau_c - n\left(F_d + F_i + F_g\right) \tag{2.53}$$

Where $q_b$ is bed load transport, $\tau_b$ the bed shear stress, $\tau_c$ the critical bed shear stress, $n$ the number of moving sediment particles, $F_d$ the drag force, $F_i$ the inertia force and $F_g$ the gravity force.

The drag force $F_d$ yields:

$$F_d \begin{bmatrix} x \\ y \end{bmatrix} = \rho g (s-1) V \mu_d \begin{bmatrix} \cos\beta_x \\ \cos\beta_y \end{bmatrix} \begin{bmatrix} \cos\alpha \\ \sin\alpha \end{bmatrix} \tag{2.54}$$

The inertia force $F_i$ yields:

$$F_i \begin{bmatrix} x \\ y \end{bmatrix} = \rho (s + C_m) V \frac{dU_b}{dt} \begin{bmatrix} \cos\alpha \\ \sin\alpha \end{bmatrix} \tag{2.55}$$

The gravity force $F_g$ yields:

$$F_g \begin{bmatrix} x \\ y \end{bmatrix} = \rho g (s-1) V \begin{bmatrix} \sin\beta_x \\ \sin\beta_y \end{bmatrix} \tag{2.56}$$

The critical shear stress is calculated from the expression for the critical Shields parameter $\theta_c$, which yields:

$$\theta_c = \frac{\tau_c}{\rho g (s-1) D} = \frac{4\mu_s}{3\alpha^2 C_d}\left(1 - \frac{1}{g(s-1)\mu_s}\frac{dU_{o,w}}{dt} sign\left(U_{o,w}\right)\right) \tag{2.57}$$

Where the term in front of the parenthesis is a measure of $\theta_{c,0}$. Here $U_{o,w}$ is the free stream velocity measured in the wave direction. Eq. (2.57) is valid for a horizontal bed. In case of a sloping bed, a corrected value for $\theta_c$ is calculated as:

$$\theta_c = \theta_{c,0}\left(\frac{-\cos\psi \sin\beta + \sqrt{\mu_s^2 \cos^2\beta - \sin^2\psi \sin^2\beta}}{\mu_s}\right) \tag{2.58}$$

Here $\psi$ is the angle between the flow and the up-slope direction.

The number of particles, $n$, can be eliminated form Eq. (2.53) using the general expression for the bed load transport rate:

$$\overline{q_b} = nV\overline{U_b} \tag{2.59}$$

The left-hand side of Eq. (2.53) can thus be written as:

$$\frac{d\overline{q_b}}{dt} = V\frac{d\left(n\overline{U_b}\right)}{dt} \tag{2.60}$$

By combining Eqs. (2.51) - (2.52) with Eq. (2.53) and Eq. (2.60) an expression for the time varying bed load transport is derived that is solved in the time domain. First the time varying bed shear stress due to the combined wave-current motion is solved using the model for the turbulent wave boundary layer of Fredsøe (1984) as described elsewhere in this manual. Secondly, the time variation of the particle velocity $U_b$ is solved in the x- and y direction using Eqs. (2.51) - (2.52). Finally, the time varying bed load transport is calculated using Eq. (2.53).

At each time step "new" particles are set into motion or become deposited at the bed. In the model the work done by the fluid to accelerate these bed particles is not included. Generally the influence of this is very small anyway.

## Influence of inertia coefficients

The correct choice of inertia coefficients is very important for the results. Experiments carried out by Meyer-Peter & Müller in 1948 and published in Smart et. al. (1983) are used for the example below.

The measurements were carried out in a flume and as such this is a pure current case. The bed load transport rate was found found from the measurements. The same conditions where simulated by LITPACK by using the default friction coefficients for $\mu_d$ and $\mu_s$.

The resulting sediment transport rates are compared in Figure 2.12.

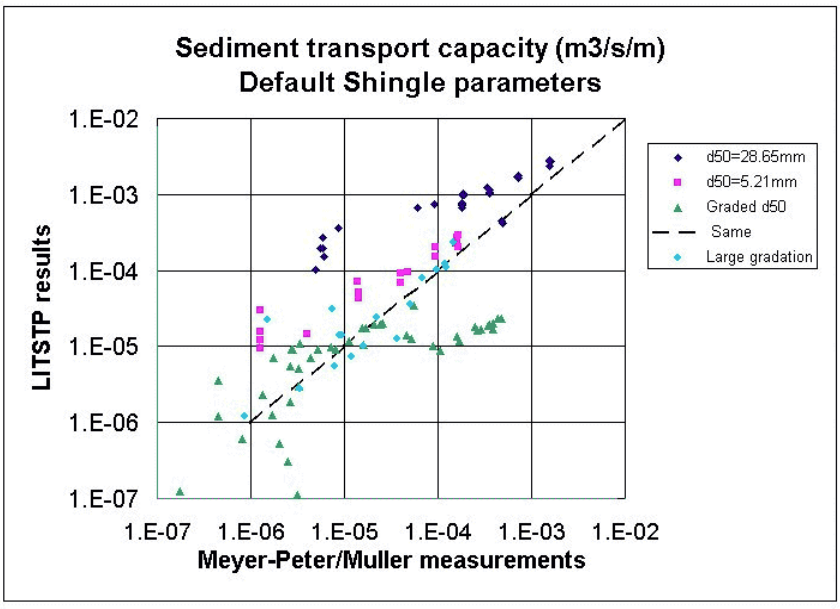


Figure 2.12 Comparison between LITPACK results and measurements of Meyer-Peter & MŸller (1948). Default friction coefficients: $\mu_d$ = 0.5, $\mu_s$ = 1.0.

The influence of the friction coefficients is shown in Figure 2.13 where the simulated sediment transport rates are found by increased values of $\mu_d$ and $\mu_s$.

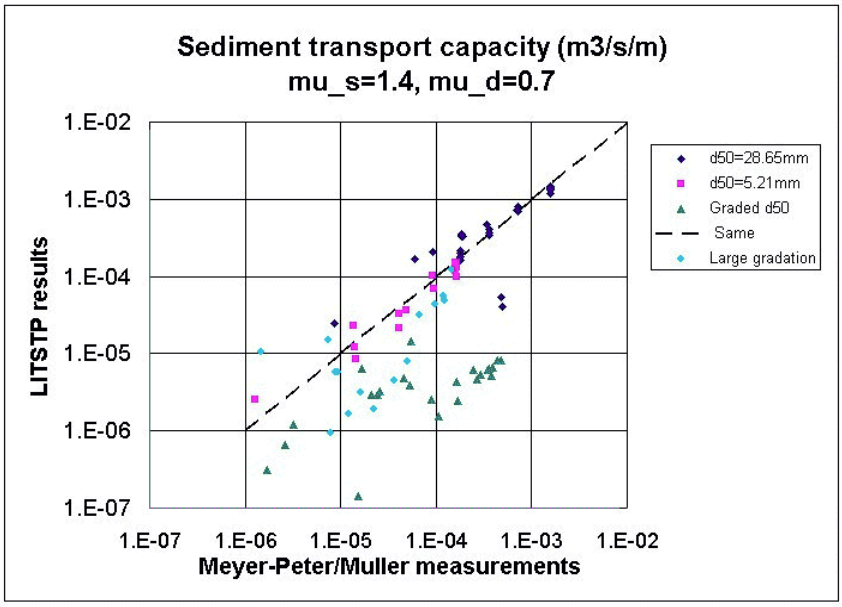


Figure 2.13 Comparison between LITPACK results and measurements of Meyer-Peter & Müller (1948). Alternative friction coefficients: $\mu_d$ = 0.7,$\mu_s$ = 1.4.

It can be concluded from Figure 2.12 and Figure 2.13 that the larger the mean grain diameter, the larger the friction parameters should be.

## 2.3.3 Suspended Load Transport

### Reference bed concentration

Once the variation of the friction velocity $U_f$ over the wave period has been determined by the boundary layer module over a flat bed, the following properties may be derived for every time step, see Engelund and Fredsøe (1976).

Shield's parameter:

$$\theta' = \frac{U_f^2}{(s-1)gd_{50}} \tag{2.61}$$

The deterministic description of the bed concentration is given by Eqs. (2.62) - (2.64):

$$p = \left[1 + \left(\frac{\frac{\pi}{6}\beta}{\theta' - \theta_c}\right)^4\right]^{-0.25} \tag{2.62}$$

$$\lambda = \sqrt{\frac{\theta' - \theta_c - \frac{\pi}{6}\beta p}{0.027 s \theta'}} \tag{2.63}$$

$$c_b = \frac{0.65}{\left(1 + 1/\lambda\right)^3} \tag{2.64}$$

Where

| | |
|---|---|
| $\rho$ | is the relative density of the sediment |
| $g$ | is the acceleration of gravity |
| $d_{50}$ | is the median grain diameter |
| $\theta'$ | is Shield's parameter determined for a plane bed |
| $\theta_c$ | is its critical value |
| $p$ | is the probability that all the particles of a layer are moving |
| $\lambda$ | is the linear concentration |
| $c_b$ | is the bed concentration |

Eq. (2.65) gives an alternative empirical description of the bed concentration by Zyserman & Fredsøe (1994):

$$c_b = \frac{0.331\left(\theta' - 0.045\right)^{1.75}}{1 + \frac{0.331}{0.46}\left(\theta' - 0.045\right)^{1.75}} \tag{2.65}$$

The empirical description of the bed concentration was developed based on a critical Shields parameter $\theta_{c0}$ for plane bed to be equal to 0.045. This value is set automatically by the model and overrules any other input of $\theta_{c0}$, if an empirical description is chosen for $C_b$.

In Figure 2.14 the bed concentration $C_b$ versus Shield's parameter $\theta'$ for both the deterministic approach and the empirical approach is shown.

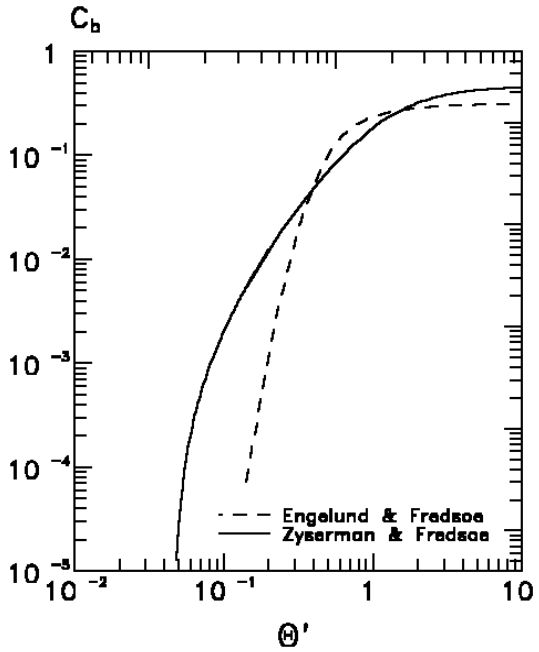


Figure 2.14 Bed concentration $c_b$ versus θ'

### Bed concentration in case of ripples

The contribution from the ripples to $c_b$ is included according to:

$$c_b(t) = \left(2 \cdot d_{50} \cdot c_b(t) + c_o \cdot h_r\right) / \left(h_r + 2 \cdot d_{50}\right) \tag{2.66}$$

In Eq. (2.66) $h_r$ the ripple height is calculated as described in Section 2.2.6. The contribution from the ripples to the bed concentration $c_0$ is given by

$$c_0 = 0.028\left(\theta'_{pn} - \theta_c\right) \cdot \frac{2}{\pi} \cos^{-1} \sqrt{\frac{\theta_c}{\theta'_{pn}}} \tag{2.67}$$

with $\theta'_{pn}$ determined by Eq. (2.32).

## Concentrations of suspended sediment

The present section describes the calculation of the concentration varying in time and over the depth. The program iterates over several wave cycles until a periodic solution is found, i.e. until the time variation of the concentration is repeated from one wave cycle to another at any position above the bed.

At the bottom the time-averaged bed concentration $c_b$ is used as a boundary condition for the initial profile:

$$c(0) = \overline{c_b} \tag{2.68}$$

The time varying concentration is calculated from the diffusion equation:

$$\frac{\partial c}{\partial t} = \frac{\partial}{\partial y}\left(\varepsilon_s \frac{\partial c}{\partial y}\right) + w \frac{\partial c}{\partial y} \tag{2.69}$$

The turbulent diffusion coefficient for the sediment $\varepsilon_s$ is taken equal to the eddy viscosity $\varepsilon$.

The boundary condition at the bottom is given by the instantaneous bed concentration:

$$c(i+1) = c_b(i+1) \qquad at \quad y = 0 \tag{2.70}$$

At the top the second boundary condition demands zero sediment flux through the water surface:

$$\varepsilon \frac{\partial c}{\partial y} + wc = 0 \qquad at \quad y = D \tag{2.71}$$

The determination of the concentration over the wave period is continued until a periodic solution is reached. In order to speed up the convergence towards periodic conditions, the initial concentration profile is determined by over-relaxation, using the previous initial profile *c'(0,j)* and the profile determined at the end of the previous calculation period *c'(n,j)*, according to:

$$c(0,j) = \frac{3}{2} c'(n,j) - \frac{1}{2} c'(0,j) \tag{2.72}$$

The primes indicate concentration values determined from the previous wave cycle.

The process of accelerating the convergence is stopped when the number of periods calculated reaches 0.75 times the *maximum number of wave cycles* prescribed. The initial concentration profile is taken as:

$$c(0,j) = c'(n,j) \tag{2.73}$$

The iteration is stopped when the relative deviation in the suspended transport in the mean current direction $q_s$ at time $t = T/4$ is less than equal to the prescribed tolerance $\nu$. $q_s$ is calculated as:

$$q_s = \int_{2d}^{D} c\left(\frac{T}{4}, y\right) \cdot U_1\left(\frac{T}{4}, y\right) dy \tag{2.74}$$

$U_1$ is the instantaneous total velocity in the direction of the mean current.

The relative deviation is determined with respect to the transport $q'_{s1}$ determined at $t = T/4$ in the previous wave cycle

$$\frac{q_{s1} - q_{s'1}}{q_{s'1}} \le \nu \tag{2.75}$$

## Mean concentration profile and centre of gravity

Having determined the variation of the concentration over time and depth as described in Eq. (2.70), the time-averaged concentration over the vertical is found as:

$$\bar{c}(y) = \frac{1}{T} \cdot \int_0^T c(y,t)\,dt \tag{2.76}$$

Figure 2.15 shows an example of the time-averaged concentration over the vertical for a non-breaking and breaking wave, respectively.

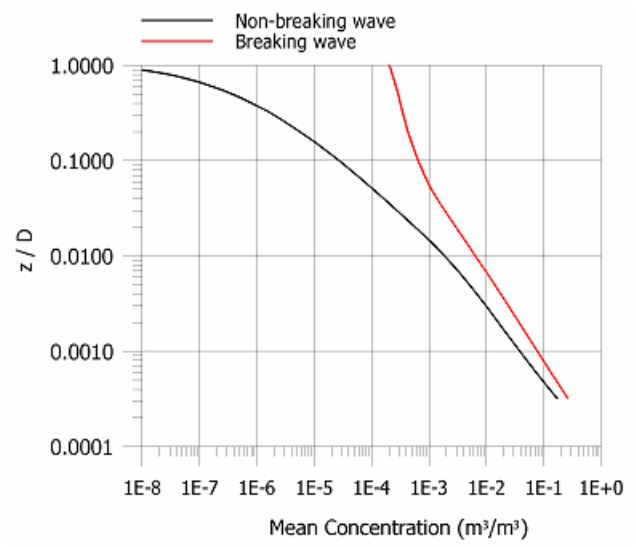


Figure 2.15 Example of time-averaged concentration profile for a non-breaking and breaking wave, respectively

The centre of concentration $y_c$ is calculated as the height of the centre of gravity of the mean concentration profile above the bottom

$$y_c = S / A \tag{2.77}$$

with

$$A = \int_{2d_{50}}^{D} \bar{c}(y)\,dy \tag{2.78}$$

$$S = \int_{2d_{50}}^{D} \bar{c}(y)\,y\,dy \tag{2.79}$$

Where $A$ is the total amount of suspended material per unit width, and $S$ is the first-order moment of the mean concentration profile with respect to the bed level.

### Time averaged transport

The instantaneous suspended load transport in the x and y direction is defined as:

$$\phi_x(t) = \int_{2d}^{D} U_x(z,t) \cdot c(z,t)\, dz \tag{2.80}$$

$$\phi_y(t) = \int_{2d}^{D} U_y(z,t) \cdot c(z,t)\, dz \tag{2.81}$$

Where $U_x$ and $U_y$ are the instantaneous resulting velocities in the x and y direction, respectively.

The resulting suspended transport over the wave period in both directions is calculated as:

$$\bar{q}_{sx} = \frac{1}{T}\int_0^T \left[\int_{2d}^{D} U_x(z,t) \cdot c(z,t)\, dz\right] dt \tag{2.82}$$

$$\bar{q}_{sy} = \frac{1}{T}\int_0^T \left[\int_{2d}^{D} U_y(z,t) \cdot c(z,t)\, dz\right] dt \tag{2.83}$$

The dimension less suspended transport is calculated as:

$$\Phi_{sx} = \bar{q}_{sx} / \sqrt{(s-1) g d_{50}^3} \tag{2.84}$$

$$\Phi_{sy} = \bar{q}_{sy} / \sqrt{(s-1) g d_{50}^3} \tag{2.85}$$

## 2.3.4 Graded Sediment Description

For a 'uniform' sediment description the geometrical characteristics of the bed material are represented through the median grain size $d_{50}$ when calculating the concentration of suspended sediment and the sediment transport numerically.

By using a 'graded' sediment description, it is possible to describe the effect that the presence of different grain size fractions have on the amount of bed load and suspended material and on the total rate of sediment transport, see Zyserman and Fredsøe (1996).

In the following it is described how the graded sediment description is included in the calculations.

### Grain curve

The sediment distribution is described by a log-normal grain curve, which is calculated on basis of the mean grain size, $d_{50}$ and the geometrical deviation or spreading $\sigma_g$ defined as $(d_{84}/d_{16})^{½}$.

Where $d_{84}$ and $d_{16}$ express the weight percentages 84% and 16%, respectively, by which the material is finer. Figure 2.16 shows the grading curves for $d_{50}$ = 0.2 mm and different values of $\sigma_g$.

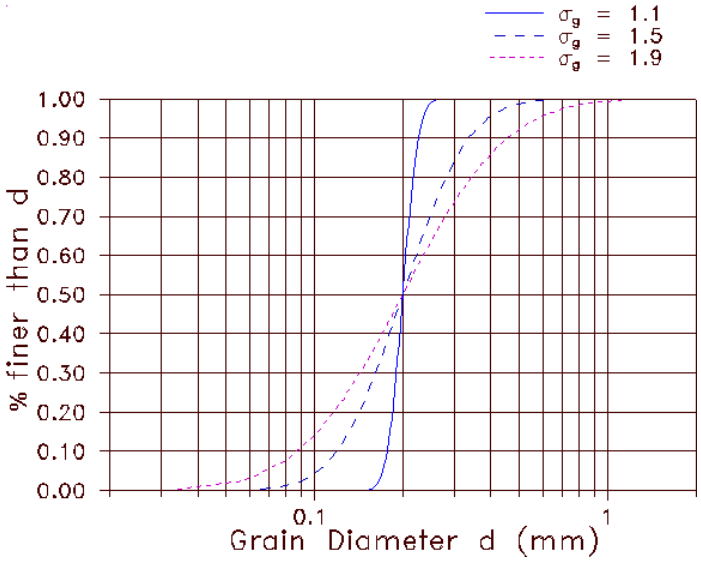


Figure 2.16 Grading curve on basis of $d_{50}$ and $\sigma_g$

The fall velocity *w* for any grain fraction with a diameter *d* is found by Eq. (2.86), Rubey's formula (1933):

$$w = \sqrt{g(s-1)d}\cdot\left(\left(\frac{2}{3}+\frac{36\nu^2}{g(s-1)d^3}\right)^{1/2}-\left(\frac{36\nu^2}{g(s-1)d^3}\right)^{1/2}\right) \tag{2.86}$$

Where *s* is the relative sediment density, *g* is gravity and $\nu$ is kinematic viscosity found by Eq. (2.87):

$$\nu = \left(1.78-0.0570812T+0.00106177T^2-8.27141\cdot10^{-6}T^3\right)\cdot10^{-6} \tag{2.87}$$

Where *T* is the water temperature in degrees Celsius.

## Bed concentration

The limiting grain size that can be brought into suspension by the flow is found using the criterion:

$$w_s \le 0.80U'_{f,\max} \tag{2.88}$$

Where $U'_{f,\max}$ is the maximum value attained by the instantaneous skin friction velocity over the wave period. The criterion simply states that only the particles having a fall velocity $w_s$ less than the threshold value given by Eq. (2.88) will be picked up from the bed. The critical diameter for suspension is indicated as $d_{crit}$, and the associated probability is called $f_{crit}$.

The value of $f_{crit}$ is then divided in *N* equal parts, where *N* is the selected number of suspended fractions, and a representative grain diameter $d_i$ *(i=1,...,N)* is related to every suspended fraction, see Figure 2.17.

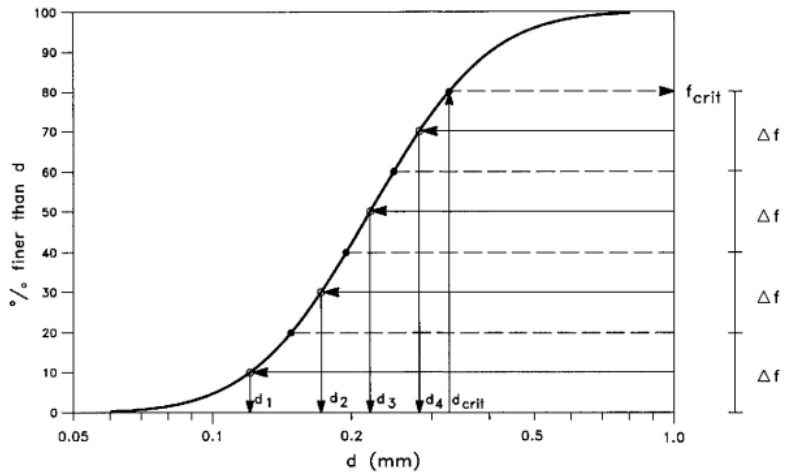


Figure 2.17 Definition of fractions of suspended sediment for N=4, $d_{50}$=0.22 mm, $\sigma_g$=1.60, $f_{crit}$=80% and $d_{crit}$=0.33 mm. $D_f=f_{crit}/N$

Next, the diffusion equation for suspended sediment is solved for each of the *N* fractions, with the settling velocity $w_i$ and the bed concentration $c_{b,i}$ calculated on the basis of $d_i$. Two conditions are applied to the concentration values and should be calculated as follows:

(i) The composition of the sediment in suspension is assumed to be equal to the composition of the original bed material (i.e. for that part finer than $d_{crit}$). If $f_i$ is a proportionality factor for fraction ***i***, this results in the following requirement for each of the *N* fractions in suspension:

$$\phi_1 M_1 = \phi_2 M_2 = \phi_3 M_3 = \ldots = \phi_N M_N \tag{2.89}$$

$M_i$ is the time-averaged total amount of sediment in suspension for fraction ***i***, defined as:

$$M_i = \int_{2d_{50}}^{D} \overline{c_i} dz \tag{2.90}$$

Where *D* is the local water depth, *c* is concentration, *z* is the vertical co-ordinate measured upwards from the bed and the over bar indicates time average. By making $\phi_N = 1$ in Eq. (2.89), the remaining $\phi_i$ can be readily calculated.

(ii) At $z=2d_{50}$, the bed concentration must be equal to the one determined on the basis of $d_{50}$ and taking into account the gradation of the sediment, i.e.:

$$Kc_b\left(\sum_{i=1}^{N} \overline{c_{b,i}}\phi_i\right) = \overline{c_{b,50}} \tag{2.91}$$

Where $K_{c_b}$ is a constant, and $c_{b50}$ is the value of $c_b$ based on $d_{50}$.

Condition (i) is a reasonable assumption under equilibrium situations, because the dispersive stresses associated with the coarser suspended fractions, which are kept in suspension closer to the bed than the finer ones, limit the capacity of the flow to pick up large amounts of fine sediment from the bed.

If the empirical description of $c_b$ is chosen, $c_{b50}$ is found directly by calculating $\theta'$ on the basis of $d_{50}$ and using Eq. (2.65).

If the deterministic description of $c_b$ is chosen, $c_{b50}$ is calculated taken into account the fact that the different grain fractions $d_i$ cover different % of the area of the bed, using Eqs. (2.61) - (2.75) where $d_{50}$ is replaced by $d_i$.

Once $Kc_b$ has been found, the bed concentration $c_b$ for each representative grain diameter $d_i$ is found by

$$c_b = Kc_b \cdot c_{b,i} \cdot \phi_i \tag{2.92}$$

## Concentration of suspended material

The concentration of suspended sediment for each of the representative grain diameters, $c_i$, is found by inserting the bed concentration $c_b$ from Eq. (2.92) into Eqs. (2.68) and (2.70).

The different contributions of the suspended concentration $c_i(z,t)$ are added directly without additional weighting by $\phi_i$.

$$c(z,t) = \sum_{i=1}^{N_{frac}} c_i(z,t) \tag{2.93}$$

# 3 Littoral Transport

## 3.1 Introduction

The present documentation for the calculation of littoral transport is made as a derivation of the basic equations followed by a description of the solution methods. Both sections comprise a description of the waves including refraction, shoaling, breaking, and directional spreading (by reduction factor), a description of the wave setup caused by wave radiation stress, and a description of the longshore current, i.e. wave radiation stress and residual current.

The longshore sediment transport is calculated by taking the hydrodynamic input parameters from the wave simulation and using the sediment transport model for combined waves and current, STPQ3D.

As for the scientific documentation of STPQ3D we refer to Section 1.

The calculation of littoral transport mainly consists of two calculation parts:

- longshore current calculation
- sediment transport calculation

The cross-shore distribution of longshore current, wave height and setup for an arbitrary coastal profile, is found by solving the long and cross-shore momentum balance equations. The longshore current model includes a description for regular and irregular waves, the influence of tidal current and non-uniform bottom friction, as well as wave refraction, shoaling and breaking.

The sediment transport rates are found directly by calls to STPQ3D.

The transport rates are integrated based on the local wave, current and sediment conditions

As a result littoral drift calculation is able to give a deterministic description of the cross-shore distribution of longshore sediment transport for an arbitrary, non-uniform, bathymetry and sediment profile. By applying a time varying wave climate, one can obtain a detailed description of the sediment budget.

## 3.2 Basic Equations – Longshore Current

### 3.2.1 Waves

In this section the incoming waves are described. The phenomena in consideration are: Depth-refraction, shoaling, breaking, and directional spreading. Finally, the effect of directional spreading of waves with respect to setup and longshore current will be discussed.

## Refraction

The angle between the wave fronts and the coastline, a is given by Snell's law:

$$\sin\alpha = \frac{\sin(\alpha^*)L}{L^*} \tag{3.1}$$

Where

| | |
|---|---|
| L | is the wave length |
| * | denotes reference point in the profile |

The wave length L is calculated explicit in each point. The expression to be used is defined by the factor $K_L$:

$$K_L = \frac{\omega^2 D}{g} \tag{3.2}$$

Where

| | |
|---|---|
| ω | is the wave frequency |
| *D* | is the water depth |
| *g* | is the acceleration of gravity |

If $K_L$ > 1.0 the expression by Fenton & McKee (1991) is applied:

$$L_o = \frac{g}{2\pi}\cdot T^2 \tag{3.3}$$

$$L = L_o \cdot \left( \tanh\left( \left( \frac{2\pi D}{L_o} \right)^{0.75} \right) \right)^{2/3} \tag{3.4}$$

Where:

| | |
|---|---|
| *T* | is the wave period, |
| $L_o$ | is the deep water wave length. |

If $K_L \le 1.0$ the expression by Wu & Thornton (1986) is applied:

$$L = \frac{2\pi D}{\sqrt{K_L}\cdot\left(1+\frac{K_L}{6}\cdot\left(1+\frac{K_L}{5}\right)\right)} \tag{3.5}$$

Where $K_L$ is found from Eq. (3.2).

## Shoaling

In case of unbroken waves the wave height is determined by the conservation of energy flux along wave orthogonals.

$$H^2 \cdot c\left(1-G\right)\cdot \cos\alpha \approx \text{ constant} \tag{3.6}$$

$$G = \frac{2kD}{\sinh\left(2kD\right)} \tag{3.7}$$

Where $c$ is the celerity of the wave ($c = L/T$).

## Breaking

As a criterion for breaking a maximum of the ratio between the wave height and the water depth is introduced:

$$\gamma = \frac{H}{D}, \gamma_2 = 0.8 \tag{3.8}$$

For broken waves γ is a function of the distance from the breaker line, $X_B$, see Andersen et al. (1983) and Deigaard et al. (1986):

$$\gamma = 0.5 + 0.3\exp\left(-0.11\frac{X_B}{D_B}\right) \tag{3.9}$$

## Orbital Motion

The near bed wave orbital motion is of importance for the flow resistance. The maximum near bed velocity is given by:

$$U_b = \frac{\pi H}{T\sinh\left(kD\right)} \tag{3.10}$$

The amplitude of the orbital motion is:

$$a = U_b \cdot \frac{T}{2\pi} \tag{3.11}$$

## The Radiation Stress Tensor

Consider a field of regular, uni-directional waves:

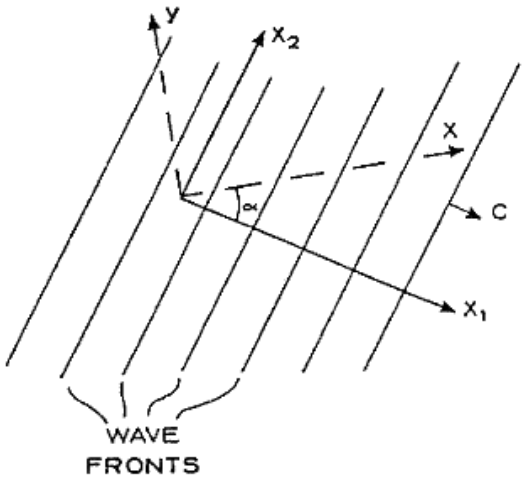


Figure 3.1 Definition Sketch

The radiation stress in the direction, $x_1$, of the wave propagation is designated $S_{11}$, and $S_{22}$ in the perpendicular direction, $x_2$. Due to symmetry no shear components are associated with these two main directions of the radiation stress field.

The radiation stress consists of an isotropic contribution, $F_p$ from the excess pressure in the waves and a momentum part, $F_m$ in the direction of wave propagation:

$$S_{11} = F_p + F_m \tag{3.12}$$

$$S_{22} = F_p \tag{3.13}$$

For $F_p$ and $F_m$ the following expressions are valid, see Svendsen and Jonsson (1980):

$$F_p = \frac{1}{16}\rho g H^2 G \tag{3.14}$$

$$F_m = \frac{1}{16}\rho g H^2 \left(1+G\right) \tag{3.15}$$

Where ρ is the density of sea water, and $G$ is defined by Equation (3.7).

Now $S_{11}$ and $S_{22}$ become:

$$S_{11} = \frac{1}{16}\rho g H^2 \left(1+2G\right) \tag{3.16}$$

$$S_{22} = \frac{1}{16}\rho g H^2 G \tag{3.17}$$

For shallow water waves $S_{22}$ is one third of $S_{11}$ , as $G$ equals one, and for deep water waves $S_{22}$ is zero, as $G$ is zero. For intermediate depths $S_{22}$ lies between these limits.

For any other direction, *x*, e.g. the coast normal in the present application, the normal and shear components of the radiation stress can be found from the application of Mohr circles. *a* is the angle between the $x_1$ and the *x* direction.

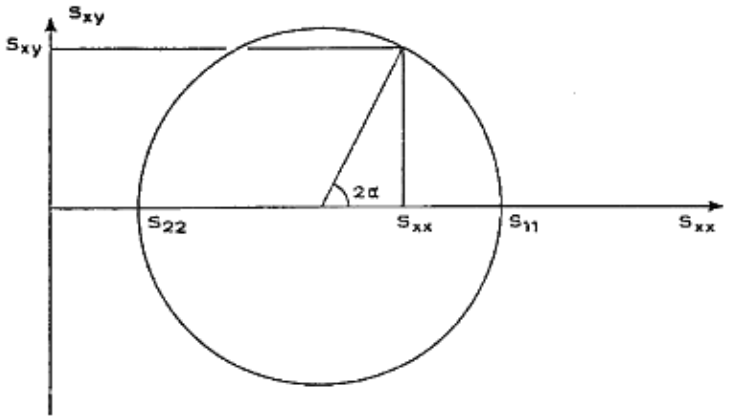


Figure 3.2 Directional Variation of Radiation Stresses

The normal radiation stress is given by:

$$S_{xx} = \frac{S_{11} + S_{22}}{2} + \frac{S_{11} - S_{22}}{2}\cos(2\alpha) \tag{3.18}$$

and the shear component is given by:

$$S_{xy} = \frac{S_{11} - S_{22}}{2}\, sin(2\alpha) \tag{3.19}$$

It is this shear radiation stress which drives the longshore current. Outside the breaker zone the energy dissipation is weak, and it can be shown that the shear radiation stress is constant when the energy flux is constant. Inside the breaker zone, the energy dissipation is strong, and the shear component of the radiation stress decreases towards the shoreline. The imbalance in the shear radiation stress must be compensated through the bed shear stresses associated with the longshore current.

## Irregular Waves

The model can be run with regular or irregular waves. For irregular waves two different approaches are included in the present model. A brief description is given below.

## The Rayleigh Wave Height Approach

The Rayleigh wave situation is described as a series of regular wave trains each characterized by its height $H_i$, and frequency of occurrence $\phi_i$. All wave trains have the same period and direction. The values of $H_i$ and $\phi_i$ are determined so that the wave heights follow the Rayleigh distribution, with a root-mean-square of the wave heights equal $H_{rms}$. Each of the wave trains is tracked across the coastal profile, which makes it possible to use the empirical non-linear wave height transformation inside the point of wave breaking for each wave train. The combined radiation stresses are found by adding the contributions from each wave train. The wave and wind setup is determined simultaneously with the tracking of the wave train, so that the variation of the mean water

surface elevation is taken into account when calculating the shoaling and breaking of the waves.

## The Model of Battjes and Janssen

The model is based on Battjes and Janssen (1978) in which the local mean rate of wave energy dissipation is modelled, based on that occurring in a bore and on the local probability of wave breaking. The results are used as a sink in the energy balance equation, which is subsequently integrated to obtain the wave height, $H_{rms}$, as a function of on-shore distance. The basis for the statistical description of the wave heights is the Rayleigh distribution.

The wave energy balance equation for a stationary situation reads

$$\frac{\partial}{\partial x}\left(C_{gs}E\right)+E_{diss}=0 \tag{3.20}$$

Where

| | |
|---|---|
| $E = 1/8\ \rho g\ H^2_{rms}$ | is the mean wave energy |
| $C_{gs} = 1/2\ c\ (1+G)\cos\alpha$ | is the group velocity in x-direction |
| $E_{diss}$ | is the time-mean dissipated power per unit area |

Based on a bore analogy, Battjes and Janssen (1978) applies following expression for the rate at which the energy is dissipated due to wave breaking

$$E_{diss}=\frac{1}{4}\alpha_{diss}\ \rho g\frac{1}{T}Q_b\ H^2_{\max} \tag{3.21}$$

Where

| | |
|---|---|
| $x$ | is an adjustable constant |
| $Q_b$ | is the fraction of breaking or broken waves |
| $H_{max}$ | is the local maximum allowable wave height |
| $\alpha_{diss}$ | is the dissipation factor |

$Q_b$ is the key variable in the formulation, and controls the rate of dissipation. The fraction $Q_b$ of the waves that are actually broken is given by the number of waves which, according to the Rayleigh distribution, would have been larger than the local maximum wave height. The Rayleigh distribution is truncated so that no wave heights exceed $H_{max}$.

$Q_b$ is given by the transcendental equation

$$\frac{1-Q_b}{\ln Q_b}=-\left(\frac{H_{rms}}{H_{\max}}\right)^2 \tag{3.22}$$

and the maximum wave height is calculated by

$$H_{\max}=\frac{\gamma_1}{k}\tanh\left(\frac{\gamma_2}{\gamma_1}kD\right) \tag{3.23}$$

Where $k$ is the wave number, $D$ the water depth and $\gamma_1$ and $\gamma_2$ are two wave breaking parameters. $\gamma_1$ controls the wave steepness condition and $\gamma_2$ controls the limiting water depth condition.

From Eq. ((3.22) and (3.23) the following limits appear

$$\text{Deep water}\left(\frac{H_{rms}}{H_{\max}}\to 0 \qquad kD>>1\right) \tag{3.24}$$

$$Q_b \to 0 \quad \text{and} \quad \frac{H_{\max}}{L}=\frac{\gamma_1}{2\pi}\approx 0.16$$

$$\text{Shallow water}\left(\frac{H_{rms}}{H_{\max}}\to 1 \qquad kD<<1\right) \tag{3.25}$$

$$Q_b \to 0 \quad \text{and} \quad \frac{H_{\max}}{D}=\gamma_2=0.8$$

The model from Battjes and Janssen (1978) has proven to be a good predictor for conditions with irregular waves and rather complex bathymetries. A detailed calibration of the model has been carried out in Battjes and Stive (1985).

## Discussion of the Directional Spreading of the Waves

Instead of one wave field, consider two regular wave fields, with the angle 2θ between the directions of migration.

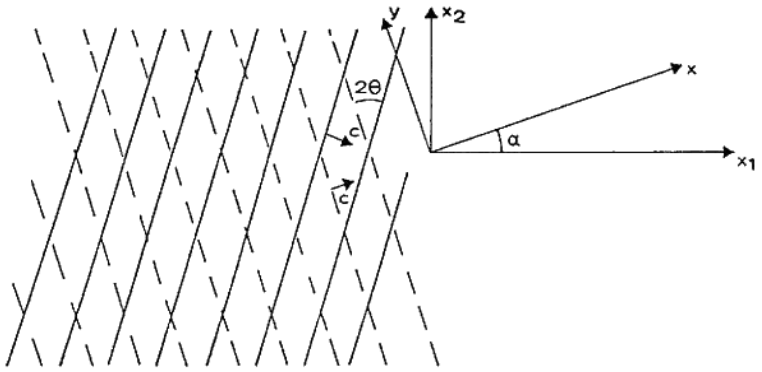


Figure 3.3 Combined Action of Two Wave Fields

Owing to symmetry the main directions $x_1$ and $x_2$ lie between the directions of the wave crests of the two wave fields.

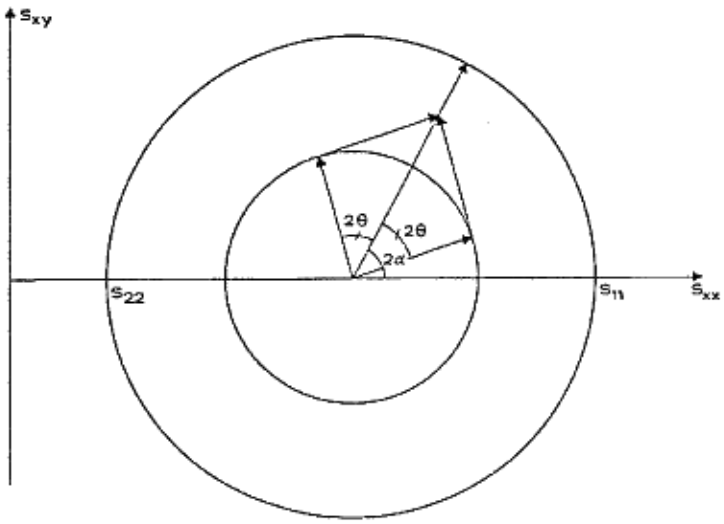


Figure 3.4 Directional Variation of Radiation Stress in Case of Two Wave Fields

The radiation stress tensor for the direction x can be found by application of the Mohr circle. It is assumed that the radiation stresses associated with each wave field is one half of the radiation stresses of the uni-directional wave field.

It can be seen that the radiation stress can be determined from a circle with the same centre as before, but with a radius reduced by the factor $R = \cos 2\theta$, which thus also is the reduction of the shear radiation stress. This reduction is rather strong even migration of the two wave fields considered.

As can be seen the shear radiation stress becomes zero when θ= 45 degrees, i.e. the two wave fields have orthogonal wave crests.

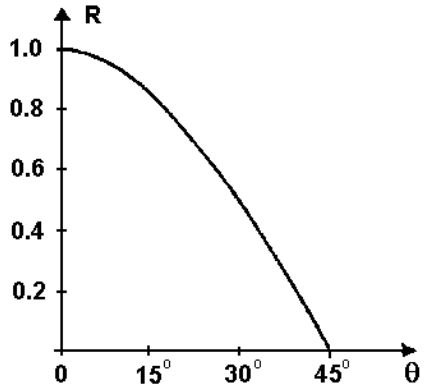


Figure 3.5 Spreading Factor vs. θ for Two Crossing Wave Fields

## The Directional Spreading Function

The situation with two wave fields is a gross simplification, as the spreading of the wave energy and radiation stress in nature is a continuous function of the direction.

A number of empirical directional spreading functions have been proposed. According to Sand (1979) one of the most commonly used functions is:

$$H(\theta) = \frac{1}{2\pi F(s)} \cos^{2s}\left(\frac{\alpha - \theta}{2}\right) \tag{3.26}$$

Where θ is the direction relative to the main wave direction α. The function $H(\theta)$ must be normalised so that the total energy is still described by the non-directional wave spectrum. The normalisation factor is given by:

$$F(s) = \frac{\Gamma(2s+1)}{2^{2s}\left(\Gamma(s+1)\right)^2} \tag{3.27}$$

Where Γ($s$) is the gamma function. The variation of $F(s)$ is shown in Figure 3.6.

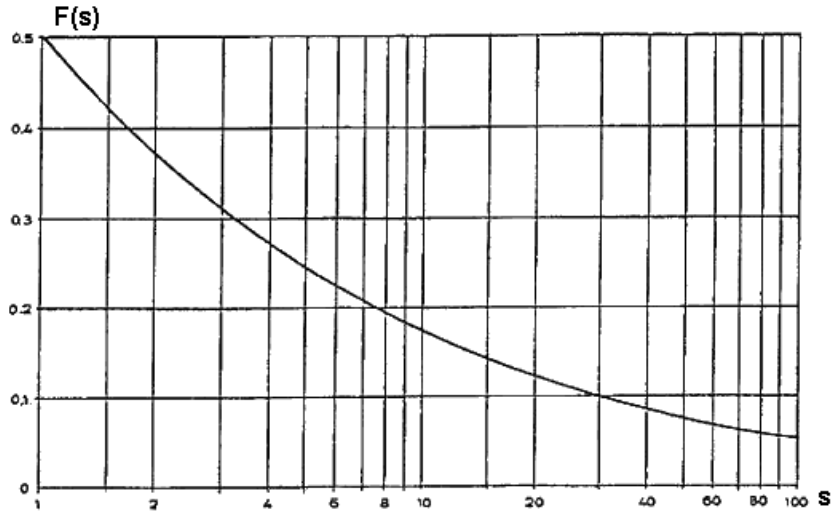


Figure 3.6 F(s) vs. s

In a natural sea state $s$ (and α) is not constant, but can vary with the frequency in the spectrum. The shape of $H(\theta)$ depends strongly on the value of $s$, and becomes more peaked for increasing s. The shape of $H(\theta)$ is indicated in Figure 3.7. According to Sand (1979) $s$ will typically lie in the range 2-20. For natural storm waves $s$ is often estimated to be about 8. This variation can occur for the different frequencies within the same spectrum. The directional distribution of the long waves is narrow (large $s$) and the locally generated high frequency waves have a wide distribution (small $s$ values). The directional spreading around the peak frequency in the spectrum will typically correspond to a H(θ) function with $s$ equal to 5.

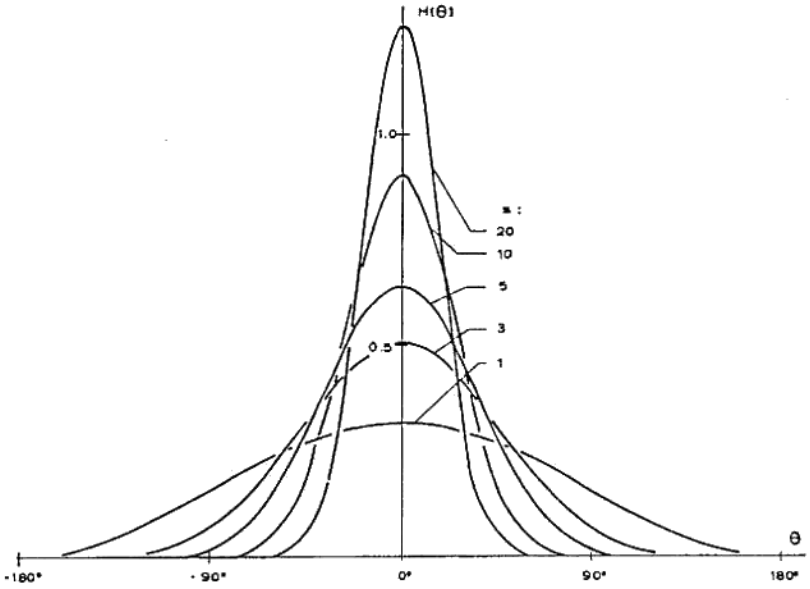


Figure 3.7 Directional Spreading Function vs. θ

For a narrow wave energy spectrum, characterised by s and α, the radiation stress tensor can be calculated. In the following $S_{11}$ and $S_{22}$ are the principle radiation stresses corresponding to a uni-directional wave field with the same energy and frequency as the part of the spectrum considered. The shear component is given by:

$$dS_{xy} = \frac{S_{11} - S_{22}}{2} H(\theta) \sin\left(2(\alpha + \theta)\right) d\theta \tag{3.28}$$

giving a mean value:

$$\overline{S_{xy}} = R(S) \frac{S_{11} - S_{22}}{2} \sin(2\alpha) \tag{3.29}$$

The normal component is given by:

$$dS_{xx} = \frac{S_{11} + S_{22}}{2} + \frac{S_{11} - S_{22}}{2} \cos\left(2(\alpha + \theta)\right) H(\theta) d\theta \tag{3.30}$$

giving a mean value of

$$\overline{S_{xx}} = \frac{S_{11} + S_{22}}{2} + R(S) \frac{S_{11} - S_{22}}{2} \cos(2\alpha) \tag{3.31}$$

It is seen that the mean radiation stress tensor for directionally distributed waves can be found by applying a Mohr circle with a radius reduced by *R* compared to the Mohr circle for the uni-directional wave field with the same energy. *R* is for the directional distribution function *H*(θ) given by:

$$R(s) = 1 - 8 \frac{F(s+1) - F(s+2)}{F(s)} \tag{3.32}$$

The reduction or spreading factor *R* vs. *s* is depicted in Figure 3.8.

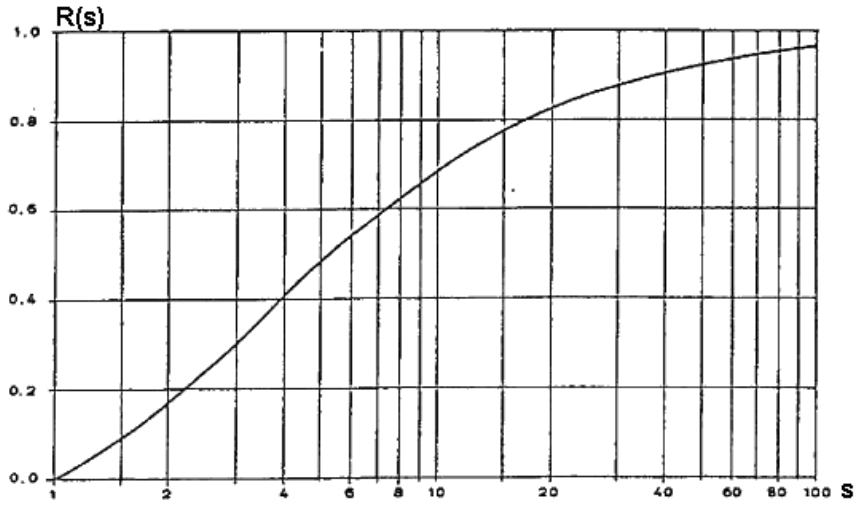


Figure 3.8 Reduction Factor R vs. s

As can be seen the shear component of the radiation stress is reduced by about 50% for the value *s* = 5, which is relevant for the peak frequency of the spectrum.

The reduction of the normal radiation stress, which is important for the wave setup, is smaller. For α = 0 degrees the reduction lies between 12% (shallow water waves) and 25% (deep water waves). For α = 45 degrees the normal radiation stress is unchanged and for larger α values it is increased.

## Inclusion of directional waves in model for wave setup and littoral current

In view of the findings described above it is indeed relevant to include the effect of the directional spreading of the waves in the simulation of wave setup and littoral current. A reduction of e.g. 50% in the driving shear radiation stress will give a reduction in the littoral current velocity of about 30%.

There are three different approaches to include the spreading in the model:

- Spectral modelling. By transformations based on shoaling, refraction and wave breaking the directional spectra are calculated in each point of the coastal profile. This approach is chosen in Battjes (1974).
- Ensemble averaging. Based on directionality of the waves at the boundary of the model an ensemble of regular wave situations with the same averaged characteristics is constructed, each individual wave situation is transformed, and the relevant parameters are calculated by averaging over the ensemble in the actual point.
- By general reduction factor. Based on the reduction factor *R*, given at the boundary of the model, the shear and normal radiation stress tensor calculated for uni-directional waves is reduced similarly.

The first method cannot be combined with the present approach for treatment of irregular wave heights in a reasonable way.

The second approach is directly applicable and expected to give fully satisfactory results. The computer costs will, however, be increased because another dimension is added to the wave description.

The third method is the most simple and gives reasonable results. The only problem arises close to the point of breaking, where the waves with different directions will be breaking at different positions. As the total driving force is the same, the effect on the littoral current is estimated to be marginal. Thus, this approach is used in the present model.

### 3.2.2 Wave Set-up and Set-down

The wave setup and set-down is caused by shoaling, refraction and breaking of the incoming waves, as the change in radiation stress, $\partial S_{ss}/\partial x$ must be counteracted by a slope in the water surface. The wave induced water level variations are calculated by integration of the mean momentum balance equation, which reads:

$$-\frac{1}{\rho}\frac{\partial \bar{S}_{xx}}{\partial x} = g(D+b)\frac{\partial b}{\partial x} \tag{3.33}$$

Where:

| | |
|---|---|
| $S_{xx}$ | is the radiation stress normal to the coast |
| $D$ | is the water depth |
| $b$ | is the wave induced water level variation |
| $\partial$ | is the density of sea water |
| $g$ | is the acceleration of gravity |

### 3.2.3 Flow Resistance

In case of pure current motion the flow resistance is caused by the roughness of the bed. For combined wave-current motion the eddy viscosity is strongly increased in the wave boundary layer close to the bed, and the near bed current velocity is retarded. The effect on the outer current velocity profile can be described by introducing an apparent “wave roughness”, $k_w$, which is larger than the actual bed roughness.

Several theories are available for description of the above phenomenon. In the present formulation the theories in Fredsøe (1981) and Fredsøe (1984) are applied. The latter is the most detailed as the instantaneous bed shear stress is calculated during a wave period, while the former has the advantage to be easily programmable as analytical expressions for the average bed shear stress are given. Comparisons show that in case of dominant wave motion the two theories give almost the same results, while in case of strong current, the flow resistance is too low in the average formulation. This problem is overcome by substituting the flow resistance terms with the usual friction factor for pure current, hence the time averaged flow description is chosen. The details of, and physical background for, this model is described in the following.

#### The wave boundary layer and friction factor

It is possible to obtain a simple analytical solution because it is assumed that the wave boundary layer thickness and friction factor can be determined by considering the wave parameters only, i.e. it is assumed that the wave motion close to the bed is dominant compared to the current.

The wave boundary layer is the region close to the bed, where the wave induced velocities deviate significantly from the free stream velocities.

According to Jonsson and Carlsen (1976), the boundary layer thickness in the rough turbulent case can be determined from the ratio between the amplitude in the near bed orbital motion and the bed roughness, *a/k*. In the calculations the lower limit for *a/k* is 2.0.

Jonsson and Carlsen (1976) gives the following explicit approximation for calculating the wave boundary layer thickness, $\delta_w$

$$\frac{\delta_w}{k} = 0.072\left(\frac{a}{k}\right)^{3/4} \tag{3.34}$$

The boundary layer thickness given above is defined for the moment when the free stream velocity is maximum. In this context the variation of $\delta w$ with time is neglected.

The wave friction factor, $f_w$, is defined by:

$$U_{fw}^2 = \frac{\tau_w}{\rho} = \frac{1}{2} f_w U_b^2 \tag{3.35}$$

Where $U_{fw}$ is the wave friction velocity, $\tau_w$ is the maximum bed shear stress and $U_b$ is the maximum wave induced velocity outside the wave boundary layer. $f_w$ is a function of *a/k*. In Jonsson and Carlsen (1976) is given the following implicit expression:

$$\frac{1}{4\sqrt{f_w}} + \log_{10}\left(\frac{1}{4\sqrt{f_w}}\right) = -0.08 + \log_{10}\left(\frac{a}{k}\right) \tag{3.36}$$

For practical calculations it is more convenient to use the following explicit approximation given in Swart (1974):

$$f_w = \exp\left(5.213\left(\frac{a}{k}\right)^{-0.194} - 5.977\right) \tag{3.37}$$

The variation in the bed shear stress is found by assuming that the instantaneous bed shear stress can be found by use of the wave friction factor:

$$\frac{\tau}{\rho} = \frac{1}{2} f_w U^2 \tag{3.38}$$

Where

| | |
|---|---|
| *U* | is the instantaneous flow velocity at y = $\delta_w$ where *y* is the distance from the bed |

By this assumption the phase between the flow velocity and the bed shear stress is neglected. This is, however, of minor importance because only the shear stress averaged over a wave period is used for the description of the mean current velocity profile.

## The mean current velocity profile

The main idea is that the velocity profile is divided into an inner and an outer region. In the inner region close to the bed the turbulence is dominated by the wave boundary layer, while the turbulence in the outer region is generated by the mean current.

## The outer region

In pure current over a rough bed the velocity, $U$, can be described by the logarithmic velocity profile:

$$\frac{U}{U_{fc}} = 8.6 + 2.5\ln\left(\frac{y}{k}\right) \cong 2.5\ln\left(\frac{30y}{k}\right) \tag{3.39}$$

$U_{fc}$ is the friction velocity and $y$ is the distance from the bed, $k$ is the bed roughness.

If the current is superimposed by waves the velocity profile in the outer region can still be assumed logarithmic, because the only contribution to the eddy viscosity originates from the current, the wave motion being a potential flow.

However, the flow resistance from the bed is increased because of the presence of the wave boundary layer. The new shear stress must be found as the average over a wave period of the bed shear stress from the combination of waves and current. The increase in flow resistance is taken into account by introducing an apparent “wave roughness”, $k_w$.

The velocity profile outside the wave boundary layer is now given by:

$$\frac{U}{U_{fc}} = 2.5\ln\left(\frac{30y}{k_w}\right) \tag{3.40}$$

Eq. (3.40) is thus identical to Eq. (3.39) with $k$ replaced by $k_w$.

## The bed shear stress

The bed shear stress from the current, $\tau_c$, is found as the time average of the instantaneous bed shear stress, $\tau$. $\tau$ is found from Eq. (3.38), inserting a vector sum of the orbital velocity, $U_b \sin(\omega t)$, and the mean current velocity $U_\delta$, at the level $y = \delta_w$.

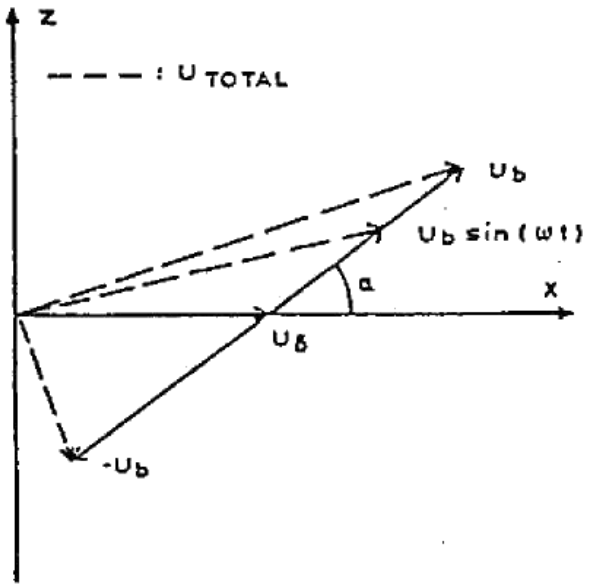


Figure 3.9 The instantaneous velocity at the top of the wave boundary layer

In a horizontal x-z coordinate system with the x-coordinate in the current direction the instantaneous flow velocity just outside the wave boundary layer can be written (see Figure 3.9):

$$\underline{U} = \begin{Bmatrix} U_z \\ U_x \end{Bmatrix} = \begin{Bmatrix} U_\delta + & U_b \sin(\omega t)\cos(\gamma) \\ & U_b \sin(\omega t)\sin(\gamma) \end{Bmatrix} \tag{3.41}$$

For this purpose the angle, γ, between the current and the direction of the wave propagation can be assumed to lie in the range from 0 to 90 degrees.

The shear velocity, $U_{fc}$, from Eq. (3.39) or (3.40) is related to $\tau_c$ by definition:

$$U_{fc} = \sqrt{\frac{\tau_c}{\rho}} = \left( \frac{2}{\pi} f_w U_b U_\delta \frac{1+\cos^2(\gamma)}{2} \right)^{1/2} \tag{3.42}$$

It may be noted that only for γ = 0 degrees and γ = 90 degrees the average shear stress vector will be in the same direction as the current. This side-effect is discussed in detail by Grant and Madsen (1979). The maximum angle between the two directions is approximately 20°. Although this deviation may be of importance in some cases it is not found to have any significance for the calculation of flow resistance for the littoral current.

## The velocity profile

The apparent wave roughness can be found from the velocity distribution given in Eq. (3.40), by expressing that the current velocity at the top of the wave boundary layer is $U_\delta$:

$$U_\delta = \sqrt{\frac{2}{\pi} f_w U_b U_\delta \frac{1+\cos^2(\gamma)}{2}} \cdot 2.5 \ln\left( 30 \frac{\delta_w}{k_w} \right) \tag{3.43}$$

For the final calculation of the velocity distribution a single parameter, characterising the current, must be known (the wave parameters are assumed to be given), i.e.

- the velocity, $U$, at $y = D$ is given
- the mean velocity, $V$, over the depth $D$ is given
- the mean shear velocity, $U_{fc}$, is given

## The inner region

The eddy viscosity distribution in a wave boundary layer without current has been described by Lundgren (1972). Close to the bed the eddy viscosity, ε, varies linearly with the distance from the bed:

$$\varepsilon = \kappa U_{fw}\, y \tag{3.44}$$

Where

κ is von Kármán's constant (~0.40)

$U_{fw} = \sqrt{\frac{\tau_w}{\rho}}$ where $\tau_w$ is the maximum bed shear stress

In pure current the eddy viscosity also varies as described by Eq. (3.44), only with the current shear velocity $U_{fc}$ inserted.

The evaluation of the resulting eddy viscosity in combined waves and current is not straightforward. Swart (1974), applied the plausible assumption that the eddy viscosity should be added vectorially. This approach yields correct eddy viscosity in the case of superposing of two currents. The resulting eddy viscosity in the inner region is thus taken to be:

$$\varepsilon_{cw} = \kappa\sqrt{U_{fc}^2 + U_{fw}^2 + 2U_{fc}U_{fw}\cos\gamma} \tag{3.45}$$

The bed shear stress due to the current is transferred in accordance with the expression:

$$\frac{\tau_c}{\rho} = U_{fc}^2 = \varepsilon_{cw}\frac{dU}{dy} \tag{3.46}$$

yielding:

$$\frac{U}{U_{fc}} = \frac{1}{\kappa}\frac{U_{fc}}{\sqrt{U_{fw}^2 + U_{fc}^2 + 2U_{fc}U_{fw}\cos\gamma}}\ln y + c \tag{3.47}$$

The constant, *c*, in Eq. (3.47) is found by requiring that the velocity distribution close to the bed corresponds to the real sand roughness of the bed, i.e. the velocity is zero at y = *k/30*.

### The transition between the two regions

Above it has implicitly been assumed that the two velocity profiles intersect each other very close to the top of the wave boundary layer, and that the velocity at y = $\delta_w$ consequently is very close to the value obtained from the velocity profile of the outer region. It appears that this assumption is well justified as several calculations have shown that the transition between the two regions indeed occurs close to y = $\delta_w$.

There is a discontinuity in the eddy viscosity between the inner and the outer region because the eddy viscosity in the outer region is determined by the current only, whereas the contribution from the wave motion in the wave boundary layer is significant. A discontinuity in the slope of the velocity profile therefore also appears. This is, however, only a mathematical result with no practical importance.

## 3.2.4 Littoral Current

As mentioned in Section 3.2.1 the incoming waves are causing a shear radiation stress, $S_{xy}$ acting in a direction parallel with the coast. The change in radiation stress, $-\partial S_{xy}/\partial x$ along a normal to the coast is responsible for the creation of a longshore current. The current is opposed by flow resistance from the bed and from the wave generated turbulence, and the velocity distribution across the coast profile is smoothed by eddies caused by waves and circulation currents.
The model for flow resistance is described in detail in Section 3.2.3 and the applied formulas are presented below.

A resistance factor *C* is introduced:

$$C = \frac{V}{U_{fc}} = \frac{V}{\sqrt{\tau_b/\rho}} \tag{3.48}$$

$$C = 2.5\left(\ln\left(\frac{D}{\delta_w}\right)-1\right)\frac{1+\sqrt{4V/Y+1}}{2} \tag{3.49}$$

$$Y = \frac{2}{\pi} f_w U_b \frac{1+\cos^2\gamma}{2}\left\{2.5\ln\left(\frac{D}{\delta_w}\right)-1\right\}^2 \tag{3.50}$$

Where:

| | |
|---|---|
| $C$ | is the resistance factor, |
| $V$ | is the mean velocity over the depth, |
| $U_{fc}$ | is the current friction factor, |
| $\tau_b$ | is the bed shear stress, |
| $\rho$ | is the density of sea water, |
| $D$ | is the water depth, |
| $\delta_w$ | is the wave boundary layer thickness, |
| $Y$ | is an intermediate parameter, |
| $f_w$ | is the wave friction factor, |
| $U_b$ | is the amplitude of the near bed wave velocity, |
| $\gamma$ | is the angle between the direction of wave propagation and the current direction. |

In the present case γ can be expressed by the angle α, which is defined in Section 3.2.1:

$$\gamma = 90° - \alpha \tag{3.51}$$

The wave boundary layer is found from:

$$\delta_w = k \cdot 0.072\left(\frac{a}{k}\right)^{3/4} \tag{3.52}$$

Where

| | |
|---|---|
| $a$ | is the near bed wave amplitude, |
| $k$ | is the bed roughness. |

For the wave friction factor the following relation is applied, see Swart (1974):

$$f_w = \exp\left\{5.213\left(\frac{a}{k}\right)^{-0.194} - 5.977\right\} \tag{3.53}$$

In case of strong current $C$ is substituted by $C_{max}$ if larger. $C_{max}$ is given by:

$$C_{max} = 2.5\left(\ln\left(\frac{30D}{k}\right)-1\right) \tag{3.54}$$

## Momentum transfer

The exchange of momentum is described by use of an “eddy viscosity type” of exchange coefficient. Several mechanisms are active in the momentum transfer, such as the turbulent fluctuations in the breaker zone and circulation currents. The exchange coefficient is less important than the bed shear stress, as its effects are more to change the distribution of the velocities across the profile than to change the magnitude of the larger velocities close to the breaker line. In the present formulation the expression for *E* derived in Jonsson et. al. (1974) is applied:

$$E = \frac{4a^2}{T}\cos^2\alpha \tag{3.55}$$

in which *a* is the near bed amplitude of the wave orbital motion and *T* is the wave period.

As shown in Jonsson et. al. (1974), large variations can be allowed in the momentum transfer coefficient *E* with only moderate changes in the longshore current as a result.

## Differential equation for V

The littoral current can be found from the equation expressing equilibrium between the following forces:

(i) Radiation stress,
(ii) Flow resistance,
(iii) Transfer of momentum.

The governing equation reads:

$$\frac{\partial \bar{S}_{xy}}{\partial x} = \tau_b - \frac{\partial}{\partial x}\left(\rho ED\frac{\partial V}{\partial x}\right) \tag{3.56}$$

Insertion of the resistance factor yields:

$$-\frac{1}{\rho}\frac{\partial \bar{S}_{xy}}{\partial x} = \frac{V^2}{C^2} - \frac{\partial}{\partial x}\left(ED\frac{\partial V}{\partial x}\right) \tag{3.57}$$

The boundary conditions are:

$$V = 0 \ \ for\ x = 0 \tag{3.58}$$

$$V \to 0 \ \ for\ x \to \infty \tag{3.59}$$

In case of additional driving forces, the equation reads:

$$-\frac{1}{\rho}\frac{\partial \bar{S}_{xy}}{\partial x} + \frac{1}{\rho}\tau_w \sin\theta + gDI = \frac{V^2}{C^2} - \frac{\partial}{\partial x}\left(ED\frac{\partial V}{\partial x}\right) \tag{3.60}$$

Where:

$\tau_w$ is the wind shear stress

$\theta$ is the angle between the wind direction and the coast normal

*I* is the longshore slope of the water surface

## 3.3 Basic Algorithms – Longshore Transport

### 3.3.1 Discretization of the Hydrodynamic Parameters

The coastal profile is described by an array, which contains from 0 to N-point consecutive points in increasing order. NEXTR is the number of the last point read, which must be located on-shore.

The water level and setup calculations yield a new coastline, which is located between points NLAST-1 and NLAST. The hydrodynamic parameters are set equal to zero inside the coast line. NLAST must be larger than 10.

The discretized coastal profile is shown in Figure 3.10.

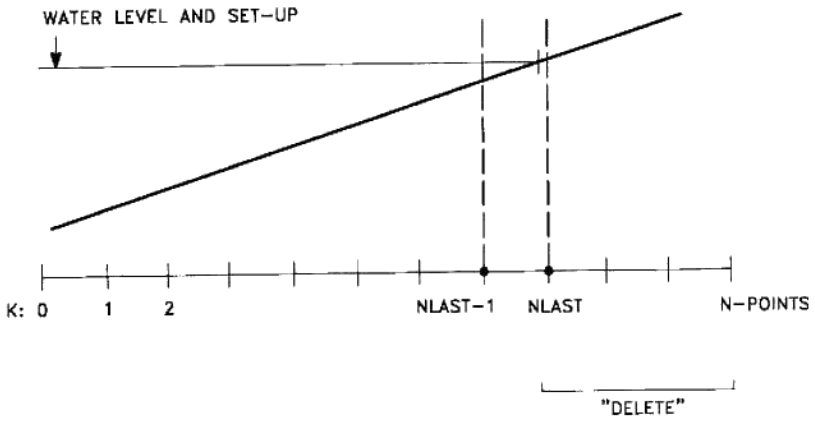


Figure 3.10 Discretized Coastal Profile

The points selected for sediment transport calculations are stored in an array along with a description of the position of zero transport, and from this the actual hydrodynamic conditions at the given points can be found.

### 3.3.2 Point Selection

Of all the points in the coastal profile a few (minimum 10) are selected for sediment transport calculations in order to reduce the computational efforts. The main purpose of the selection algorithm is to make the best estimate of the integrated total sediment transport over the coastal profile and to a lesser degree, describe the exact distribution of the transport over the profile.

It is known in advance that the actual combination of hydrodynamic and sediment models yields local maxima in the sediment transport capacity close to the local maxima of the longshore current and close to the position of wave-breaking. This is mainly due to two phenomena, which are described by the models:

(i) the transport increases with the current velocity,

(ii) the maxima in the longshore current profile are caused by wave breaking at low water depth, hence the transport is increased by high bottom shear stresses and strong turbulence under the broken waves.

In order to suppress small current velocities, $V$, the points are selected according to the velocity raised to a certain power, as the transport capacity increases non-linearly with $V$. From experience $V^3$ is found to be appropriate.

The transport capacity increases by a decrease of the grain diameter. From experience $d^{-3/2}$ is found to be appropriate.

The magnitude of the transport increases near the position of wave-breaking. Thus the relation between wave height and water depth, $H/D$, is included in the analysis.

On basis of the above, the point selection parameter $S$ is defined in Eq. (3.61).

$$S = \frac{V^3}{d^{2/3}} \cdot \frac{H}{D} \tag{3.61}$$

This definition introduces an extra option: parts of the profile may be defined as non-erodible by introducing fictitious large grain diameters.

The selection procedure is outlined below, and the individual steps, a) to f), are shown in Figure 3.11:

a. Find global maximum and minimum, $S_{max}$ and $S_{min}$.

b. Set zero points if $|S| < 0.01 (S_{max} - S_{min})$.

c. Find local maxima in S and check if it is distinct
$S_{max,L} - S_{min,L} |S| > 0.01 \cdot (S_{max} - S_{min})$.

d. Loop over profile to determine calculation points where $S$ differs more than $(S_{max} - S_{min})/5$ from $S$ at the previous calculation point.

e. Determine extra points if the distance between two calculation points is more than 0.1 · NLAST.

f. Remove excess 0-points if any.

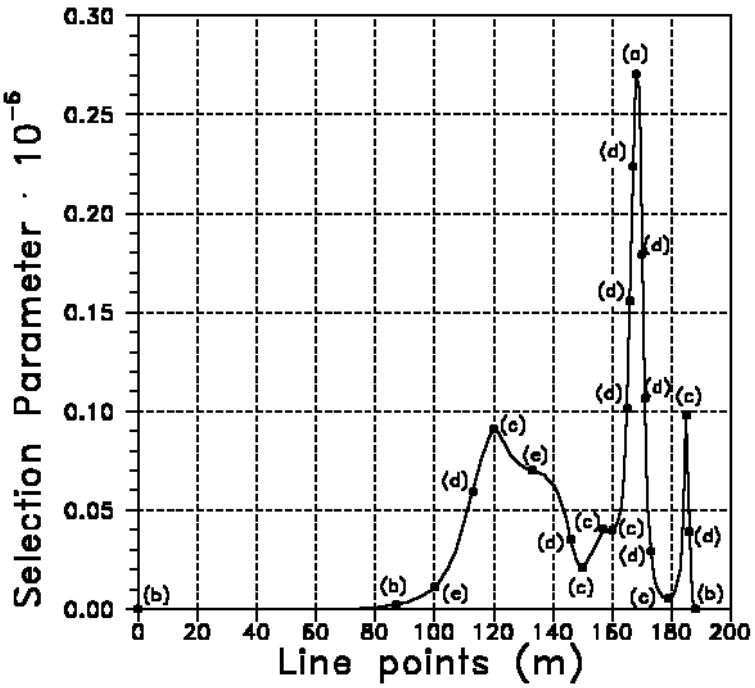


Figure 3.11 Point Selection. The letters refer to the single steps of the selection procedure and the figures refer to the point types

### 3.3.3 Sediment Transport Calculation

#### Input to STPQ3D

At the points selected, the sediment transport rate in the longshore direction is calculated by the model STPQ3D.

The sediment transport model is called at the selected points with the local values of the hydrodynamic and sedimentological parameters as input:

- Water depth
- Wave height, *H*
- Wave period, *T*
- Current velocity
- Angle between current and waves, $\delta_{cw}$
- Broken/non-broken waves
- Bed level gradient
- mean grain diameter
- fall velocity/sediment spreading

The definition of angles in the littoral drift calculation is shown in Figure 3.12.

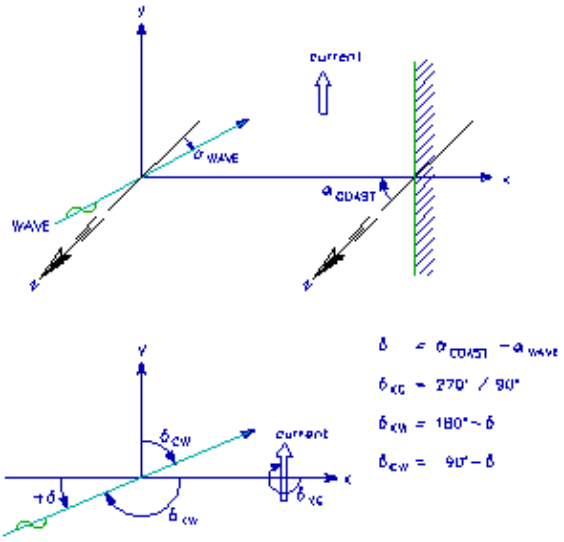


Figure 3.12 Definition of angles in the littoral drift calculations

## Irregular Waves

At the bed the wave period, $T$ and the root-mean-square of the local wave height, $H_{rms}$ are used to determine the bed concentration, the near-bed diffusion coefficient and the associated near-bed concentration profile.

In the surf zone only a fraction of the waves break due to the irregularity. As in the case of regular waves, the effect of breaking or broken (in the following denoted broken) waves is modelled by describing the production, vertical spreading and decay of turbulence generated by the passage of the front of a spilling breaker or a broken wave. The extra input parameters, wave height, $H_{diss}$, and period, $T_{diss}$, are introduced to reflect the conditions in the surf zone for irregular waves: the turbulent energy from the wave-breaking is calculated on the basis of $H = H_{diss}$ and $T = T_{diss}$.

The representative wave period is described as

$$T_{diss} = \frac{\sum T_i \phi_i}{\sum \phi_{bi}} \tag{3.62}$$

Where subscript '*diss*' indicates that only broken waves are considered.

The representative wave height is determined from the energy dissipation, using a bore to characterize the dissipation in the passing wave fronts. The dissipation is thus proportional to the cube of wave height, giving:

$$H_{diss}^3 = \frac{\sum {}^3_{bi} \phi_{bi}}{\sum \phi_{bi}} \tag{3.63}$$

This wave height and period are thus used at each location to characterize the production of turbulence by passing broken waves. The turbulence from the broken waves is time averaged.

### Breaking waves

To examine whether the waves are behaving as breaking or non-breaking waves, the three different spectral wave descriptions have separate checking routines. The following conditions must be fulfilled if the wave is breaking:

$$\text{Regular description: } \frac{dS_{xy}}{dx} > 0.00001 \tag{3.64}$$

$$\text{Rayleigh description: } H_{diss} > 0.0 \tag{3.65}$$

$$\text{Battjes \& Janssen description: } T_{diss} < \frac{T}{0.005} \tag{3.66}$$

## 3.3.4 Integration of Transport Rates

After sediment transport calculation in the selected points, the transport is interpolated and integrated across the profile. The transport is assumed to vary linearly between the selected sediment calculation points.

The sediment transport capacity is transferred from solid transport into volume by introducing the porosity:

$$Qs_{volume} = \frac{1}{(1 - porosity)} \cdot Qs_{solid} \tag{3.67}$$

## 3.3.5 Algorithms for Annual Littoral Drift

The annual drift is found by the contribution of transport from each of the wave incidents occurring during the year.

When calculating the annual drift, the wave climate in the calculations is described in a time series file where each set of items describe the characteristics of one wave incident and the bathymetric conditions at the time. In addition, the duration of the individual wave incident is considered.

Thus, the total annual drift $Q_{annual}$ is found as the sum of the contributions from all wave incidents.

$$Q_{annual} = \sum_{i=1}^{NSETS} Qs(i) \cdot Duration(i) \tag{3.68}$$

Where *NSETS* is the total number of wave incidents, and Duration (*i*) is the duration of the wave incident.

The definition of annual drift $Q_{annual}$ is provided that the total duration in the wave climate file is one year. Otherwise the total drift is found per design period (= total duration in simulation.

# 4 Littoral Drift Table Generation

## 4.1 Introduction

In order to reduce computation time during the simulation of coastline evolution, the transport rates are found by interpolation in pre-generated littoral drift transport tables rather than calculating the instant littoral drift for each location of the coastline.

The tables are composed by numerous littoral transport rates for an envelope of hydrodynamic conditions and generated by successive calls to the littoral transport engine. The calculation method for each of the representative events are similar to that described in Chapter 3 (Littoral Transport).

The entry for the interpolation process is the conditions present at the breaker line. Hence the limits and intervals of the littoral drift transport table axis are derived from the specified conditions as described in Section 4.3.1.

## 4.2 Table Layout

The total transport rates $Q_t$ ($I_g$, *wl*, *T*, $h_b$, $\alpha_b$, *i*) as well as the related cross-shore distribution $Q_d$ ($I_g$, *wl*, *T*, $h_b$, $\alpha_b$, *i*) are tabulated for an envelope of hydrodynamic conditions and cross-shore profiles:

| | |
|---|---|
| $I_g$: | Slope of water surface due to regional current |
| *wl*: | Water level |
| *T*: | Wave period |
| $h_b$: | Wave height at breaking |
| $\alpha_b$: | Wave angle at breaking |
| *i*: | Cross-shore profile |

The tables are specified by a global name, *Name*, that are common for all the files that combined represents a littoral drift transport table. The table consist of four different types of files as described in Table 4.1.

Table 4.1 List of files contained in a littoral drift transport table

| File name | Format | Description |
|---|---|---|
| *Name*.val | Ascii | This file contains information of the input parameters related to the transport rates in the tables |
| *Name*qtt.*i* | Binary | This file contains the total sediment transport rates $Q_t$ for cross-shore profile no. *i* |
| *Name*qtd. *i*0*j* | Binary | This file contains the values of the distributed sediment transport rates $Q_d$ across the profile for cross-shore profile no. *i* and surface slope no. *j* |
| *Name*nqd.*i*0*j* | binary | This file contains the positions of the distributed sediment transport rates across the profile for profile no. *i* and surface slope no. *j* |

NOTE: Some combinations of $I_g$, *wl*, *T*, $h_b$ and $\alpha_b$ cannot exist for the given bathymetric conditions. In these cases the sediment transport rate will be given a very small default value below $10^{-7}$ $m^3/s$.

### 4.2.1 Main outline

The outline of the littoral drift transport table is give in *name*.val as shown in Figure 4.1.

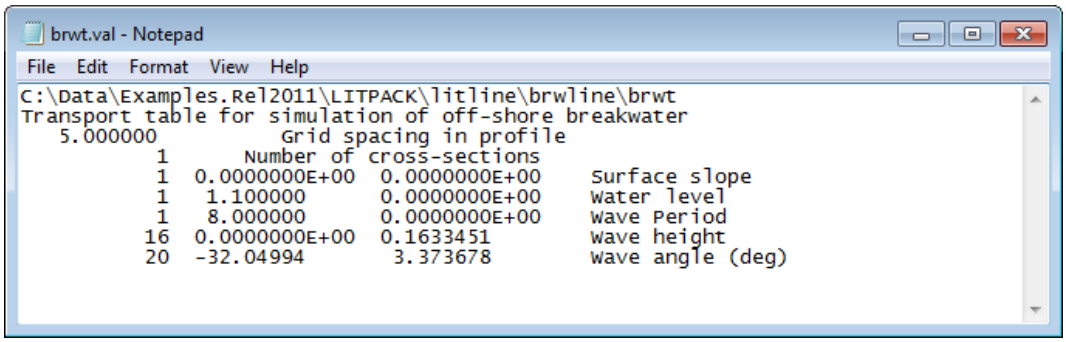


Figure 4.1 Outline of littoral drift transport table

The file contains 9 lines:

1. string containing path to global name of table during generation
2. descriptive string
3. Grid spacing of cross-shore profile(s)
4. Number of cross-sections (e.g. cross-shore profiles)
5. Description of representative surface slope (derived from regional current)
6. Description of representative water level
7. Description of representative wave period
8. Description of representative wave height at breaking point
9. Description of representative wave angle at breaking point

The description of representative events are made by the number of values, the minimum value and the interval in combination. E.g. the k'th value of the breaking wave height, $h_b(k)$, is derived by $h_b(k) = h_{b,min} + (k-1)*\Delta h_b$ .

### 4.2.2 Total transport rate

The binary QTT file contains the total transport rates for all the representative events. If the transport table utilize several cross-shore profiles, each profile relates to a separate QTT file.

For each representative event in the table one value is written to the QTT file.

### 4.2.3 Distributed drift

The binary QTD and NQD tables contains information about the distributed littoral drift across the profile. If the transport table utilize several cross-shore profiles or surface slopes, each profile, surface slope relates to a separate QTD/NQD file.

For each representative event in the table the distributed transport values with the corresponding grid point numbers for the given profile are written to the files:

- First the number of selected calculation points are written to the NQD file
- Next all the selected calculation grid point numbers are written to the NQD file
- Finally the distributed transport rates ($m^3/s/m$) for the selected calculation points point are written to the QTD file.

## 4.3 Basic Algorithm

### 4.3.1 Determining table limits

First you have to specify the cross-shore profile(s) you want to include in your table. Note, that it is not possible to extend the transport table later.

The type of input parameters for the table generation are similar to the ones applied for calculating the littoral drift. By using the knowledge about the hydrodynamic conditions in the area the minimum and maximum values of each of the following input parameters is defined: wave height, wave angle, wave period, water level and regional current.

The wave angles are related to the coastline normal, See Figure 4.2. As such the default minimum and maximum value of the wave angles is +/- 89 degrees.

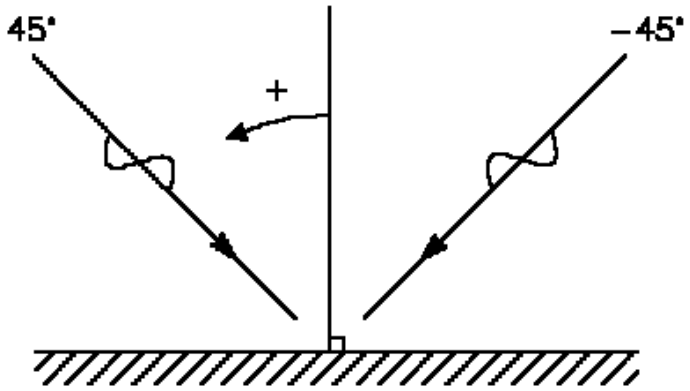


Figure 4.2 Definition of incoming wave angle in transport tables

NOTE that in general the specified maximum value should be greater than or equal to the maximum value expected to be used as input to the calculations of coastline evolution. The number of each of the input parameters is selected in order to have a representative envelope of conditions.

The wave conditions are then transformed internally to conditions at the breaking line, $h_b = 0.8*D$, through refraction/shoaling.

Based on the findings the minimum and maximum values for the breaking wave height and wave angle is used to outline the representative events in the littoral drift transport table.

The definition of input water level and wave period is considered the same at the breaking point as in the reference point. If regional current is applied the program will automatically calculate the corresponding surface slope that is assumed constant across the profile.

The outline of the transport table is defined in the resulting .val file (see Section 4.2.1).

### 4.3.2 Populating table

For each combination of the hydrodynamic conditions at the breaker line, as defined in the main outline of the littoral drift transport table, the wave conditions at the start of the given profile is found by backwards refraction and shoaling. These conditions are then applied in the calculation of the littoral sediment transport (as described in chapter 3), and the results saved in the various parts of the transport table.

Note that the calculations involved in the process of creating the tables may take several minutes or hours, dependent on the defined size of the tables and cross-shore profiles.

The order of the calculations and storage of data into the binary output files is as described in the following flow charts.

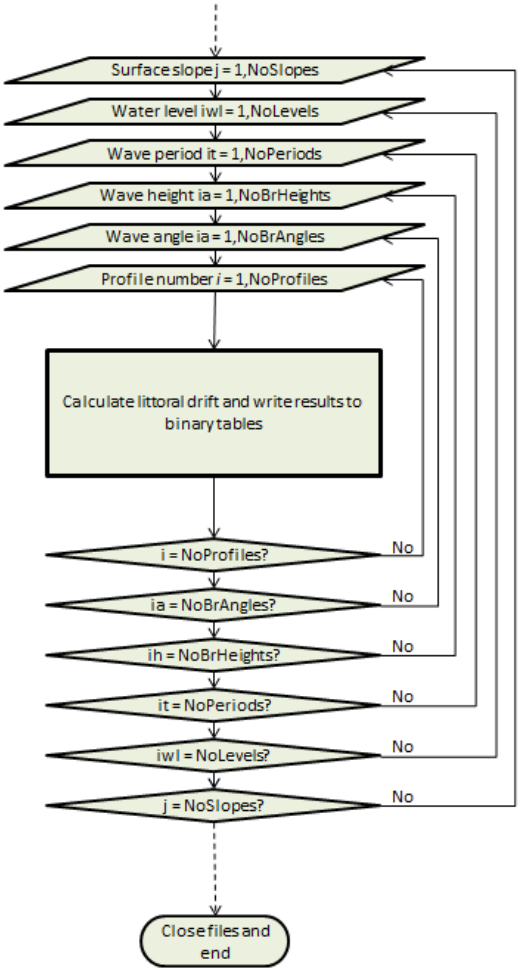


Figure 4.3 Outline of calculation order for populating littoral drift transport tables

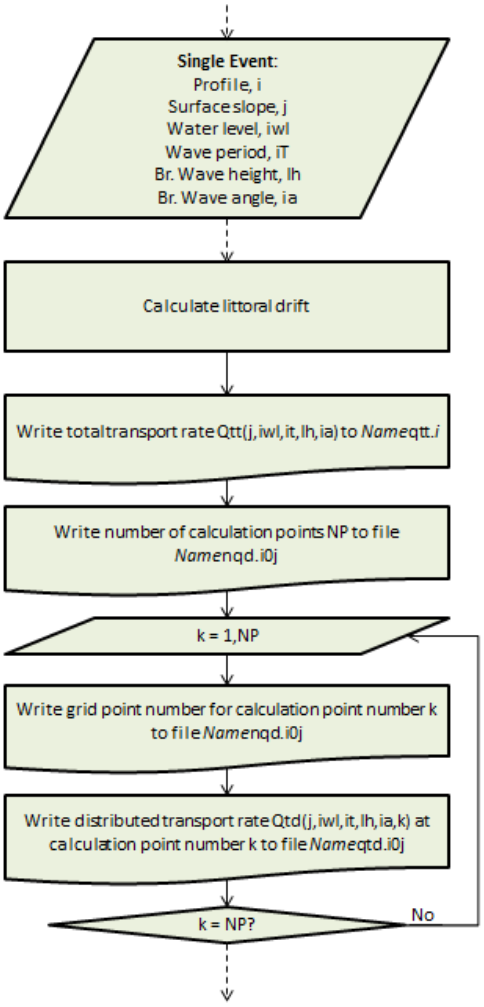


Figure 4.4 Outline of process for calculating littoral transport rate and store results for a single event in the littoral drift transport table

# 5 Coastline Evolution

## 5.1 Introduction

The aim of this section on the scientific background is to provide the user with a more detailed description of the theory and methods used for the calculation of coastline evolution than is supplied in other sections of the manual. This should provide the user with a better understanding of the various input parameters, the limitations of the model and finally, enable the interpretation of the results obtained by using the model.

After a brief description of the main equation and the flow diagram of the model, a more detailed explanation to e.g. the various structures and their influence on the transport will be given.

To eliminate any sources of confusion, a few terms, which are used in the documentation, will be briefly described.

The coastline evolution calculations are based on a co-ordinate system in which the x-axis is a baseline that runs parallel to the primary coastline orientation, while the y-axis runs from the baseline in offshore direction, see Figure 5.1. $y_c(x)$ is the distance from the baseline to the coastline.

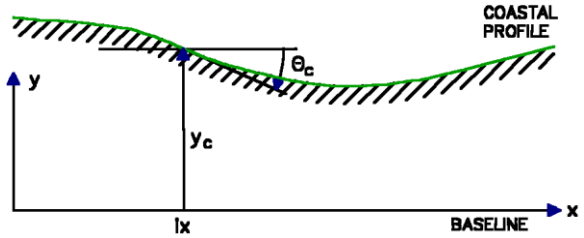


Figure 5.1 Co-ordinate system in the coastline evolution calculation

"Coastal- or coastline profile" is used to denote the variation of $y_c$ in the longshore (x) direction, while the cross-shore profile denotes the water depth (bottom position) as a function of the cross-shore position relative to the coastline position $y_c$. "Up- and downstream" positions are often used with respect to waves, such that "upstream" means in the longshore direction from where the waves are coming.

## 5.2 Continuity Equation for Sediment Volumes

The main equation in the coastline evolution calculation is the continuity equation for sediment volumes expressed by:

$$\frac{\partial y_c(x)}{\partial t} = -\frac{1}{h_{act}(x)}\frac{\partial Q(x)}{\partial x} + \frac{Q_{sou}(x)}{h_{act}(x)\Delta x} \tag{5.1}$$

in which the symbols are

| | |
|---|---|
| $y_c(x)$ | distance from the baseline to the coastline |
| $t$ | time |
| $h_{act}(x)$ | height of the active cross-shore profile |
| $Q(x)$ | longshore transport of sediment expressed in volumes |
| $x$ | longshore position |
| $\Delta x$ | longshore discretization |
| $Q_{sou}(x)$ | source/sink term expressed in volume |

$h_{act}(x)$ and $Q_{sou}(x)$ are calculated based on user specifications, while the longshore transport rate $Q(x)$ is determined from tables relating the transport rate to the hydrodynamic conditions at breaking. $\Delta x$ is user specified, while the internal timestep $\Delta t$ is determined from stability criteria. From an initial coastline position $y_{init}(x)$, the evolution in time is determined by solving Eq. (5.1), using an implicit Crank-Nicholson scheme.

## 5.3 Flow Diagram

The flow diagram in the coastal evolution calculations is crudely sketched in Figure 5.2. Much of the effort (and code + computational time) is put into the determination of *Q(x)*.

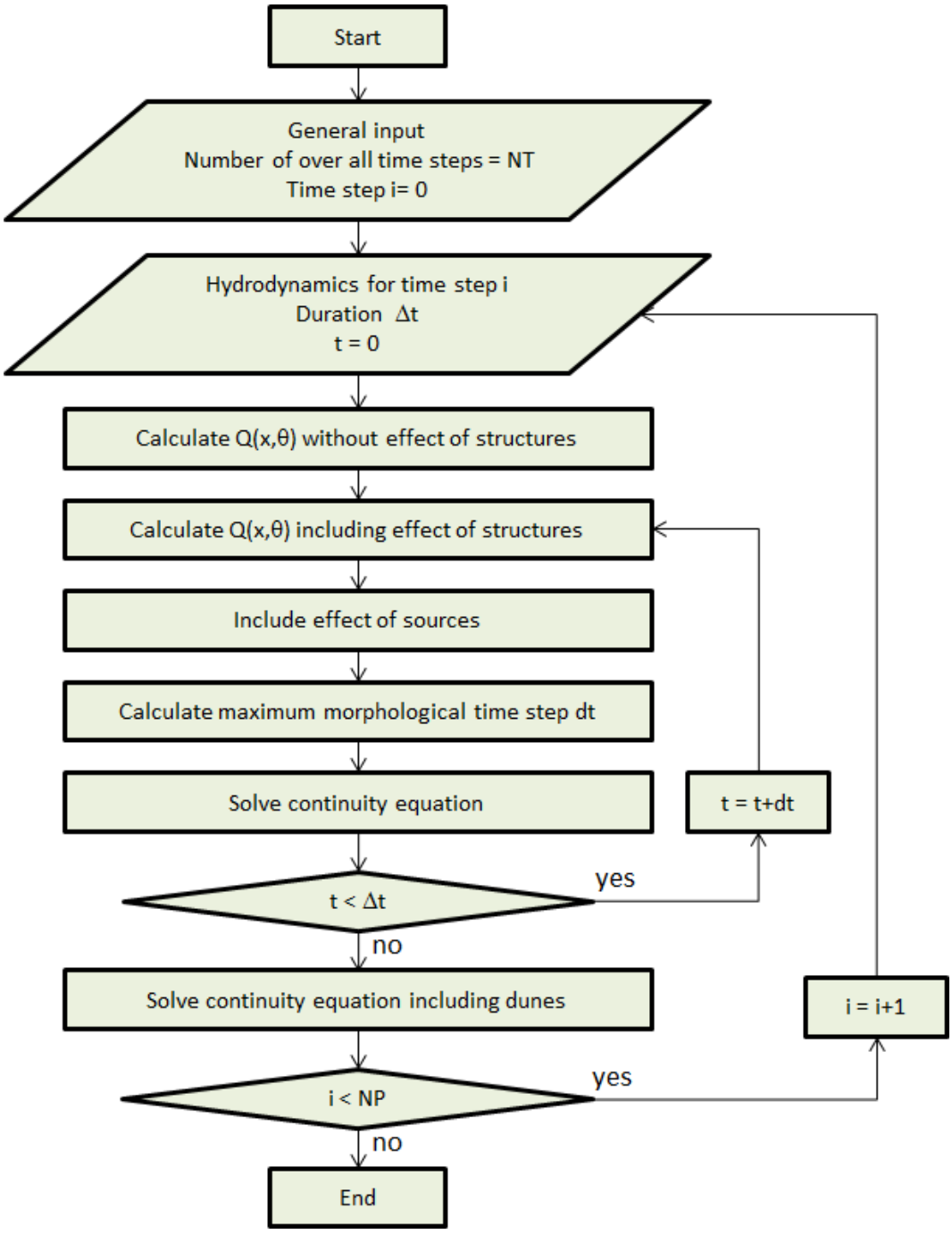


Figure 5.2 Sketch of flow diagram

## 5.4 Modification of Transport Tables

The undisturbed longshore transport rate $Q$ at a given position is a function of the wave climate, current, cross-shore profile, sediment properties and the coastline orientation (angle between wave and coastline normal).

The total transport rate as well as the cross-shore distribution of the transport for given coastal profiles are calculated and saved in tables prior to the execution of the coastal evolution calculations (see Chapter 3). To determine the transport rate and distribution under certain conditions, interpolation in the tables is performed among values of the water level (*wl*), the slope of the surface (*ig*) due to regional (not wave generated) currents, the wave period ($T$), the height $h_b$ and angle $\alpha_b$ of the wave at the breaking line.

Generally, the wave angle (compared to the coastline normal) and the wave height at breaking are the most important parameters.

A structure as a groyne or jetty will cause accretion with a resulting change in the coastline orientation on the updrift side. Shoreward of the active depth, $D_{act}$, the depth contours are assumed to follow the local orientation of the coastline. Furthermore, the littoral current and sediment transport are assumed to be in local equilibrium with the driving forces, primarily radiation stresses due to breaking waves. The radiation stresses strongly depend on the wave angle at breaking. If the cross-shore length of the structure is small compared to the width of the surf zone, the above-mentioned assumptions of local equilibrium between the coastline orientation and the transport rates may cause severe overestimation of the blocking effect of a groyne, as the transport gradient will be higher than in nature!

One way of avoiding this effect is to modify the transport tables to only include the transport occurring shoreward of a certain specified cross-shore position. All transport offshore of the distance specified is omitted in the tables containing the total transport rates as well as the tables containing the cross-shore distribution of the transport. Caution should be taken when the transport tables are modified. If changes in transport rates due to eg. a general change in coastline orientation are present, they will be underestimated. The change in transport rates counts for the entire coastline.

## 5.5 Local Wave Conditions

### 5.5.1 Reference Wave Conditions

The nearshore wave climate represented by the following parameters

| | |
|---|---|
| $H_0$ | Wave height at start of profile ($H_{rms}$ for irregular waves) |
| $\alpha_0$ | Wave angle at start of profile |
| $T$ | Wave period |
| *wl* | Water level (discrepancy from mean water level) |
| $V_c$ | Longshore regional current |

are assumed to remain constant throughout the duration step, $\Delta T$. $\Delta T$ may vary during the simulation. $V_c$ is due to regional currents (not wave driven) and specified for a start position of the cross-shore profile corresponding to a specific depth and roughness of the bed. This information is transformed to a slope "*ig*" of the water surface.

The wave climate can be constant or vary along the coast.

### 5.5.2 Breaking Wave Conditions

For a given longshore position $X_{cal}$, the wave is refracted and shoaled to the breaking line in two steps. Refraction is performed according to Snell's law of refraction:

$$\sin(\alpha_2) = \frac{L_2}{L_1}\sin(\alpha_1) \tag{5.2}$$

in which $\alpha_1$, $L_1$ and $\alpha_2$, $L_2$ are wave angle and wave length at positions 1 with depth $D_1$ and position 2 with depth $D_2$, respectively. Snell's law of refraction assumes straight and parallel depth contours. Shoaling calculations are based on an assumption of conservation of energy flux along wave orthogonals, leading to:

$$h_2 = h_1\sqrt{\frac{\cos(\alpha_1)(1+G_1)\tanh(k_1D_1)}{\cos(\alpha_2)(1+G_2)\tanh(k_2D_2)}} \tag{5.3}$$

in which $k$ is the wave number defined by

$$k = \frac{2\pi}{L} \tag{5.4}$$

and $G$ is given as

$$G = \frac{2kD}{\sinh(2kD)} \tag{5.5}$$

The two steps of refraction/shoaling involved to bring the waves from the reference depth to breaking are:

1. From the reference depth $D_{ref}$ to the limiting depth for offshore contours $D_{offshore}$ using the specified “offshore” orientation of the depth contours. The orientation of the offshore depth contours is only a function of $x$ and remains constant in time. If the offshore contours are specified by position, the “offshore” orientation is calculated internally.

2. From the limiting depth for offshore contours, the wave is refracted/shoaled until the breaking condition $h/D$ = 0.8 is satisfied. In this range, the orientation of the depth contours is determined by the local coastline orientation θ. This provides the wave height $h_b$ and angle $\alpha_b$ between the coastline normal and the incoming wave at breaking.

The values for the wave height, wave period, wave angle and water level at the breaking point are used together with a possible surface slope derived from regional currents to interpolate in the sediment transport tables for the calculation of coastline evolution.

## 5.6 Determination of Q(x,θ)

### 5.6.1 Interpolation in Transport Tables

For given wave properties, the total longshore transport of sediment *Q* is determined as a function of the longshore position and the local coastline orientation θ.

With known values of *ig*, *wl*, *T*, $h_b$, and $\alpha_b$, the total longshore transport *Q* corresponding to the applied value of θ can be determined by interpolation in the transport tables. For each value of $X_{cal}$, step 2 is repeated for eg. 20 different values of θ to provide a "discrete" $Q(X_{cal}, \theta)$ relation, as shown by the solid line in Figure 5.3.

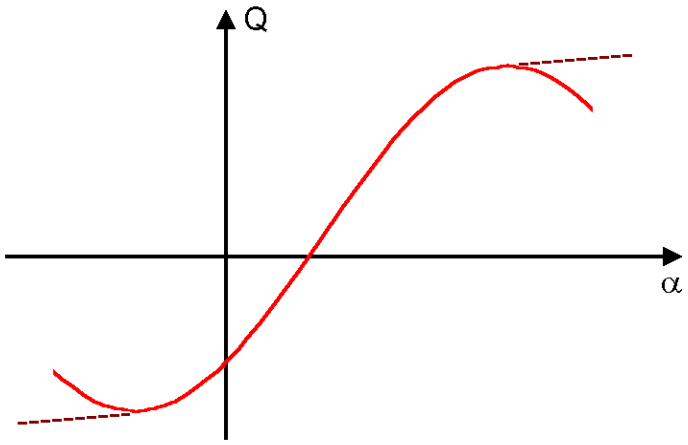


Figure 5.3 $Q(X_{cal}, \alpha)$ for varying α

To ensure stability in the simulation of the coastline evolution it is necessary that the transport curve maintains a positive transport gradient. Thus the transport curve can be modified as shown by the stippled line in Figure 5.3 when morphological feedback is required (i.e. evolution of the coastline).

If different transport tables are specified in the longshore direction (eg. due to different cross-shore profiles, varying sediment properties, etc.) the transport capacity for each value of θ is found by linear interpolation in the x-direction between values corresponding to the nearest table on either side of $X_{cal}$.

### 5.6.2 Q(x,θ) along Coastline

The values for $Q(X_{cal},\theta)$ are calculated for all points along the coastline.

Within a certain duration step corresponding to a particular wave event, the longshore sediment transport $Q(x)$ at x-positions, which is not influenced by any structures, can be found by interpolation in the $Q(x, \theta)$ relation based on the local coastline orientation $\theta_{coa}(x)$.

## 5.7 Structures

Structures in the coastal zone may cause changes in the wave angle and height at breaking, leading to altered transport rates. How this is handled for each type of structure is described in the following. It is strongly emphasized that for each structure type there are limitations to the capabilities of the model. Not all natural effects are included in the model, and proper evaluation of the results requires a good understanding of the mechanisms behind the physical processes as well as the modelling.

The calculation of coastline evolution includes two structure types with a longshore span:

- Breakwaters are basically separated from the coastline and located outside the breaker zone. Diffraction calculations are performed around the two structure heads.
- Revetments are situated at the coastline or further inshore. The coastline is not allowed to erode further back than the revetment, but the depth in front of the revetment is allowed to increase up to a certain fraction of $D_{act}$.

Structures with a cross-shore span are divided into two types classified as jetties and groynes. Both structure types extend in the offshore direction perpendicular to the baseline, and both give rise to a blocking of the longshore transport. The difference is related to the calculation of the sheltering effect of the structure on the downdrift side:

- Jetties are regarded as relatively long structures, with a structure tip outside the breaker zone. Diffraction calculation around the tip of the structure is carried out.
- Groynes in the model represent relatively short structures, and the sheltering effect is determined through a simple reduction of the “undisturbed “transport rates.´

### 5.7.1 General Parameters

#### Blocking of transport

The maximum active length, $L_{act,max}$ , is used when calculating bypass of sediment in case of structures at the coastline.

In the sediment transport tables the cross-shore distribution of the sediment transport rates are saved in non-equidistant space intervals, to secure a detailed description in the surf zone.

In the case of structures at the coastline the program internally describes the cross-shore distributed sediment transport by 50 equidistant space intervals in order to calculate the rate of bypass.

The spacing, $d_i$ , describes the number of cross-shore grid steps in each 'block'. This is calculated by

$$d_i = \mathrm{int}\left(\frac{L_{act,\max}}{(dy \cdot 50)}\right) + 1 \qquad (5.6)$$

Where *dy* is the cross-shore grid spacing in the profile data files.

Usually $L_{act,max}$ is only important by very long profiles with small grid spacing, and in the case of several tables in the simulation.

The parameter that influences the coastline evolution directly is the active depth that is given in the coastline data file.

### Interaction between several structures

Generally the calculation of coastline evolution is set up on the assumption of long and uniform coastlines that at a few places might be interrupted by structures. The effect of the structures is to a large extend based on empirical knowledge of the coastal processes.

The effect from other structures is incorporated similarly to the estimation of the wave height distribution in coastal waters:

$$H = H_0 \cdot K_c \cdot K_s \cdot K_r \cdot K_f \tag{5.7}$$

Where $K_c$ , $K_s$ , $K_r$ and $K_f$ are the dobbler coefficient, shoaling coefficient, refraction coefficient and friction coefficient, respectively.

Following this idea the sediment transport along the coastline is modified as follows: each structure have a coefficient. In the following example 6 structures is used in the calculations:

$$Q_{final} = Q_{open} \cdot K_{b1} \cdot K_{b2} \cdot K_{g1} \cdot K_{g2} \cdot K_r \cdot K_j \tag{5.8}$$

Where the coefficients $K_{b1}$ and $K_{b2}$ refer to the effect from two breakwaters, $K_{g1}$ and $K_{g2}$ refer to the effect from two groynes, $K_r$ refers to the effect of a revetment and $K_j$ referx to the effect from a jetty. For each single structure the coefficient is found with the assumption that it is the only structure along the coastline.

It must be stressed that the basic assumption in LITPACK is the long and uniform coastline. This assumption is violated by the structures. For a single structure the effect of the structure on the coastline is well predicted as well for a small number of structures. In the case of a large number of structures, say 20 groynes, great care must be taken. In some cases it might be an advantage to simplify the set-up. For instance a large number of groynes can in some cases be modelled as one revetment. It must be stressed that these adjustments must be performed from a sound coastal engineering point of view.

## 5.7.2 Theoretical Adaptation Length

The following presents a simple estimation of the length scale for the re- establishment of the longshore current in the case where a structure is located on an otherwise straight coast. This interruption can be in the form of a groyne or a jetty but could be a headland as well.

The total distance, $L_t$, from the structure to the point where the flow has attained its equilibrium value for uniform flow is related partly to the length of the structure and partly to the bed friction:

$$L_{total} = \max\left(L_s, L_{sep}\right) + L_f \tag{5.9}$$

The first part of the relation is related to the groyne itself. This contribution may be either due to the area related to the wave sheltering provided by the groyne, $L_s$, or the length of

the separation zone downstream of the groyne, $L_{sep}$. The former can be found by geometrical considerations:

$$L = L_{groyne} \tan(\delta) \tag{5.10}$$

Where δ = direction of wave at the tip of the structure and measured relative to the orientation of the groyne. The length of the separation zone is related to $L_{groyne}$ as well but is also related to the friction. In the case where the friction is very small the length of the separation zone, $L_{sep}$, is around 6 times the groyne length.

The second term, $L_f$, is related to the distance required before the radiation stress and the bed friction is in balance; i.e. before the longshore current is fully developed. The length scale for this process can be obtained from the momentum equation in the longshore direction (y-direction):

$$\rho D \frac{dV}{dt} = \frac{\partial S_{xy}}{\partial x} - \frac{1}{2}\rho f_w V^2 \tag{5.11}$$

Where the left side is the acceleration (ρ = density of water, $D$ = water depth (a function of the cross-shore coordinate, $x$, only), $V$ = longshore velocity, $t$ = time), and the right side is the wave forcing ($S_{xy}$ = radiation stress) and the friction ($\tau_{by}$ = bed shear stress). The wave forcing is assumed to be constant and the advective term ($d(U\,V)/dx$) is ignored.

Introducing the following variables (not functions of $y$)

$$\alpha = \frac{1}{\rho D}\frac{\partial S_{xy}}{\partial x} = \frac{S_{xy}}{\rho D}, \quad \beta = \frac{1}{2}\frac{f_w}{D} \tag{5.12}$$

Equation (5.11) can be rewritten:

$$\frac{dV}{\alpha - \beta V^2} = dt \tag{5.13}$$

Introducing:

$$V = \frac{dy}{dt} \Rightarrow dt = \frac{dy}{V} \tag{5.14}$$

Where $y$ is the distance from the structure in Eq. (5.13), the equation can be written:

$$y = \frac{\log\left(\alpha - \beta V^2\right)}{2\beta} + K \tag{5.15}$$

Where $K$ = constant. If $V = V_0$ at $y = 0$ then:

$$K = \frac{\log\left(\alpha - \beta V_0^2\right)}{2\beta} \Rightarrow$$

$$V = \sqrt{\frac{\alpha}{\beta}\left(\frac{\alpha}{\beta} - V_0^2\right)\exp(-2\beta y)} \tag{5.16}$$

if $V_0 = 0$ (groyne longer than the width of the surf zone) then

$$V = \sqrt{\frac{\alpha}{\beta} - \exp(-2\beta y)} = V\infty\sqrt{1 - \exp\left(-\frac{y}{K}\right)} \tag{5.17}$$

Where

$$K_f = \frac{D}{f_w} \quad and \quad V\infty\sqrt{-\frac{S_{xy}}{\frac{1}{2}\rho f_w}} \tag{5.18}$$

V ∞ is the fully developed velocity and $K_f$ is the length scale factor for adaptation of the longshore current. For example, the distance $x_L$ required for the longshore current to attain 95% of the fully developed longshore current is:

$$X_L = -K_f \ln\left(1 - \left(\frac{V}{V_\infty}\right)^2\right) = 2.3K_f \tag{5.19}$$

## Numerical examples

The analytical model is verified by considering a long straight coast interrupted by a groyne (length = 360m). The numerical results (obtained by MIKE 21 Nearshore Spectral Wave Module and MIKE 21 Flow Model, Hydrodynamic Module) are compared with the above equation. Both the Manning number, wave height and wave direction is investigated.

The orientation of the groyne is 270 deg.N and is blocking the longshore current entirely. The depth at offshore boundary where waves are imposed is 20m. Grid spacing is 5m. Examples of the flow field are given in Figure 5.4.

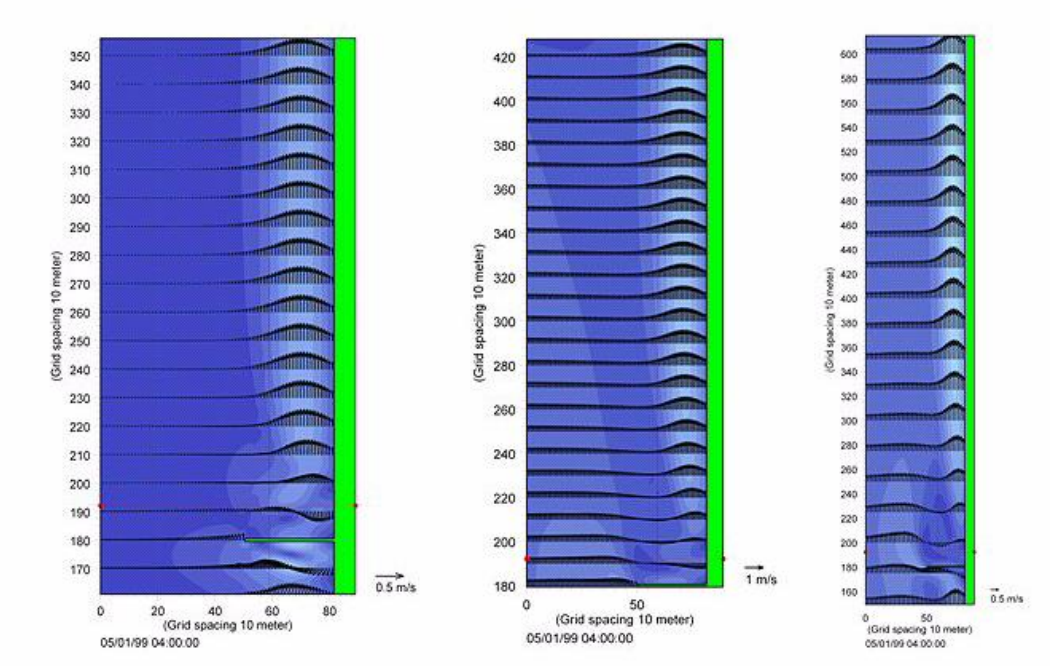


Figure 5.4 Flow fields for different Manning numbers

In Figure 5.5 the non-dimensional longshore velocity at the break line as function of the alongshore coordinate is presented for three cases. In the upper part of Figure 5.5 curves for the longshore current are shown for different Manning numbers. In the middle and lower part of Figure 5.5 the variation with offshore wave height and wave direction is presented. The wave-sheltering length ($L_S$) has been added in the results, whereas the length of the separation zone (behind the groyne) has not been added. The later length is not possible to estimate correctly, other than it will be dependent on the Manning number and such that it will always be less then approximately 6 times the length of the groyne (when the bed friction is very small and the groyne is located within the surf-zone).

The results shown in Figure 5.5 for the Manning number (upper part of Figure 5.5) probably show a too large dependency on the Manning number, *M*, since the numerical model has not included the apparent (wave-related) roughness. The waves will certainly entail roughness heights, which are equivalent to values of *M* smaller than 50m$^{1/3}$/s.

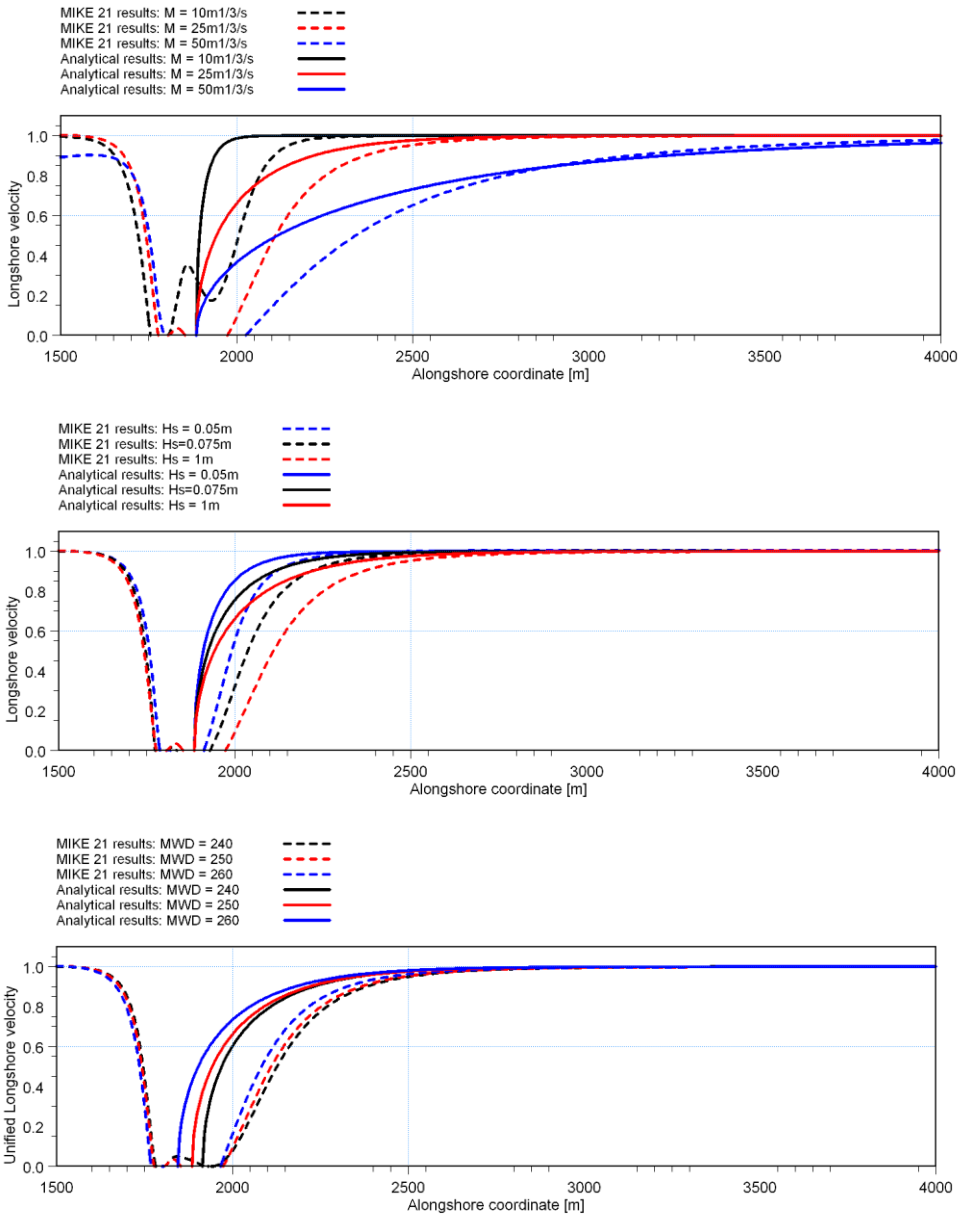


Figure 5.5 Non-dimensional longshore velocity at break line vs. longshore coordinate. Upper : MWD=250 deg.N and $H_S$=1 m; Middle: MWD=250 deg.N and M=25 m$^{1/3}$/s; and Lower: M=25 m$^{1/3}$/s and $H_S$=1 m.

## Adaptation length in the calculation of coastline evolution

The influence of any structure to the littoral drift along a coastline is a two-dimensional phenomenon, which has to be simplified in one-line models. In the calculation of coastline evolution two different approaches are possible; groynes and jetties.

In coastline evolution calculations the influence on the littoral drift depends on the type of structure, length of structure and the properties of the incoming wave. More information about the influence of groynes and jetties can be found in Section 5.7.5 Groyne and Section 5.7.4 Jetty, respectively.

Figure 5.6 shows an example of the downstream sediment transport rates for a groyne, a jetty and a theoretical structure, respectively. The theoretical result is calculated using wave sheltering and adaptation length, as the length of the separation zone cannot be calculated accurately.

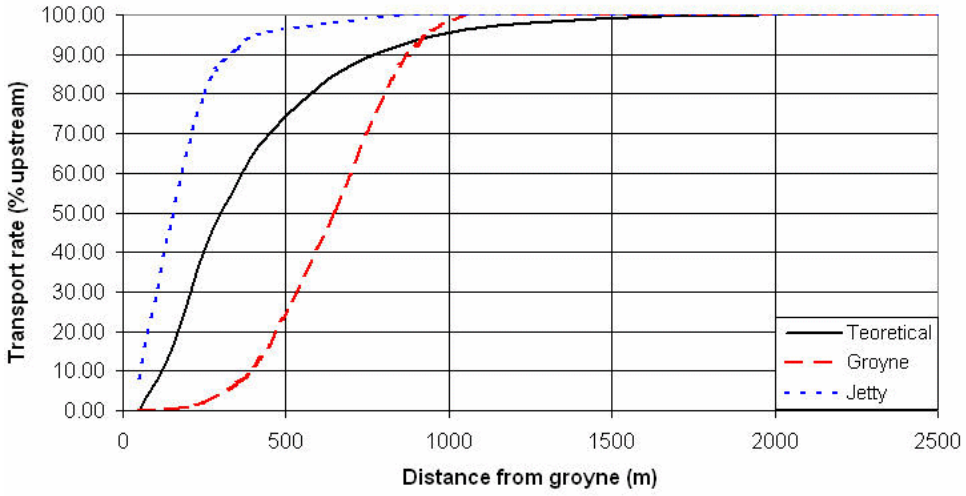


Figure 5.6 Sediment transport rates downstream a structure. Incoming wave height is 1 m and wave angle 20 degrees to the coastline. The structure extends 300 m from the coastline. The theoretical adaptation length is calculated with by use of Eq. (5.10) and Eq. (5.17), with $K_f$ = 300 and $Q_s$~V2.

As seen from Figure 5.6 the downstream transport rates clearly depends on the type of structure. The theoretical transport rates are different from the results of both approaches (groyne and jetty) in the coastline evolution calculations, but comparable. Please note that it is very important to calibrate the model and to consider what kind of structures to use.

## 5.7.3 Breakwaters

### Introduction

The flow around a breakwater comprises complicated two-dimensional circulations, which cannot be fully assessed by any one-dimensional model. With respect to coastline evolution modelling, the prime effect of a breakwater is its sheltering effect of the incoming waves. In the shadow region between the breakwater and the coastline, the wave disturbance and the driving forces for a longshore current are reduced (and may even reverse, depending on the relative size and proportions of the breakwater). This will lead to a decrease in the longshore sediment transport $Q(x)$. It is this effect that is modelled in the coastline evolution calculations, and it is solely used to assess the stability of the local coastline through the changes to the longshore transport rates. Thus this feature is preferred to be applied for structures far away from the breakerline, e.g. offshore breakwaters. If 2D effects, as for example local scour, are important; a 2D-model as MIKE 21 should be used.

A breakwater in coastline evolution calculations is assumed to be surface piercing and run close to parallel to the baseline. It is described solely by the positions of the two structure heads. Further, the breakwater is assumed impermeable and non-reflective. The wave heights are reduced and the wave angles altered behind it due to diffraction, refraction and shoaling. Transport capacities are determined from the transport tables based on the altered values of $h_b$ and $\alpha_b$.

### Wave conditions at a breakwater

The first step is to determine the wave conditions at the tip of the breakwater. Based on the distance between the tip of the breakwater and the coastline, the depth at the breakwater tip is determined through interpolation in the two closer cross-shore profiles. Waves are shoaled and refracted to the tip of the breakwater based on the local depth contours (offshore contours offshore of $D_{offshore}$ and an orientation corresponding to the local coastline orientation shoreward of $D_{offshore}$). If breaking occurs offshore of the breakwater, the wave height at the tip of the breakwater used in the diffraction calculations is set to $h_{tip} = 0.8 * D_{tip}$, and the bypass of sediment is determined (see section about bypass).

### Calculation points

Based on the wave angle at the tip of the breakwater, the shadow area (see Figure 5.7a) is determined by extending the incoming wave ray at the breakwater to the coastline.

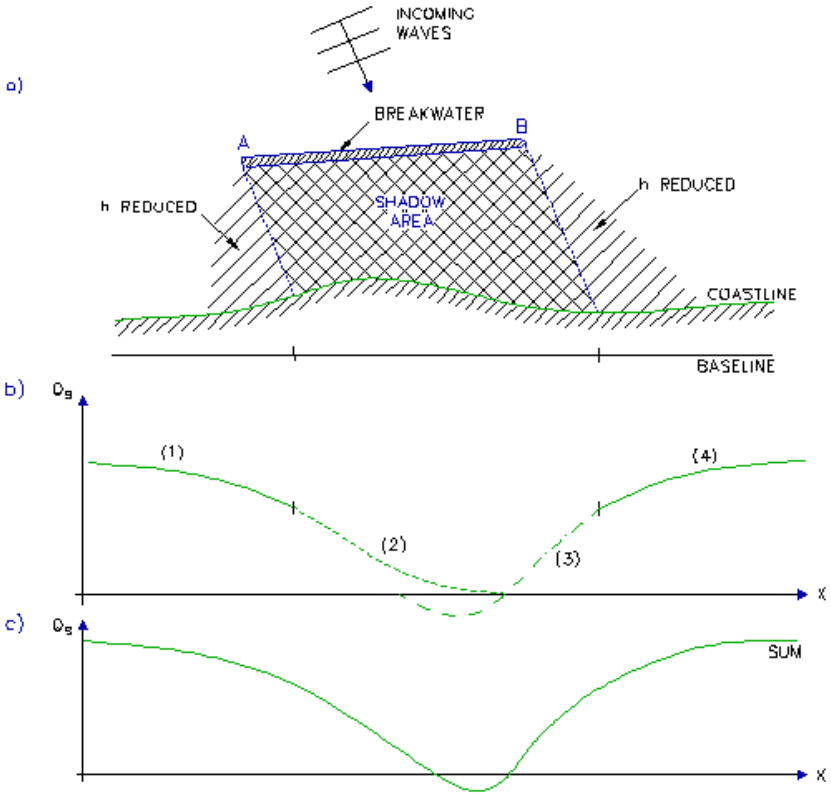


Figure 5.7 a) shadow area due to breakwater, b)+c) transport rates due to diffraction

the effect of the breakwater on the longshore transport is determined in all points within the shadow area as well as the point in adjacent areas on either side, where the influence of the breakwater also plays an important role.

The extension of the affected coastline is found on the basis of the location of the breakwater tips and incoming wave angle:

- The coastline is affected in the shadow area as outlined in Figure 5.7.
- The coastline is affected upstream from the limit of the shadow area and 2*$L_{tip}$ further updrift, where $L_{tip}$ is the distance from the upstream tip of the breakwater to the coastline.
- The coastline is affected downstream from the limit of the shadow area and 2*$L_{tip}$ further downdrift, where $L_{tip}$ is the distance from the downstream tip of the breakwater to the coastline.

## Longshore transport

Outside, but close to the shadow area (see Figure 5.7a), the wave heights are reduced due to a flux of energy into the shadow area. Here, the wave height is calculated based on the local diffraction coefficient, while the wave angle relative to the coastline normal is calculated from refraction, as without a breakwater. Figure 5.7b shows a schematic representation of transport levels. The segments (1) and (4) show reductions in the transport capacities from the undisturbed levels away from the breakwater towards the shadow area.

The transport in the shadow area between the breakwater and the coastline is calculated based on diffraction of the waves around the two structure heads, A and B in Figure 5.7a. $Q(x)$ is determined as the sum of the transport due to waves diffracted around the two structure heads A and B, respectively. For each component, the wave angle and height at breaking is determined by refraction and shoaling of the diffracted waves to the point of breaking. For irregular waves, the diffraction calculations are based on $H_{rms}$. (2) and (3) in Figure 5.7b represent the transport due to diffraction around A and B, respectively. Figure 5.7c shows the total transport rates along the coast.

For short breakwaters compared to their distance from the coastline, the waves diffracted into the shadow region from the left tip of the breakwater may give rise to a small transport rate to the right of the shadow region ((2) in Figure 5.7b is greater than zero to the right of the shadow region). In this case, (2) and (3) are added together to determine the total transport rate (Figure 5.7c).

## Bypass of sediment

If the breakwater is situated on relatively shallow water, there may be sediment bypassing on the offshore side of the breakwater. The amount of bypass, $Q_{byp}$, is calculated from the cross-shore distribution of the transport at the upstream tip of the breakwater (see Figure 5.8). If the transport tables change in the longshore direction, interpolation is as usual performed among the closest table specified on either side.

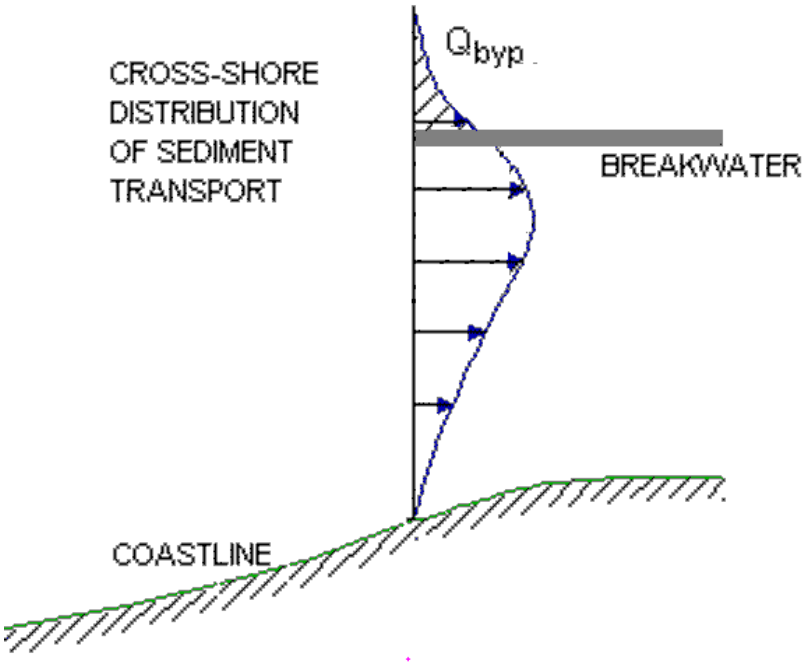


Figure 5.8 Determination of $Q_{byp}$ from cross-shore distribution of transport

Further checks on the calculated bypass rates are introduced. Unless the coastline has advanced all the way to the upstream breakwater tip, $Q_{byp}$ is not allowed to exceed the transport in the first upstream point (for waves coming from the left, $Q_{byp}$ = min. ($Q_{byp}$ ,$Q_{ibrw1}$ in which *ibrw*1 is the position of the left limit of the breakwater). Furthermore, the coastline is not allowed to develop beyond the upstream tip of the breakwater unless the downstream tip also becomes embedded in the coastline. If both tips of the structure become embedded in the coastline due to general accretion in the area, the breakwater is disregarded in the calculations.

Please note that this should be avoided as the theory behind breakwaters will be violated. In general the wave breaking point should always be located shorewards of the breakwater.

In the shadow area, $Q_{byp}$ is added to the transport capacities calculated from diffraction. Outside the shadow area, the reduction in the transport capacities will be less when bypass is present because breaking may occur offshore of the breakwater, prior to the reduction in wave height due to flux of energy into the shadow area. In this case, the local longshore transport is calculated through:

$$Q = Q_{byp} + \left(Q_{un} - Q_{byp}\right)\frac{Q_{dif}}{Q_{un}} \tag{5.20}$$

in which $Q_{un}$ is the "undisturbed" transport without reducing the wave height according to the diffraction, and $Q_{dif}$ is the transport calculated though diffraction corresponding to no bypass. The transport occurring shoreward of the breakwater is reduced proportionally to what the total transport would have been reduced if no bypass had been present.

The model includes an option to disregard the bypass in the breakwater calculations. This option can eg. be used to investigate how large a fraction passes offshore of the breakwater by comparing similar runs with and without bypass included, respectively.

## Combined effect of separate breakwaters

The combined effect of several breakwaters can be included as long as they do not shadow for each other (the wave conditions at the tip of a breakwater is assumed unaffected by other structures and is calculated by refraction/shoaling from $D_{ref}$ to the depth at the breakwater tip).

## Angles in diffraction calculations

The angle between the normal to the baseline and the incoming wave, $\alpha_{tip}$, is determined by refraction of the wave to the depth at the breakwater tip. For a certain longshore position ix, $\theta_L$ is the local angle between the baseline normal and a line from the breakwater tip to *yc*(*ix*), see Figure 5.9.

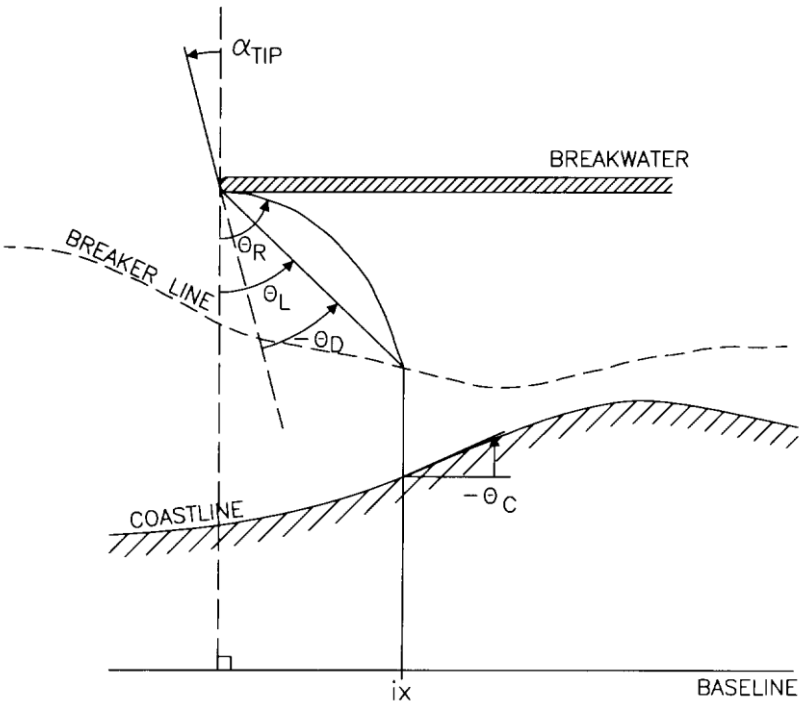


Figure 5.9 Angles involved in diffraction calculations

The diffraction coefficient $k_D$ is based upon the angle between the incoming wave and the diffracted wave $\theta_D = \alpha_{tip} - \theta_L$. $\theta_L$ corresponds to a certain value of *ix* on the cross-shore position where wave breaking occurs (according to the usual criteria *h/D* = 0.8).

Due to the sloping bottom, refraction and shoaling also has to be included to transform the wave conditions at the breakwater tip to conditions at breaking. The angle $\theta_R$ corresponding to a wave ray that will break at the longshore position "*ix*" is determined through an iterative process.

The effect of the above mentioned approximations involved in determination of the angles has been investigated. Generally, the impact on transport rates is small and insignificant compared to the effect of other approximations/assumptions involved in the model. Just to mention one example related to a 1D-model, it is assumed that the bottom contours behind the breakwater are "locally straight and parallel", and follow the local coastline orientation. This assumption is necessary for the refraction calculations.

Once the diffraction coefficient $k_D$ and the wave angle of a wave ray corresponding to a certain position, *ix*, has been determined, the wave is refracted and shoaled to breaking according to the criteria

$$\frac{h_{shoal} \cdot k_D}{D_b} = 0.8 \tag{5.21}$$

in which $h_{shoal}$ is the wave height corresponding to refraction/shoaling without diffraction from the wave height at the breakwater tip to the depth at breaking, $D_b$.

## Diffraction scheme

For the diffraction calculations, a method described by Goda et al. (1978) is used. Compared to conventional diffraction schemes, which utilize the Sommerfeld solution for monochromatic waves, Goda et al. includes a directional spectrum in their calculations of the diffraction coefficients. Figure 5.10 shows the diffraction coefficient $k_D$ as a function of the diffraction angle $\theta_D$ for various values of the wave concentration parameter $S_{max}$ at the breakwater tip.

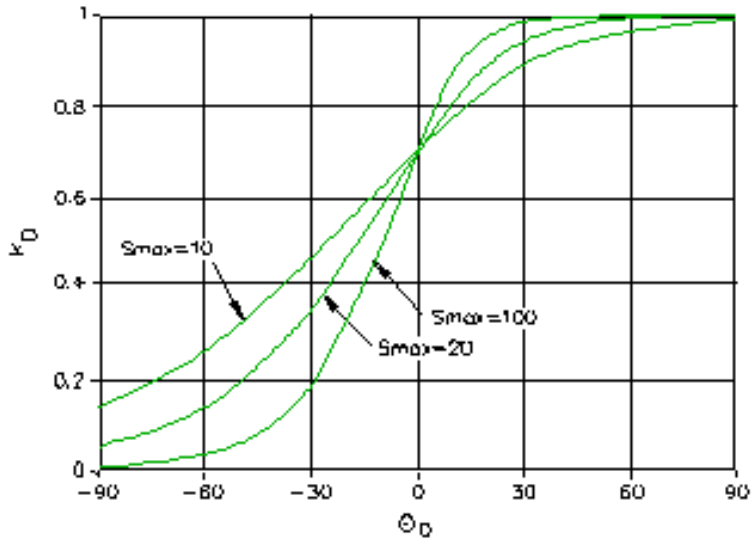


Figure 5.10 Diffraction curves

The diffraction curves in Figure 5.10 are determined from the best-fit approximations by Kraus (1984) to the original curves given by Goda et al. (1979). The formulation by Kraus is very effective with respect to calculation speed and only introduces very minor errors compared to the original curves.

$S_{max}$ represents the degree of directional spreading in the wave field. A value of $S_{max}$ corresponding to deep water, $S_{max0}$, must be specified in the input when diffraction calculations are included (breakwaters and jetties). Goda et al. (1979) proposed the values for $S_{max}$ given in Table 3.1.

Table 5.1 Directional spreading, Smax0, in deep water for different wave types

| Wave type | $S_{max0}$ |
|---|---|
| Wind waves | 10 |
| Swell with short to medium decay distance | 25 |
| Swell with medium to long decay distance | 75 |

Refraction leads to a narrowing of the spectrum. The value of $S_{max}$ at the tip of the breakwater is found from Figure 5.11, which depicts $S_{max}$ as a function of the local depth to deep-water wavelength. The original curves of Goda also include the influence of the angle of the waves at deep water, but as this effect is relatively small, the curves corresponding to an angle of 30 degrees have been selected. For practical calculations in coastline evolution, the curves have been tabulated and the value of $S_{max}$ at the tip of the breakwater is determined through interpolation in the table.

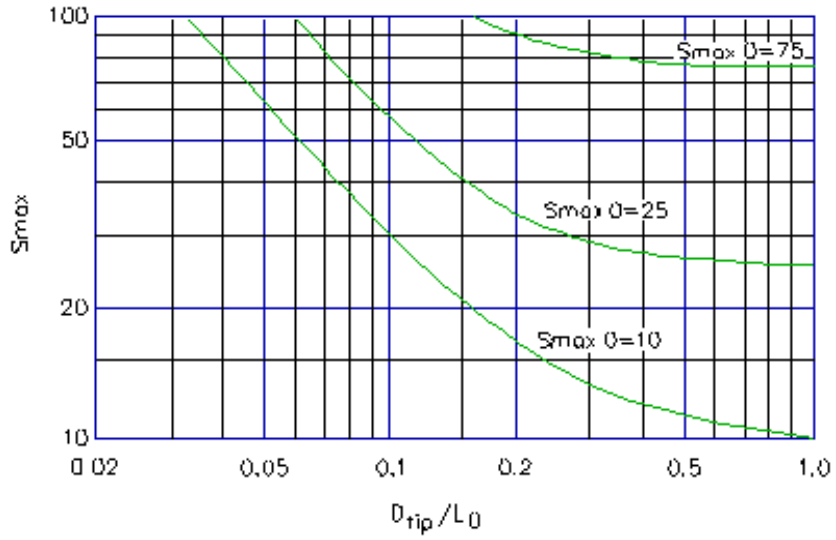


Figure 5.11 $S_{max}$ as function of local water depth to deep water wave length (Goda et al. 1978)

## Model limitations

It should always be kept in mind that essentially the coastline evolution calculation behaves as 1D-model while diffraction is a 2D-effect. It is important to use a good deal of sound judgement when setting up the tasks and evaluating the results from the model. A few aspects, which might cause inaccurate or incorrect results in relation to a breakwater, will be mentioned here.

Precautions must be taken with respect to the relative dimensions of the breakwater. The diffraction diagrams used are valid for semi-infinite breakwaters. If the length of a breakwater is small compared to its distance from the coastline, the energy dispersion from the illuminated area into the shadow area from either side of the breakwater is likely to be overestimated (energy entering at one end of the breakwater does not influence the calculation of diffraction coefficients at the other end). This will lead to an underestimate of the wave heights and thereby the transport rates in the illuminated areas on either side of the breakwater.

Momentum-effects with respect to the longshore current are not included in the model. The calculated sediment transport rate at any point corresponds to equilibrium between the local values of the driving forces (radiation stresses due to wave breaking) and the longshore current. The acceleration terms due to longshore changes in the driving forces are neglected. With respect to a breakwater, the momentum of the longshore current may in some cases play a significant role close to the ends of the breakwater, where the littoral current is first subject to deceleration when entering and later acceleration when leaving the sheltered area. Disregarding the acceleration effects in the breakwater case may cause the model to shift the areas of accretion and erosion in the up-stream direction.

## 5.7.4 Jetty

### Introduction

A jetty is defined as a relatively long structure extending in the offshore direction perpendicular to the baseline. Diffraction calculations are performed around the structure head.

The jetty is specified through its longshore position (point no. $I_{jet}$), a length $L_{jet}$ (the distance from the baseline to the tip of the jetty) and a bypass length, $L_{jet,bypass}$. the apparent length found by $L_{jeta} = L_{jet} - L_{jet,\ bypass}$ represent the effective length for blockage of the longshore sediment transport.

A jetty has two main effects on the longshore sediment transport:

1. The littoral current and sediment transport is blocked partially or fully by the jetty, depending on its effective length $L_{jeta} - y_c$ compared to the active width (in cross-shore direction) of the cross-shore profile.

2. The structure has a sheltering effect for the wave action on the beach downstream. The wave height and direction in the sheltered region is determined through diffraction.

Generally, the blocking of the transport will lead to an advancing coastline upstream and erosion with a retreating coastline downstream of the structure. The upstream coastline profile is determined by the relation between the transport rates and the orientation of the local coastline. For a given wave direction, the coastline will approach an equilibrium profile. Downstream, there is a lack of sediment due to the blocking effect of the structure. The local transport rate is influenced by the local coastline orientation as well as the sheltering effect of the jetty.

### Bypass calculations

To determine the bypass of sediment (the amount of sediment passing offshore of the tip of the jetty) the wave is refracted/shoaled to the breaking line based on conditions (coastline orientation and position) just upstream of the jetty. With the hydrodynamic parameters determined, the cross-shore distribution of the sediment transport can be found from the transport tables. Due to three-dimensional effects with local scour around the structure tip, the entire length of the jetty is not effective in blocking the transport. For this reason, the apparent length, $L_{jeta}$, on which the bypass calculation is based, has been implemented (see Figure 5.12).

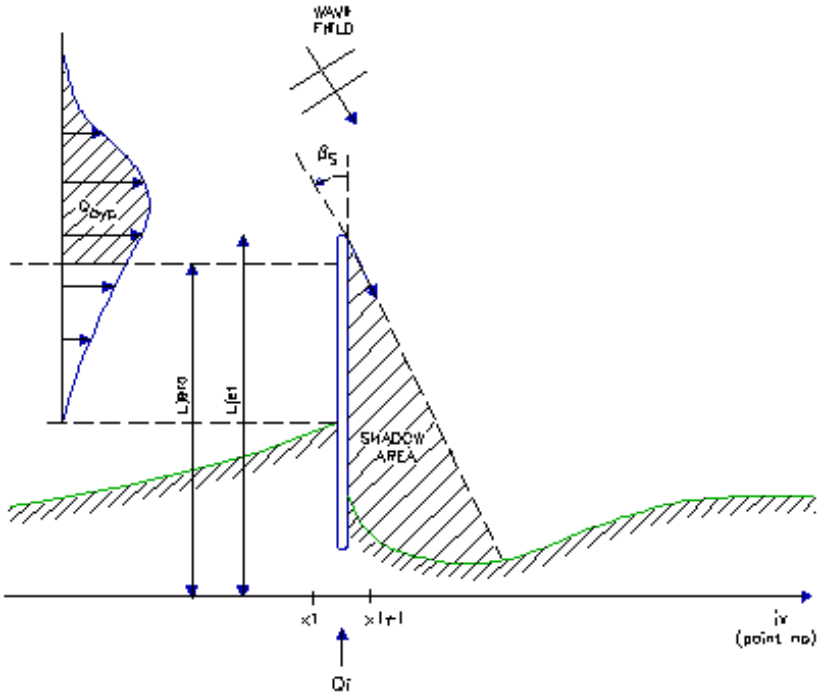


Figure 5.12 Terms related to jetties and groynes

Further checks on the calculated bypass rates are introduced. Unless the coastline on the upstream side of the jetty has reached the apparent length of the jetty, $Q_{byp}$ is not allowed to exceed the transport in the first upstream point. Further, the coastline is not allowed to develop beyond the apparent length of the jetty unless the tip also becomes embedded in the coastline on the downstream side. The structure may become completely embedded in the coastline due to general accretion in the area, in which case the jetty is disregarded in the calculations.

A jetty should never be situated in the sheltered area of a breakwater; in this case the calculations carried out for a groyne are better suited. Further, the possible effects from nearby breakwaters on the wave climate at the tip of the jetty are not taken into account.

However, the sheltering effects from nearby jetties or groynes on the wave climate at the tip of the jetty are taken into consideration. If the tip of the jetty concerned is situated in the shadow area of another jetty or groyne, the wave height and angle at the tip of the jetty are altered through a diffraction calculation based on the angles sketched in Figure 5.13.

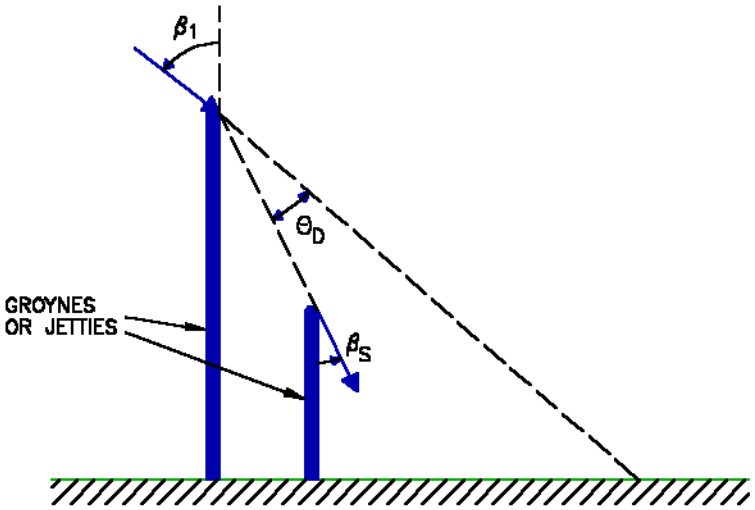


Figure 5.13 Lee from other structures

The sediment bypassing the jetty is distributed evenly over the downstream shadow area.

## Sheltering of waves

The sheltering effect of the jetty on the down-stream wave climate and the associated reduction in transport capacity is calculated through diffraction.
Based on the upstream length of the jetty $L_{up} = L_{jet} - y_c$, the depth at the breakwater tip is determined through interpolation in the two closer cross-shore profiles. Waves are shoaled and refracted to the tip of the jetty based on the upstream depth contours (offshore contours offshore of $D_{act}$ and an orientation corresponding to the upstream coastline orientation shoreward of $D_{act}$). This provides the wave angle $\beta_s$ and the wave height $h_{tip}$ at the tip of the jetty.

If breaking occurs offshore of the tip, the wave height used in the diffraction calculations is set to $h_{tip} = 0.8 * D_{tip}$. Should the tip of the breakwater be situated in the shadow area of another jetty or a groyne, the wave height and angle are adjusted as described in the previous section.

The sheltered (shadow) area is calculated based on $\beta_s$ (Figure 5.12). Within this area, the wave height and angle at breaking is found through combined diffraction, refraction and shoaling. The diffraction scheme used is the same as the one described under breakwaters ( Figure 5.10 and Figure 5.11). In the illuminated area just downstream of the shadow area, the wave angle is not influenced by the jetty, while the wave height is still reduced due to energy dispersion into the shadow area.

## Angles in diffraction calculations

$\beta_s$ was determined by refraction of the wave to the depth at the tip of the jetty or through diffraction calculations if the tip of the jetty lies within the shadow region of another structure. For a certain longshore position, $x_{cal}$, in the shadow region, $\theta_L$ is the local angle between the coastline normal and a line from the structure tip to $y_c(ix)$ (see Figure 5.14).

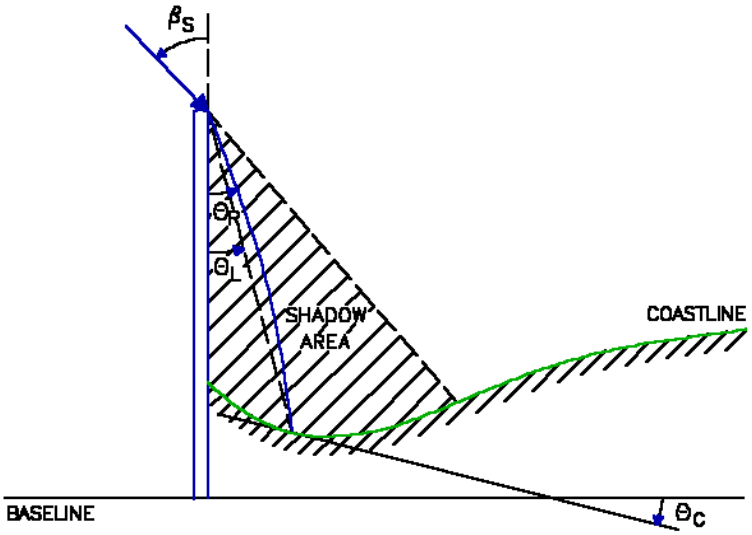


Figure 5.14 Definition of angles in diffraction calculations

The diffraction coefficient $k_D$ is based upon the angle $\theta_D = \theta_L - \beta_s$ between the incoming wave and the diffracted wave. Like the case for breakwaters, $\theta_L$ corresponding to a certain value of $x_{cal}$ should ideally be based on the cross-shore position where wave breaking occurs (according to the usual criteria $h/D = 0.8$), but to simplify calculations and save computer time, $\theta_L$ is approximated from the local position of the coastline. In this case, the diffraction coefficient and thereby the transport rate is slightly underestimated.

Due to the sloping bottom, refraction and shoaling also have to be included to transform the wave conditions at the tip of the jetty to conditions at breaking. The angle $\theta_R$ corresponding to a wave ray that will break at the longshore position of $x_{cal}$ could be determined through an iterative process. Again, to simplify calculation procedures and save computer time, $\theta_R$ is estimated through

$$\theta_R = \theta_L + \frac{x_{cal} - x_{jet}}{x_{sha} - x_{jet}}\left(\beta_s - \theta_L\right) \tag{5.22}$$

$x_{jet}$ is the longshore position of the jetty and $x_{sha}$ is the longshore position of the limit between the shadow area and the illuminated area.

The discussion in the section on breakwaters regarding the influence of the approximations related to the determination of the involved angles is also valid for this case.
Once the diffraction coefficient $k_D$ and the wave angle of a wave ray corresponding to $x_{cal}$ have been determined, the wave is refracted and shoaled to breaking according to the criteria

$$\frac{h_{shoal} \cdot k_D}{D_b} = 0.8 \tag{5.23}$$

in which $h_{shoal}$ is the wave height corresponding to refraction/ shoaling of $h_{tip}$ without diffraction, and $D_b$ is the water depth at breaking.

### Diffraction outside shadow area

In the illuminated area downstream of the shadow area, the diffraction coefficient $k_D$ is still based upon the angle $\theta_D = \theta_L - \beta_s$ between the incoming wave and the diffracted wave. The wave angle at breaking is determined by refraction and shoaling to breaking from the input wave angle and height at the reference depth.

### Calculation points

Diffraction calculations are performed in all longshore points occurring in the shadow area and selected points in the downstream illuminated area. The points in the illuminated area are selected similarly as for the breakwater:

- The affected coastline downstream the breakwater extends from the limit of the shadow area and twice the effective length of the jetty downstream.

## 5.7.5 Groyne

### Introduction

A groyne in the calculation of coastline evolution is defined as a relatively short structure extending in the offshore direction perpendicular to the baseline. The sheltering effect downstream of a groyne is incorporated by a scheme to reduce the longshore sediment transport that would have occurred if the groyne had not been present.

Similar to a jetty, the groyne is specified through its longshore position (point no. Igro), a length $L_{gro}$ (the distance from the baseline to the tip of the groyne) and a bypass length, $L_{gro,bypass}$. The apparent length $L_{groa}$, found by $L_{groa} = L_{gro} - L_{gro,bypass}$, represents the effective length for blockage of the longshore sediment transport.

A groyne basically has the same effects on the longshore sediment transport as a jetty:

1. The littoral current and sediment transport are blocked partially or fully by the groyne, depending on its effective length $L_{groa} - y_c$ compared to the active width (in cross-shore direction) of the cross-shore profile.

2. The structure has a sheltering effect for the wave action on the beach downstream. The sediment transport in the sheltered area is estimated by a scheme to reduce the “undisturbed” transport capacity.

Generally, the blocking of the transport will lead to an advancing coastline upstream and erosion with a retreating coastline downstream of the structure. The upstream coastline profile is determined by the relation between the transport rates and the orientation of the local coastline. For a given wave direction, the coastline will approach an equilibrium profile. Downstream, there is a lack of sediment due to the blocking effect of the structure. The local transport rate is influenced by the local coastline orientation and the position relative to the groyne.

## Bypass calculations

If the groyne is not situated behind a breakwater, the bypass of sediment for a groyne is basically determined analogously to the case with a jetty. The wave is refracted/shoaled to the breaking line based on conditions (coastline orientation and position) just upstream of the groyne. If the tip of the groyne in concern is situated in the shadow area of another groyne or a jetty, the wave height and angle at the tip of the groyne are altered through a diffraction calculation based on the angles sketched in Figure 5.13. With the hydrodynamic parameters determined, the cross-shore distribution of the sediment transport can be found from the transport tables. The calculation of the bypass is based on the apparent length, $L_{groa}$, similarly to the case for a jetty (see Figure 5.12).

Further checks on the calculated bypass rates are introduced. Unless the coastline on the upstream side of the groyne has reached the apparent length of the groyne, $Q_{byp}$ is not allowed to exceed the transport in the first upstream point. Further, the coastline is not allowed to develop beyond the apparent length of the groyne unless the tip also becomes embedded in the coastline on the downstream side. The structure may become completely embedded in the coastline due to general accretion in the area, in which case the groyne is disregarded in the calculations.

Unlike jetties, the groyne may be situated “behind” a breakwater, although the results should be assessed with a good deal of physical judgement.

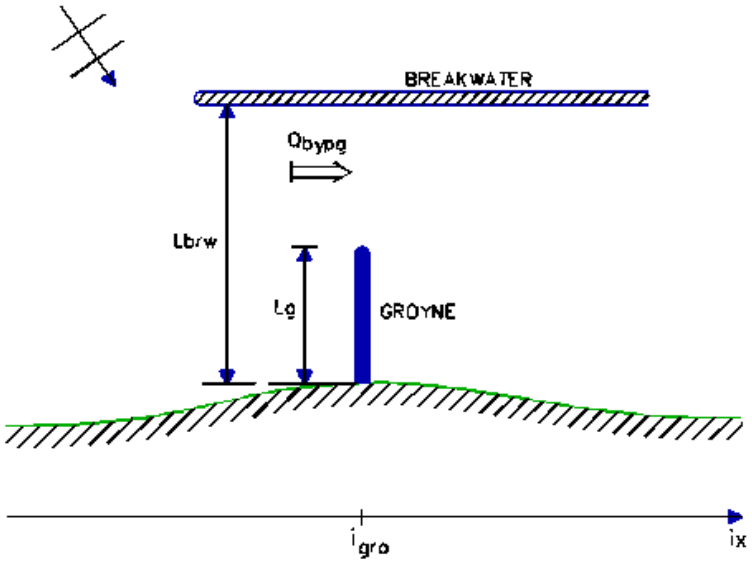


Figure 5.15 Bypass between groyne and breakwater

The breakwater is assumed to be situated further offshore than the tip of the groyne. In this case, the bypass of sediment between the tip of the groyne and the breakwater, $Q_{bypg}$, is determined by a simple linear blocking of the transport rate, $Q(i_{gro})$ that would have occurred if the groyne had not been present (see Figure 5.15:

$$Q_{bypg} = \frac{L_{brw} - L_g}{L_{brw}} \cdot Q\left(i_{gro}\right) \tag{5.24}$$

## Downstream sheltering

The sheltering effect of the groyne on the down-stream wave climate and the associated reduction in transport capacity is included by reducing the “undisturbed” transport rates in the sheltered area. The wave angle $\beta_s$ at the tip of the groyne is calculated based on upstream conditions. The sheltered area in the case of a groyne is confined by the groyne on the upstream side and ten times the distance to the crossing between a line from the tip of the groyne with the angle $\beta_s$ and the coastline on the downstream side (Figure 5.16). This has shown to predict the coastline evolution to a reasonable accuracy when compared to the observed shoreline evolution and to full 2D-calculation of the sediment transport around a groyne.

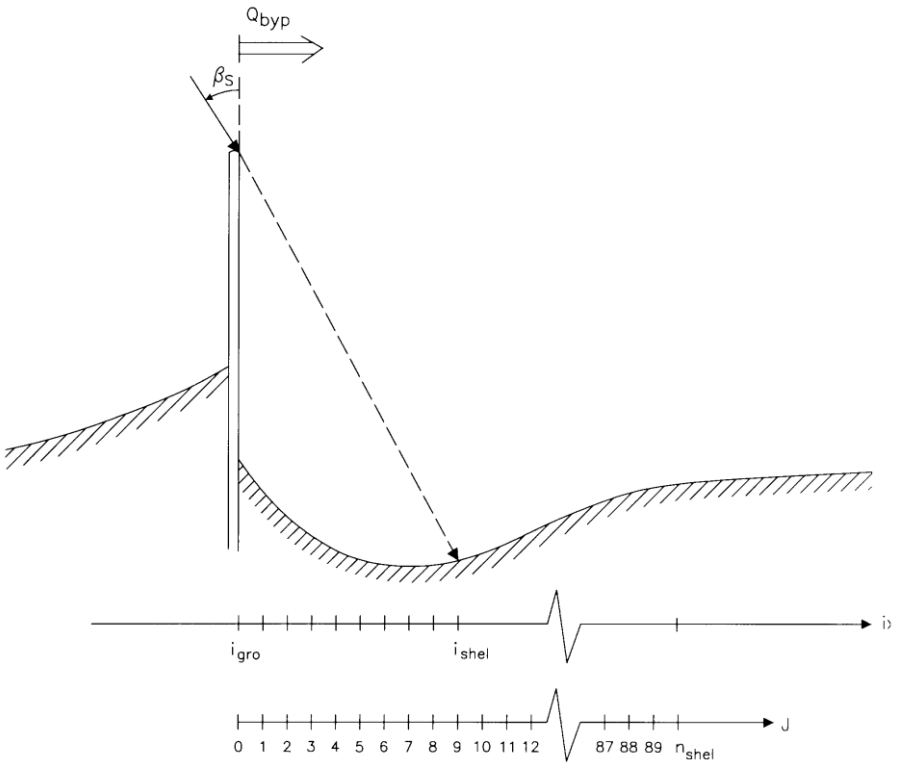


Figure 5.16 Definition sketch related to sheltering by groyne.

The transport downstream of the groyne is determined through:

$$Q(j) = Q_{byp} + \left(Q_{un}(j) - Q_{byp}\right) \cdot \sin^4\left(\frac{j}{n_{shel}} \cdot \frac{\pi}{2}\right) \tag{5.25}$$

Where $n_{shel} = 10 \cdot \Delta i_{shadow} = 10 \cdot \left(i_{shel} - i_{groyne}\right)$

$Q_{un}$ is the transport capacity based on the wave climate and possible effects from breakwaters, jetties, and other groynes situated upstream. This procedure gives a result that qualitatively and quantitatively resembles the results from a diffraction calculation carried out for similar conditions.

## 5.7.6 Revetment

### Introduction

A revetment is a structure that over a certain longshore stretch restricts the retreat of the coastline. When an eroding coastline reaches a revetment, the retreat is stopped, but the depth increases in front of the revetment due to continued imbalance in the longshore transport. As the depth in front of the revetment increases, the longshore transport is reduced to become zero when the local depth is equal to the active depth.

A revetment is defined by its cross-shore position $y_{rev}(x)$ compared to the baseline and the positions of its limits in the longshore direction. It can be situated behind other structure types.

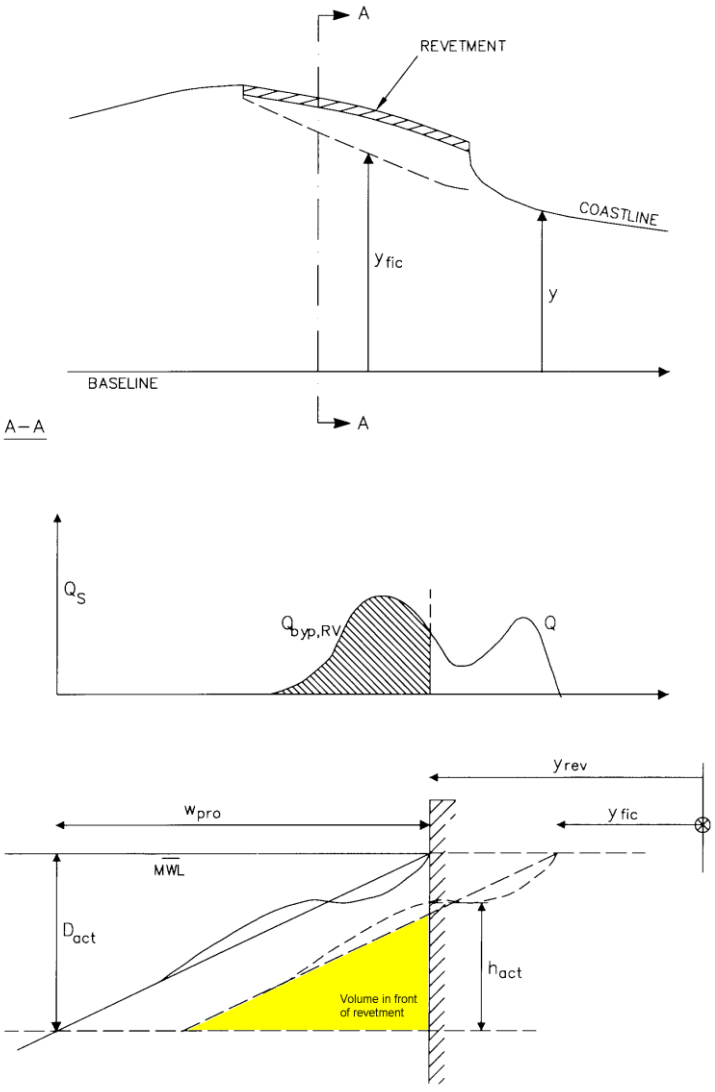


Figure 5.17 Definitions related to revetments

### Reduction of longshore transport

For calculations with revetments, the cross-shore profile is assumed to be represented by a certain active width, $W_{pro}$, which is user specified as the maximum retreat. When erosion has occurred in front of a revetment, LITLINE calculates with a fictive coastline,

$y_{fic}$ (see Figure 5.17). The “undisturbed” longshore sediment transport is reduced corresponding to the distribution of the transport of the cross-shore profile, $Q_{byp,rev}$. $Q_{byp,rev}$ is shown as the shaded area in Figure 5.17.

## Reduction of active height in continuity equation

The “area” of the cross-shore profile changes when the profile is eroded in front of a revetment. This is taken into consideration in the continuity equation through the active height of the profile. $h_{act}$ is found by reducing $D_{act}$ proportionally to the retreat of the fictive coastline. However, to ensure stability in the calculations, $h_{act}$ is always set to be greater than or equal to 0.01*$D_{act}$.

Note: The accumulated volume of the material in front of the revetment is calculated assuming a straight profile (see Figure 5.17).

## Downstream lee-effect

Because the revetment causes a decrease in the longshore transport, the coastline will generally erode just downstream of the revetment. If the coastline recedes sufficiently far, the downstream edge of the revetment will give rise to a sheltering effect similar to the one caused by a groyne.

If the user chooses to include the lee-effect, it is calculated in a similar manner as for the groyne.

The sheltered area is confined by the end of the structure on the upstream side and ten times the distance to the crossing between a line from the structure tip with the angle $\beta_s$ and the coastline on the downstream side similar as for a groyne sketched in Figure 5.16. The transport downstream of the revetment is determined through:

$$Q(j) = Q_{byp} + \left(Q_{un}(j) - Q_{byp}\right) \cdot \sin^4\left(\frac{j}{n_{shel}} \cdot \frac{\pi}{2}\right) \tag{5.26}$$

Where $n_{shel} = 10 \cdot \Delta i_{shadow} = 10 \cdot \left(i_{shel} - i_{groyne}\right)$

$Q_{un}$ is the transport capacity based on the wave climate and possible effects from breakwaters, jetties and groynes situated upstream.

# 5.8 Sources

## 5.8.1 Introduction

A sediment source is used to simulate eg. sediment discharge from a river or beach nourishment. In case the source magnitude is negative, the source behaves like a sink.Two types of sediment sources can be included in the model:

- Point sources are related to a specific longshore position "*IS*" with a certain sediment discharge rate $Q_p$. Point sources are typically used to simulate discharge from a river.
- Distributed sources are related to a stretch of the coastline from $IS_{Start}$ to $IS_{End}$, with a total discharge rate of $Q_d$. Distributed sources are typically used to simulate beach nourishment.

## 5.8.2 Distribution in Longshore Direction

In order to avoid large discontinuity in $Q_s(x)$, the sediment discharge from point sources is distributed to the specified position "*IS*" of the source and the neighbouring points according to the sketch in Figure 5.18a.

The sediment discharge corresponding to a distributed source is distributed evenly over the "length of the source", see Figure 5.18b.

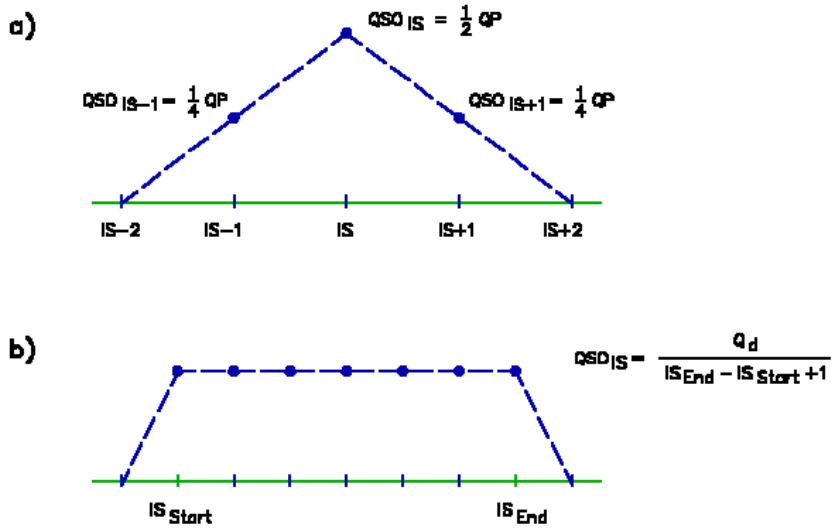


Figure 5.18 Distribution of sediment discharge from a) point source and b) distributed source

## 5.8.3 Including Sources in the Model

Each source on the coastline is defined by the position on the coastline and the magnitude of the source.

It should be noticed that the discharge rates are given in porous volumes (taking the porosity of the sediment into account).

Except for the distribution to neighbouring points, no "diffusion" is included for the sources. The coupling between the local coastline orientation and the longshore transport

rate is the only mechanism responsible for “smoothing out” the effects of sediment sources.

Note that the *Q*-θ relation behind a breakwater is less pronounced, and the model is not set up for including sources here.

## 5.9 Active Height in Continuity Equation

The coastline evolution model is based on the one-line principle, which means that the cross-shore profile at a given longshore position is kept constant and moved back and forth in cross-shore direction with the coastline position y. This is sketched for a specific longshore position in Figure 5.19 where a change of Δy in the cross-shore coastline position leads to a parallel displacement of the cross-shore profile.

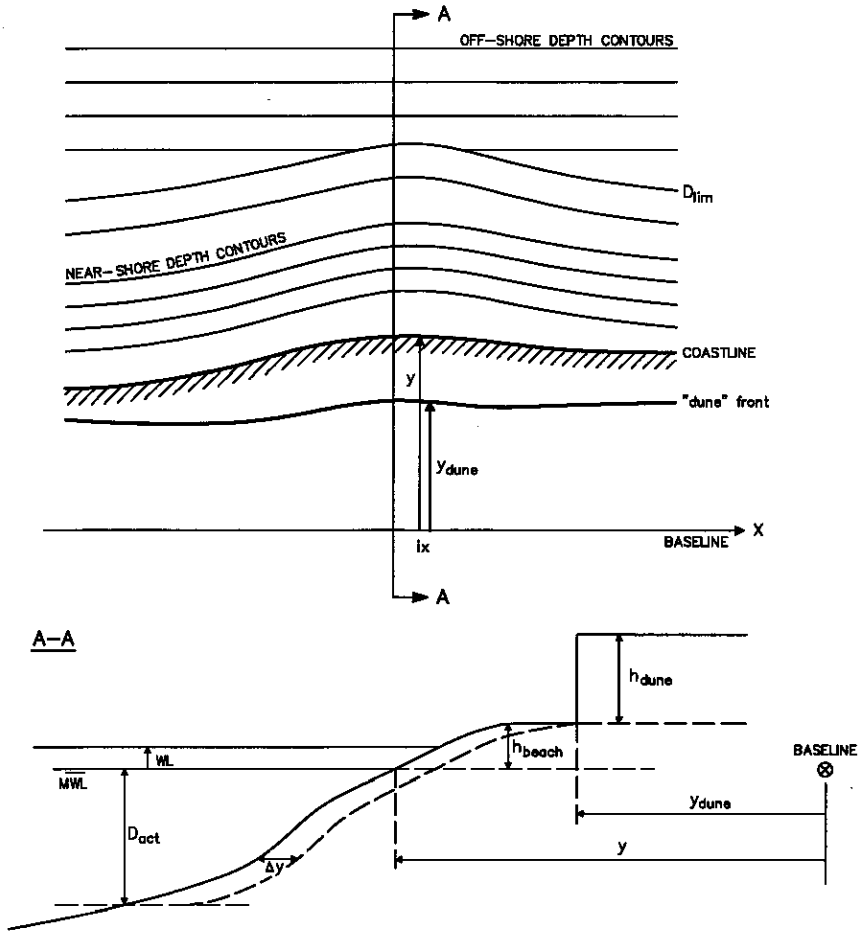


Figure 5.19 Components in active height

Shoreward of the limiting depth, $D_{lim}$, the bottom contours are assumed to run parallel to the local coastline, while the orientation of the depth contours offshore from $D_{lim}$ are specified separately.

As sketched in Figure 5.19, the active height of the cross-shore profile, $h_{act}(x)$ is composed of two components

$$h_{act}(x) = D_{act}(x) + h_{beach} \quad (5.27)$$

$D_{act}$ is the active depth, which, as a function of the longshore position, is kept constant in time regardless of the contemporary water level, wave conditions etc. $h_{beach}$ is the height of the "front beach" or berm. $h_{beach}$ is included in the continuity equation both during erosive and accretive processes. $h_{beach}$ is specified in the input as a constant height above mean water level.

When the coastline has reached a revetment, $h_{act}$ is determined as a fraction of $D_{act}$, see Section 5.7.6 Revetment.

## 5.10 Dune Erosion in Continuity Equation

As sketched in Figure 5.19, $h_{dune}$ is the height above $h_{beach}$ of possible dunes or sand cliffs as a function of the longshore position. The "dunes" are further defined by a position of their front relative to the baseline. The sediment volume from dune erosion is defined as a source term at a given position along the coast in the continuity equation if the beach is eroding and the coastline has reached the front of the "dune". Hence, the "dune" is only eroded and cannot move forward on the beach.

Note that the effect of dune erosion is calculated in a separate continuity equation and is not influencing the morphological time step in the calculations. Large time steps may thus cause an overestimation of the dune erosion.

## 5.11 Effect of Water Level

The discrepancy "*wl*" from the mean water level "*mwl*" (see Figure 5.19) has two effects in the model:

1. It is included as a parameter in the transport tables where it may have a relatively weak influence on the total transport rates, while it can have a larger effect on the cross-shore distribution of the transport.

2. *wl* is included when calculating the bypass of sediment by structures, thus increasing and decreasing the blocking effect of the structure by high tide and low tide, respectively.

The water level discrepancy is included in the time series input.

## 5.12 Regional Currents

Regional currents may in some cases play an important role for the sediment transport. Due to varying cross-shore profile etc., the current speed may vary along the coastline and for varying wave climate. To be able to transfer information from the transport tables to the calculation of coastline evolution, the tables are defined by a slope of the water surface in the longshore direction representing a driving force. The slope is assumed constant in the longshore direction.

The regional current in the calculations is defined by a current speed and direction in the start of the cross shore profile. This information is transformed to a surface slope, which is used for the interpolation in the transport tables.

Relatively strong regional currents may in some cases cause problems with respect to structures. If the waves drive a current in the opposite direction of the regional current, the cross-shore profile of the sediment transport will reverse somewhere across the profile (see Figure 5.20). If the regional current is strong compared to the wave driven current, the net transport may be directed in the opposite direction of the waves. This may cause problems with respect to the calculation of bypass and sheltering effect, which are usually calculated on basis of the wave direction.

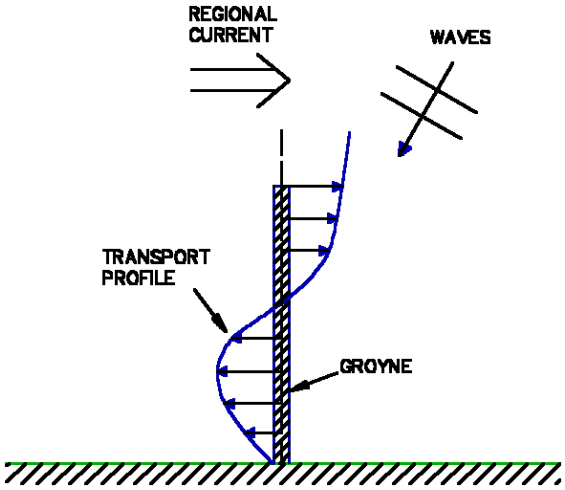


Figure 5.20 Reversing transport profile for oppositely directed waves and current

## 5.13 Time Series Approach

The coastline evolution calculations may be based on either a real-time approach or by a scenario approach.

In the case of a wave climate given by scenarios, eg. yearly wave statistics for a certain location, the set-up of the input has to be performed with some care. The duration of each event as well as the sequence (especially with respect to wave angle) in which they appear in the time series is of significance to the final result. Events of unrealistic long duration should be avoided, and the wave angle variation in the time series should represent a realistic sequence. To assess the influence of the set-up of the time series, different series containing the same components may be simulated, leading to “an envelope” for the resulting coastline evolution.

## 5.14 Morphological Time Step

Each morphological time step Δt in the calculation is calculated on the basis of the maximum gradient in the longshore transport rate. A Courant number for the morphological evolution is defined by:

$$Cou_{\max} = \frac{\left|\frac{\partial y}{\partial t}\right|_{\max} \cdot \Delta t}{\Delta y} = \frac{\left(\frac{\Delta Q_{\max}}{\Delta x \cdot h_{act}}\right) \cdot \Delta t}{\Delta y} \tag{5.28}$$

The Courant number is given as input and each morphological time step is calculated through:

$$\Delta t = \frac{Cou_{\max} \cdot \Delta y \cdot \Delta x \cdot h_{act}}{\Delta Q_{\max}} \tag{5.29}$$

in which $\Delta Q_{\max} = \left|Q(i) - Q(i-1)\right|_{\max}$

The default value of the Courant number is 1.0. Higher values will speed up the calculations but may result in stability problems.

High values of the Courant number or a large gridspacing may result in the coastline upstream of a structure to advance beyond the structure tip.

## 5.15 Solution of Continuity Equation

The continuity equation for sediment volumes, Eq. (5.1), is solved through an implicit Crank-Nicholson scheme. The discretization in longshore direction is sketched in Figure 5.21.

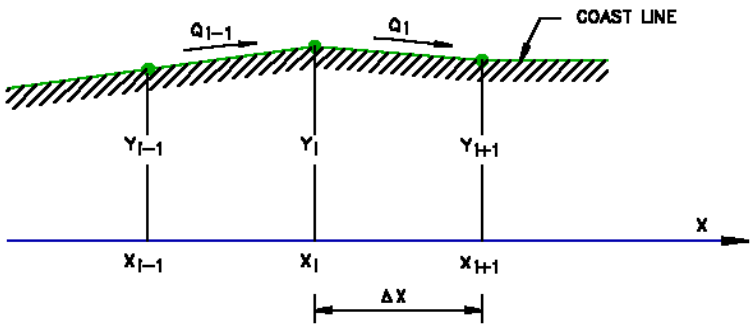


Figure 5.21 Longshore discretization

$Q_i$ denotes the transport rate between $x_i$ and $x_{i+1}$, while $dQ_i$ denotes the change in the transport rate with respect to change in coastline orientation (for values of θ close to the local orientation $\theta_0$).

$$dQ(x) = \frac{\partial Q}{\partial \theta}(x, \theta_0) \tag{5.30}$$

A subscript "*t*" denotes (known) values of the present time step, while subscript "*t+1*" denotes (unknown) values of the next time step. Transport rates corresponding to time step *t+1* are estimated through:

On the basis of a Crank-Nicholson scheme the continuity equation in Eq. (5.1) can be written as

$$a_i y_{i-1,t+1} + b_i y_{i,t+1} + c_i y_{i+1,t+1} = d_i \tag{5.31}$$

in which

$$a_i = (1-\alpha) dQ_{i-1}$$

$$c_i = (1-\alpha)\,dQ_i$$

$$b_i = \frac{\Delta x^2 \cdot h}{\Delta t} - a_i - c_i$$

$$d_i = a_i y_{i-1,t} + b_i y_{i,t} + c_i y_{i+1,t} - \Delta x \cdot \left(Q_{i,t} - Q_{i-1,t} - QS_i\right) \quad (5.32)$$

Where $QS_i$ is the contribution from possible sources.

$a_i$, $b_i$, $c_i$ and $d_i$, can be found for the present time step, and with two boundary conditions, the system of equations for all longshore positions can be solved by Gauss-elimination.

The boundary conditions applied assume a zero transport gradient through each boundary. This causes the coastline orientation at the boundaries to be constant. Structures should be placed at an appropriate distance from the boundaries not to be influenced by the boundary conditions.

The parameter α is the Crank-Nicholson factor. It determines how implicit the solution scheme is. A value of 0 gives a fully implicit solution. A value of 1 gives a fully explicit solution.

### 5.15.1 Dune Erosion

The contribution of sediment to the coastline evolution from dune erosion is included as a source term in the continuity equation.

In case dune erosion is found to occur, the dune front is updated accordingly and the continuity equation in Eq. (5.31) is solved once more, now defining the value $d_i$ as

$$d_i = a_i y_{i-1,t} + b_i y_{i,t} + c_i y_{i+1,t} - \Delta x \cdot QD_1 \quad (5.33)$$

Where $QD_i$ is the contribution of sediment volume from the dune expressed by

$$QD_i = \left[ y_{i,t} - \left(y_{dune}\right)_{i-1,t} \right] \frac{\left(h_{dune}\right)_i}{\Delta t} \quad (5.34)$$

## 5.16 Cross-sections

The cross-shore profile and the related cross-section are basically used for two purposes in the coastline evolution calculations:

- Determination of the total longshore transport rates and the cross-shore distribution of the transport rates. This is done during the table generation and the information is stored in the tables specified by the cross-sections.
- Determination of the depth at a certain distance from the coastline. This is used to determine the depth at structure heads, which goes into the refraction/shoaling calculations. The depth is defined by the specified profiles.

It is possible to vary the profile along the coast. The procedure may, however, not seem straightforward and it is therefore described in some detail in the following.

As a first approach it is recommended always to perform a simulation in which the profile and the cross-section are kept constant. This will help to evaluate the effect of changing the profile compared to other variations.

### 5.16.1 Longshore Variation

If the coastal profile exhibits a large-scale trend which can significantly change the transport conditions in the longshore direction, e.g. an increase in the gradient profile or a change from a profile without bars to one with bars, it may be important to include this variation in the simulation.

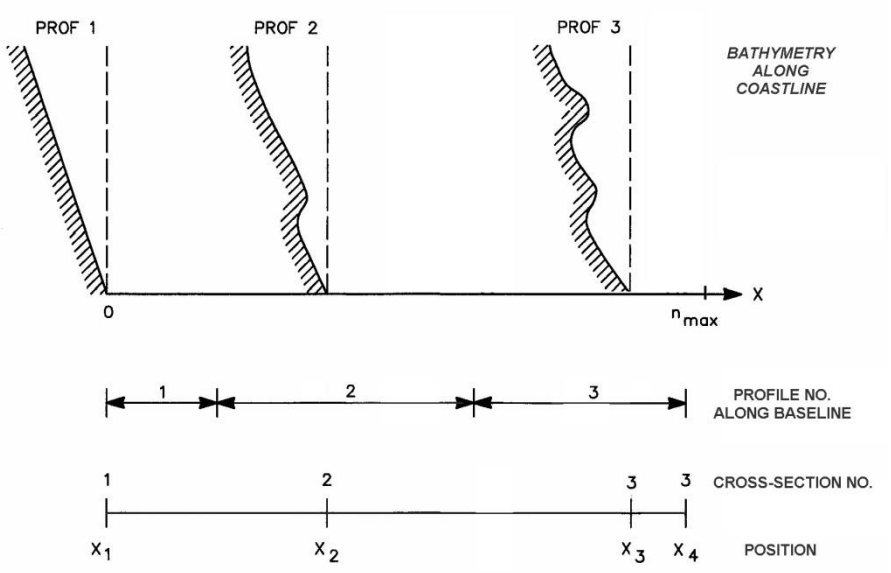


Figure 5.22 Variable profiles along coastline

The procedure is best illustrated with an example. Figure 5.22 illustrates a coastline where the profile in the x-direction changes from a uniform slope (prof1) at the position $x_1$ to a 1-bar profile (prof2) at $x_2$ and finally to a 2-bar profile (prof3) at $x_3$.

#### Profile files

The three cross-shore profiles have to have the same length and Δy, and the shoreline (MWL) should be situated at approximately the same grid point. For the present example the profiles are named prof1, prof2 and prof3.

#### Tables

An envelope of tables containing three cross-sections corresponding to prof1, prof2 and prof3 has to be generated beforehand.

By specifying the three profiles in the Table Generation set-up, a profile reference number is connected to each cross-section. For the present example, the profile number corresponds to the cross-section number in increasing order, but this does not have to be

the case. The profile numbers are just reference numbers, which can be defined to suit any desired order.

Running the table generation with the above (and other necessary) specifications will generate an envelope of tables with one global name containing three sets of tables each carrying a reference number (1, 2 and 3, respectively).

## Coastline file

The results in the transport tables are based on the profiles used, but the tables carry no information to the coastline evolution calculation on which profiles were used. This has to be specified in the input. Here the reference number for the profiles is specified as a function of the longshore position.

## Cross-sections

The next step is to specify the transport tables. First, the global name is specified. Secondly, the longshore variation of the transport tables should be defined. The cross-section should per default resemble the cross-shore profile locations. This, however, is not mandatory, since minor differences may help the calibration.

At the specified positions, transport rates will be taken directly from the specified cross-sections table, while the depth-distance relation is taken from the profile corresponding to the number specified in the space-varying profile location array.

Conditions in between the selected cross-sections are found from interpolation, both in the tables and in the depth-distance relation.

# 6 References


/1/ Andersen, O.H., and Fredsøe, J.(1983): *Transport of Suspended Sediment along the Coast*. Progress Report No. 59, ISVA, Technical University of Denmark.

/2/ Battjes, J.A.(1974): *Computation of Set-Up, Longshore Currents, Run-Up and Overtopping due to Wind-Generated Waves*. Delft Technische Hogeschool.

/3/ Battjes, J.A., and J.P.F.M. Janssen (1978) *Energy Loss and Set-Up due to Breaking of Random Waves*. Proc. of the 16th Int. Conf. on Coastal Eng. pp. 569-587, Hamburg.

/4/ Battjes, J.A., and Stive, M.F. (1985) *Calibration and Verification of a Dissipative Model for Random Breaking Waves*. J. of Geophys. Res., 90:9159-67, September.

/5/ Brøker Hedegaard, I. (1985), *Wave Generated Ripples and Resulting Sediment Transport in Waves,* Series paper No. 36, Inst. of Hydrodynamics and Hydraulic Engineering, Technical University of Denmark.

/6/ Dally, W.R. and Brown, C.A. (1995), *A modeling investigation of the breaking wave roller with application to cross-shore currents,* J. of Geophys. Research, Vol. 100, No. C12, pp. 24.873-24.883.

/7/ Deigaard, R., Fredsøe, J., and Brøker Hedegaard, I. (1986) *Mathematical Model for Littoral Drift.* Journal of Waterway, Port, Coastal and Ocean Engineering, ASCE, Vol. 112, No. 3, pp. 351-369.

/8/ Deigaard, R., Fredsøe, J., and Hedegaard, I.B. (1986), *Suspended sediment in the surf zone*, Jour. of Waterway, Port, Coast. and Ocean Eng., ASCE, Vol. 112, No. 1, pp. 115-128.

/9/ Deigaard, R., Asp Hansen, E., Justesen, P. and Brøker, I. (1994), *Sediment transport in the surf zone due to oblique incident waves,* MAST Gregynog Workshop, Gregynog, Wales.

/10/ Doering, J.C. and Bowen, A.J. (1995), *Parameterization of orbital velocity asymmetries of shoaling and breaking waves using bispectral analysis,* Coastal Engineering (26)1-2, pp. 15-33.

/11/ Elfrink, B., Brøker, I., Deigaard, R., Hansen, E.A. and Justesen, P. (1996), *Modelling of 3D Sediment Transport in the Surf Zone,* Conf. of Coastal Engineering 1996, Proceedings.

/12/ Engelund, F. and Fredsøe, J. (1976), *A sediment transport model for straight alluvial channels,* Nordic Hydrology, 7, pp. 296-306.

/13/ Fenton, J. (1985), *A fifth-order Stokes theory for steady waves,* J. Coastal, Port, Waterway and Ocean Eng., ASCE, Vol.111, pp. 216-234.

/14/ Fenton, J. (1990), *Non-linear wave theories,* The Sea, Vol. 9, Ocean Eng. Science, Part A, Wiley, N.Y.

/15/ Fenton, J.D. & W.D. McKee (1991): *On calculating the lengths of water waves*, Coastal Engrg., 15 pp.499-513. Elsevier Science Publishers B.v., Amsterdam.

/16/ Fredsøe, J.(1981): *Mean Current Velocity Distribution in Combined Waves and Current*. Progress Report No. 53, ISVA, Technical University of Denmark.

/17/ Fredsøe, J.(1984) *Turbulent Boundary Layers in Combined Wave Current Motion.* Journal of Hydraulic Engineering, ASCE, Vol. 110, No. HY8, pp. 1103-1120.

/18/ Fredsøe, J. and Deigaard, R. (1992), *Mechanics of Coastal Sediment Transport,* Advanced Series on Ocean Engineering, Vol. 3, World Scientific.

/19/ Fredsøe, J., Andersen, O.H., and Silberg, S. (1985), *Distribution of Suspended Sediment in Large Waves,* Journal of Waterway, Port, Coastal and Ocean Engineering, ASCE, Vol. III, No. 6, pp. 1041-1059.

/20/ Goda Y., Takayama T., and Suzuki Y. (1978). *Diffraction diagrams for directional random waves*. Proceedings of the 16th Coastal Engineering Conference. ASCE, Vol. 1, 1978, pp. 628-650.

/21/ Isobe and Horikawa (1982), *Study on water particle velocities of shoaling and breaking waves*, Coast. Eng. in Japan, Vol. 25, pp. 109-123.

/22/ Jonsson, I.G., Skovgaard, O., and Jacobsen, T.S.(1974) *Computation of Longshore Currents.* Proc. Coastal Engineering Conference, pp. 699-714.

/23/ Jonsson, I.G. and N.A. Carlsen (1976): *Experimental and Theoretical Investigations in an Oscillatory Turbulent Boundary Layer*. J. Hyd. Res. 14,1 pp. 45-60.

/24/ Kraus N.C. (1984). *Estimate of breaking wave height behind structures.* J. of Waterway, Port, Coastal and Ocean Engineering. Vol. 110, No. 2, 1984.

/25/ Lundgren, H. (1972): *Turbulent Currents in the Presence of Waves.* Coastal Eng. Conf., pp. 623-634).

/26/ Nielsen, P. (1979), *Some Basic Concepts of Wave Sediment Transport*, Institute of Hydrodynamic and Hydraulic Engineering, Technical University of Denmark, Series Paper 20.

/27/ Raudkivi, Arved J. (1988), *The Roughness Height under Waves,* Journal of Hydraulics Research, Vol. 26, 1988, No.5.6.

/28/ Rubey, N.W. (1933), *Settling Velocities of Gravel, Sand and Silt Particles,* Amer. J. of Science, 5th Series, Vol. 25, No. 148, pp. 325-338.

/29/ Sand, S.E.(1979) *Three-Dimensional Deterministic Structure of Ocean Waves*. Series paper No. 24, ISVA, Technical University of Denmark, 1979.

/30/ Smart, G.M. and M.N.R. Jaeggi (1983) *Sediment Transport on Steep Slopes.* VAW Mitteilung 64, pp. 104-106 and pp. 11-117.

/31/ Svendsen, I.A., and Jonsson, I.G.(1980): *Hydrodynamics of Coastal Regions*. Den Private Ingeniørfond, Technical University of Denmark.

/32/ Swart, D.H.(1974) *Offshore Sediment Transport and Equilibrium Beach Profiles*. Delft Hydr. Lab. Publ. 131, Delft University Technology Diss., Delft.

/33/ Swart,D.H (1982), *The nature and analysis of random waves in shallow water,* CSIR Research report 388/2, Stellenbosch, South Africa.

/34/ Wu & Thornton (1986): *Wave numbers of Linear Progressive waves,* JWPCO., ASCE, Vol.112, WW4, July, pp.536-540.

/35/ Zyserman, J.A. and Fredsøe, J. (1994), *Data analysis of bed concentration of suspended sediment,* Journal of Hydraulic Engineering, ASCE, Vol. 120, No. 9, pp. 1021-1042.

/36/ Zyserman, J.A., and J. Fredsøe (1996), *Validation of a deterministic sediment transport model for sheet-flow conditions,* Progress Report 76, pp. 1-7, Institute of Hydrodynamics and Hydraulic Engineering (ISVA), Technical University of Denmark.